BILINGUAL PUBLISHING CO.
Pioneer of Global Academics Since 1984

Journal of Environmental & Earth Sciences

Volume 4 • Issue 1 • April 2022 ISSN 2661-3190(Online)

Editor-in-Chief

Editorial Board Members

Volume 4 Issue 1 • April 2022 • ISSN 2661-3190 (Online)

Journal of Environmental & Earth Sciences

BILINGUAL PUBLISHING CO.
Pioneer of Global Academics Since 1984

BILINGUAL PUBLISHING CO.
Pioneer of Global Academics Since 1984

Volume 4 | Issue 1 | April 2022 | Page1-71
Journal of Environmental & Earth Sciences

Contents

Articles

Review

BILINGUAL PUBLISHING CO.
Pioneer of Global Academics Since 1984

Journal of Environmental & Earth Sciences
https://ojs.bilpublishing.com/index.php/jees

REVIEW

Petroleum Filling Stations and Their Impact on the Environment in Nigeria

Ruth Oghenerukevwe Eyankware Ulakpa[1*] Wisdom Chukwuemeke Ulakpa[2]
Oghenegare Emmanuel Eyankware[3]

1. Department of Environmental Management and Pollution Control, Nigeria Maritime University, Okerenkoko, Nigeria
2. Federal University of Technology, Minna Niger State, Nigeria
3. University of Port-Harcourt Rivers State, Nigeria

ARTICLE INFO

Article history
Received: 9 November 2021
Accepted: 16 December 2021
Published Online: 22 February 2022

Keywords:
Petroleum filling stations (PFSs)
Environment
Health
Impact
Department of Petroleum Resource (DPR)

ABSTRACT

The poor state of the environment, especially in urban areas, has become a major global issue, with developing countries such as Nigeria voicing growing concern. There is a scarcity of knowledge on the environmental impact of PFSs as a result of the loss of life and property, as well as other serious socio-economic implications of non-compliance with PFSs siting criteria. The historical literature on the impact of residential buildings, the environment, and human health on PFSs in Nigeria, as well as the study's gap, is examined in this research. It also outlines DPR compliance with PFSs location as well as established criteria for prohibiting PFS sitting in Nigeria's states. Relevant publications on PFSs-related topics were downloaded from Google Scholar. The goal of this study is to look back on a previous essay about PFSs in Nigeria and its impacts on the environment and human health. This study's main purpose is to give a complete overview of Nigerian PFSs. According to the article analyzed, the majority of PFSs were located close to residents, with setbacks from the road and residential areas of less than 30 m in 90% of the filling stations. As a result, the landowners can band together to argue that a facility that is improperly sited cannot be built. A great deal of public participation is required. A campaign should be launched to raise awareness among filling station owners and other developers of the dangers of non-compliance with established norms. All violators of the established norms, as well as corrupt officials of enforcement agencies/bodies, should face open punishment so that others might learn their lessons. Finally, appropriate planning is required to allow future road expansion.

*Corresponding Author:
Ruth Oghenerukevwe Eyankware Ulakpa,
Department of Environmental Management and Pollution Control, Nigeria Maritime University, Okerenkoko, Nigeria;
Email: rutheyankware@yahoo.com

DOI: https://doi.org/10.30564/jees.v4i1.4073

1. Introduction

Volatile organic compounds (VOCs) are a diverse collection of substances distinguished by their relatively high vapor pressures. Exposure to these substances can cause asthma, headaches, mucosal symptoms [1], and, in some situations (e.g., benzene), an elevated risk of cancer [2,3]. In Europe, benzene is the only VOC that is officially regulated in terms of air quality (Directives 2000/69/EC and 2008/50/EC). VOCs have indirect health consequences due to their role as ozone and other photochemical pollution precursors. PFSs are frequently the largest source of VOCs in metropolitan settings. Additional sources include traffic and small-scale companies that employ organic chemicals as solvents (paint, glue, etc.). Petrol stations as VOC emission sources have been the topic of much research in recent years, with a special focus on the design and evaluation of control systems in an effort to reduce environmental concerns and emissions [4,5]. Mostly those concerning their effects on employees and environmental issues [6-11].

Several studies in the worldwide literature have looked at local projections of petroleum vapours on petrol station workers' health and the impact of petrol stations on their immediate surroundings, and gas stations as a major source of VOCs [12,13]. The inclusion of petrol stations within residential zones in human settlements was determined by the uncontrolled and rapid sprawl of built-up houses unique to Romanian urban ecosystems [14]. This is why we're interested in doing a temporal analysis of incompatible land use and land-cover to find evidence for the velocity of change in terms of locational conflicts between residential areas and gas stations. The high VOC pressure on air quality provided a legislative framework at the European level: Directive 1999/13/EC which promotes the reduction of VOC emissions caused by the use of organic solvents in certain activities and installations; and Directive 94/63/EC, which highlights that VOC emissions contribute significantly to air pollution [15,17].

Although Spanish petrol stations were traditionally located in relatively empty areas, the country's continual urbanization has resulted in numerous petrol stations being established within metropolitan areas surrounded by structures in recent years. This issue has sparked a debate between residents whose homes are close to gas stations and the authorities in charge of land management. With oil products, the residential areas-gas stations' relationship can cause fires, increased traffic, noise, pollutants, waste, and wastewater [16]. The climate zone, road network features, and urban agglomeration all amplify these effects [17]. The haphazard expansion of built surfaces in Romania, particularly residential areas, has resulted in the replacement of the terrain profile, from one prodct to one consumer, as well as the residential areas' closeness to opposing functions [18]. In general, gas stations are positioned only for economic reasons, with little consistency in issuing building certificates and no proper oversight of conformity with territorial planning requirements. Environmental endowments are modest, and environmental components are only superficially monitored at these gas stations. All of them are linked to excessive VOC emissions (particularly benzene), which cause structural disequilibrium in environmental components.

In physical planning practices throughout the world, the easy-going methods and littering of fuel filling stations in approved residential land uses are unsafe, pervasive, and forbidding. Even though anthropogenic actions such as petrol filling stations and related commercial land use development continue to fail the environmental impact evaluation test of acceptance, compatibility, suitability, and standard on a daily basis in developing countries around the world, are common in residential neighborhoods. In Sub-Saharan Africa, however, formal analysis of other land uses, such as fuel filling stations, in order to determine their social and environmental advantages and disadvantages in terms of layout or residential neighborhoods is no longer required. The reasons for this exceptional rise are not difficult to imagine. The oil business became a major source of energy with the start of the industrial revolution at the turn of the twentieth century, owing to the rise of the vehicle industry. Although oil is an important petrochemical feedstock, it is also a source of energy for the global economy [19]. As can be seen from the above data, oil has played a significant role in the growth of technology in our day. However, oil finding, like any other technique, has its drawbacks. One of these disadvantages is its harmful impact on the earth's biosphere, which includes the release of pollutants and greenhouse gases into the environment, as well as ecosystem damage from occurrences like oil spillage [20]. As a result of this predicament, developed countries are beginning to

place a greater emphasis on a cleaner, more environmentally friendly energy source. Nigeria's energy needs are provided by petroleum and natural gas reserves, which are plentiful. The Nigerian economy is heavily reliant on crude oil exports. The recent population growth in Nigeria has prompted a rise in demand for petroleum goods, and many marketers have taken advantage of this need by arbitrarily constructing service stations without considering the potential impact of their locations [21]. The rapid growth of built-up gas filling stations in primarily residential neighborhoods in developing nations, including Nigeria, is concerning and poses issues for a sustainable environment as well as violations of land use arrangements and environmental aesthetics [22]. Opinions show the accumulating and obstinate glassiness of these phenomena in Nigerian residential zones, exacerbated by quick approval, poor evaluation, and control of such developmental projects in residential areas by the relevant agencies, which are safekeeping physical planning and urban development without regard for the attendant environmental and health implications.

The condition can also be a result of land use modification or conversion, such as the continued presence of escalating petrol stations in various types of residential areas. It causes problems since extremely flammable petroleum products are frequently stored in residential zones in constructed underground tanks for retail purposes. Furthermore, the inability of petrol station developers to comply with the necessary laws guiding the development of such activities, as well as a lack of strict control by appropriate agencies, contribute to the location of such commercial land use in the residential domain of Nigerian urban areas, as more filling stations are built in order to meet demand. As a result of the current scenario, it is becoming increasingly frequent to find fueling stations positioned close to residential areas. The consequence of this development is increased air pollution due to the ongoing release of hazardous chemicals into the atmosphere. These emissions come from a variety of sources, including gasoline delivery to stations, tank breathing caused by temperature and pressure fluctuations during vehicle refueling, emissions from loosely closed tanks, and leakage caused by the mishandling of petroleum [21]. There is also the emission of combustion products from the station's vehicle engines [23]. PFSs, as retail outlets for highly flammable petroleum resources such as gas, gasoline, and kerosene, must be strategically situated in relation to other operations to minimize the damage to the nearby environment. Petrol stations along the route were found to be too close together; some were even built side by side, resulting in a greater likelihood of massive and wide-ranging consequences on the nearby environment. The positions of gas stations in relation to road crossings and U-Turns, as well as their setbacks from the expressway, a high-tension power line, and adjacent land uses, have generated concerns about the area's safety. Because the power supply in Nigeria is known to be unreliable, many, if not all, of the stations are planned to use privately owned generating facilities, which may cause some noise and air pollution in the immediate environment. Another source of concern is the rowdiness at and near gas stations, especially when there is a shortage of fuel. Economic expansion is now widely acknowledged as a major contributor to developing environmental challenges, particularly when such development is not sustainable.

The following are the objectives of this article: To examine the effects of the expansion of PFSs in new locations on the environment and human health; examine EIA requirements for PFS site suitability; and examine the impact of their locations in order to find a long-term solution to the problems.

Description of the Study Area

Nigeria is located in the West African sub-region between longitudes 30 and 140E and latitudes 40 and 140N as shown in Figure 1. It has a total area of 923,768 square kilometers. It is bordered to the North by the Republics of Niger and Chad, and to the West by the Republic of Benin. It shares Eastern borders with Cameroon all the way down to the Atlantic Ocean's coasts, establishing the Nigerian Territory's Southern boundaries.

Despite being totally inside the tropics, Nigeria's climate ranges from tropical on the coast to sub-tropical in the interior. The wet season runs from April to October, with the dry season being from November to March. The extreme maximum temperature in Southern coastal locations can reach 370 °C, while the extreme low is 100 °C. Temperature extremes can vary from 400 to 5000 degrees Celsius further north, and the climate is drier [24].

Figure 1. Nigerian map depicting the federating states [24].

2. Methods

In Nigeria, a similar technique was used to review PFSs, and the same was used in order to assess the environmental impact of petrol pumping stations near residential areas in Nigeria, as well as to suggest mitigating techniques, articles from the last 5-10 years were examined [25]. Articles relevant to this study were found using Google search engines and open access journal sites. These articles and papers were reviewed in their entirety, and the data was entered into a database containing the authors' names, publication details, study site, time period, strategy, and technique for studying the impact of filling stations on man and the environment, as well as the major conclusion.

Furthermore, multiple methods were employed for this study with some modifications to satisfy the goal and objectives of this paper, which was to interpret the status and quality of work done within and outside Nigeria. The following approaches were used to evaluate the quality of the articles; the environmental and human health consequences of the proliferation of PFSs in previously uncharted territory; to research EIA standards for PFS site selection suitability, and to assess the impact of their sites in order to provide a long-term solution to the difficulties.

3. Results and Discussion

3.1 Impacts of the Proliferation of PFSs with Their Unprecedented Locations It Has on the Environment

Several researches have demonstrated the problems associated with the environmental impact of PFSs in Nigeria. The manner in which petrol fuel outlets are sandwiched in residential zones of Nigerian urban centers without regard for the health and environmental consequences is not encouraging. An empirical study was conducted on contaminants released from PFSs and their impact on air quality [26]. Their findings revealed that the main contaminants identified in the environment air were volatile organic compounds, methane, and carbon monoxide, with impurity levels exceeding the FEPA air quality limit. Over 98 percent of PFSs met the minimum

reserve of 100 meters from health care centers and various gas stations in order to achieve the 400-meter basic station distance guideline [27]. PFSs have been found to be abundant near roadways and residential buildings in previous research. Similar research has demonstrated that the locational pattern of nearby petrol filling stations has the propensity to cluster in a specific zone. The study recommends that petrol stations be closed or restricted in and around the town's built road flight path and strictly designated residential zones [28].

The buffer analysis and descriptive statistics to evaluate the proximity of PFSs to residential buildings in the Bucharest suburbs discovered that the presence of PFSs has resulted in malfunctions, highlighting a disadvantaged area due to environmental issues, unplanned development, overburdened infrastructure, and pollution of each environment component [29,30]. They evaluated the survival of filling stations and urban infrastructure to qualify check maintenance on compliance. In their research, they discovered that while 50% of gas stations followed the rules, the remaining 50% did not. According to the researchers, preparedness should be based on the adequacy, functionality, and sophistication of available extinguishing facilities. Setback standards and safety preparedness policies should be improved for long-term urban development [31]. The study on the locational distribution of petrol stations and the underlying ramifications in Osun City, Nigeria's commercial density shows that about 56% of PFSs followed the area coverage standards, implying that the petrol stations' clustering was endangering the area's safety [32].

Land-use activities along arterial highways in several Nigerian cities are not regulated or coordinated, exposing the region to threats such as traffic bottlenecks, pollution, accidents, fire explosions, and other environmental issues. These filling stations serve as a major contributor to traffic problems such as traffic congestion, pollution, fire, and explosion in densely populated regions [33]. According to him, the degree of these varies depending on factors such as location, size, and distance from the road, among others. It is believed that the air quality near fuel stations and their environs (which is mostly influenced by vapor emissions from unburned gasoline) differs from the ratio seen in city air, which is primarily influenced by traffic emissions [21]. Petroleum distribution is a complicated task that entails carrying and storing across the country [34]. The location of filling stations and their impact on the environment in different parts of Nigeria was investigated [33,35,36]. In Kaduna North the spatial distribution of filling stations was analyzed, from the result it was discovered that the 22 PFSs in the area are irregularly dispersed and largely clustered along key highways [33]. The analysis did not consider the impact of the spatial distribution of these filling stations on traffic flow along the highway which contradicts [35]. According to research conducted in Spain, gas stations contribute significantly to ambient benzene concentrations in their vicinity as a result of the non-conformity of filling station locations to statutory criteria on traffic flow [37]. Table 1 shows the results.

In Romania the haphazard growth of PFSs and their closeness to residential buildings, made residents in Ro-

Table 1. A brief comparison of the distance between PFSs in Nigeria.

From	To	Location	Kilometer	Meter	References
NNPC Mega Conoil	Federal road	Abuja- Keffi road	0.05	50	[21]
Oando	Residential Buildings	Isoko road Ughelli	0.05	50	Field Study, 2021
Conoil	Businesses centers	Kubuwa Abuja	0.1	100	Field Study, 2021
Century	New path	Okpanam road Asaba	0.3	300	Field Study, 2021
Texaco	Total	Abuja-Keffi road	0.1	100	[21]
Total	Mobil	Isoko road Ughelli	0.2	200	Field Study, 2021
Rain oil	Federal road	Asaba-Agbor road	0.1	100	Field Study, 2021
Conoil	Residential Buildings	Rumuokuta -Mgbuoba road	0.2	200	Field Study, 2021
Total	State road	Agbani-Enugu road	0.3	300	Field Study
NNPC mega stations	State road	Douglas road Owerri	0.05	50	Field Study
AA Rano Nig. Ltd.	Federal road	Mararaba	0.1	100	Field Study
Mobil	State road	Kurunduma	0.5	500	Field Study
Oando	State road	Kuchikau	0.14	140	Field Study
Total	State road	Masaka	0.14	140	Field Study
NNPC	Federal road	Ado	0.75	750	Field Study

mania believe that the affiliation of home gasoline stations can cause fires, increased traffic, noise, pollution, trash, and wastewater by using oil products [18,17]. This is consistent with the findings of the location and spatial distribution of PFSs in Ilaro, Ogun State [38]. The study of PFSs in Ilesa, Osun State, Nigeria concludes that numerous filling stations were haphazardly spread along with it, with some more under construction, and that filling stations along the road was discovered to be too close to each other; some were even developed side-by-side, implying a higher propensity for massive and wider effects on the immediate environment [39]. A variety of factors impact the location of a petrol station in the Accra district [40]. The study's findings revealed that factors such as promotion, brand, pump pricing, service quality, opening hours, local authority assessment, and location size influenced sitting. As a consequence of the study's findings, a fuel station placed in a high-traffic region, a struggle along the road, the area's land use activities, and the road's condition, including environmental and regulatory requirements, are all desirable. In the Nigerian city of Port Harcourt, there is an agreement that the spatial attribute for locational analysis of petroleum stations is that filling stations have been converted to residential houses, and 14 filling/petrol dispensable engines are located near the road, and one is located near a high tension line [17,40].

Research on the impact of PFSs on petrol stations in Kampala, Uganda was compared to studies on the level of compliance of PFSs with development control requirements in Anambra, Nigeria [41,42]. As the distances between the filling stations sampled from the road and the setback standards are significantly different, the results of their study suggested that the aforementioned explain why houses located 100 meters from stations were prone to sensible height and those 50 meters' analyses were rated the peak of the risk, as the distances between the filling stations sampled from the road and the setback standards are significantly different. Further studies revealed that the environmental problems of developed fuel filling stations in the residential domain are also numerous, including volatile organic compounds, methane, and carbon monoxide, to name a few in Port Harcourt Rivers State [22].

The increase in the global population has outpaced, and automobiles, including Premium Motor Spirit (PMS), have posed a serious threat to human health in terms of providing the Liquified Natural Oil, Kerosene, Dual Purpose Kerosene masses with the necessary infrastructure, enact, and (DPK), Aviation Turbine Kerosene are sold [43]. As the population of completed white petroleum products grows, so does the number of automobiles that run on flammable vapour at very low temperatures.

The fact that certain hydrocarbons found in PFSs are effective inducers of cytochrome P450 was demonstrated in the introduction section of the research, which could lead to biological and physiological effects. Following car refueling, a significant level of benzene was observed in the pulmonary zone of PFSs [44]. Benzene and similar hydrocarbons produced by PFSs are metabolized by a highly reactive intermediate epoxide that binds to hepatic microsomal proteins and nucleic acids, causing lethal consequences in humans [45]. Because petroleum hydrocarbons and other related carbon-containing compounds, particularly mammalian liver and kidney cells, are converted into free radicals or activated metabolites during oxidation in cells it was deemed necessary to assess the extent of PFSs' impact on human health and, if possible, quantify it [45]. Unlike decades earlier, when PFSs were sporadically spread, most of the activities of PFSs were connected to contemporary day development in some way.

It is believed that PFSs hydrocarbons activated metabolites, when reacted with some cellular components, such as membrane lipids, to form lipid peroxidation products, could contribute to membrane alteration [46]. They went on to say that this could react with enzymes and cause inactivation by oxidizing proteins and/or breaking DNA strands. Because their metabolites can attach to proteins and nucleic acids, they can trigger these latter effects. Studies have also shown that PFS exposure has resulted in significant alterations in the activity of numerous enzymes in China particularly in the tissues of the liver, kidneys, and lungs [47,48]. The potential health risks of Owerri's petrol station personnel were assessed [49]. The results show a significant increase in alkaline phosphatase, analine, and aspartate amino transfer activities in people exposed to petrol vapour for 6-10 years. Individuals exposed to petrol vapour had significant amounts of serum urea, creatinine, and urine protein, according to the findings.

Qualitative interviews were conducted to confirm the discovered parameters of PFSs in Ife-Central using an inductive manner. The findings show that all of the PFSs violate the principles and criteria because the distribution was clumped, negatively impacting the residents' well-being, the environment, and their socioeconomic situation [50]. PFSs siting has resulted in the release of volatile organic compounds such as benzene and toluene, as well as toxic gases such as carbon monoxide and traces of soot, all of which have been shown to have a negative impact on general health and environmental hazards [51]. Table 1 shows the results.

Table 2. Benzene concentrations ($\mu g.m^{-3}$) measured by personal (R) or by fixed site monitors (S) placed in or around of petrol station.

Local	Period	Observations (n)	Study Type (Sx)	References
United States	1981-83	72	Rnc	[52]
Europe	1986-1992		Rnc	[53]
United Kingdom	1995	-	Rnc Rc	[54]
Valencia (Spain)	-	7	R	[55]
Kolkata (India)	2005-2006	35	R	[56]
Ioannina (Greece): - urban - rural	2006	30 30	Rc	[57]
Ioannina (Greece) - urban - rural	2006	32 32	Rc R	[58]
Owerri (Nigeria)	2005-2007	40	Rnc	[59]
Italy	-	28	R	[60]
Kano (Nigeria)	2008	214	Rnc	[38]
Illorin (Nigeria)	2018	297	Rc	[61]
Anambra (Nigeria)	2019-2020	270	Rnc	[42]
Ife- central (Nigeria)	2021	52	Rnc	[50]
Ede Osun state (Nigeria)	2021	14	Rnc	[62]

-: the requested information was not found; Rnc: refueling without an installed emission control system; Rc: refueling with an installed emission control system; R: refueling without knowing whether or not an emission control system is in place; Sx: a study conducted at a maximum distance of x meters around a petrol station.

3.2 EIA Requirements for Suitability of Site Selection of PFSs

Construction activities are anticipated to cause severe environmental harm, which is a major worry. Rail projects, fuel pumping stations, and infrastructural facilities all have the potential to impact the environment, including soil degradation, air pollution, and water contamination [50,63-66]. The main challenge for developers today is to establish and implement a strategy for sustainable building operations that is both environmentally friendly and long-term [67-69]. Continuous urbanization creates a fair demand for automobiles, resulting in increased fuel consumption and filling station demand [70]. In the same line, the bulk of PFSs in Ede Osun state did not adhere to planning criteria. Implementing a public awareness campaign among residents and enforcing planning standards in existing PFSs and other land uses will go a long way toward addressing the issues of low perception and non-compliance with planning standards. Filling stations and electric charging stations for future cars meet the increased demand for fuel. The PFSs have a significant potential to harm the site and the surrounding environment, according to reports. It also has an effect on socioeconomic losses, environmental deterioration, geological disintegration, and water contamination [71-73]. One of the most serious hazards of PFSs is fire, which is compounded by other factors such as electricity [70] and pipe and underground storage tank leakage, which can lead to groundwater contamination [74]. Furthermore, it causes air pollution from aromatic compound concentrations [75] as well as traffic congestion [70]. The PFSs facility is necessary, but it is also dangerous. As a result, particular care must be used when selecting such a facility. Any company project's site selection is crucial [76,77]. Several incidences involving fires at gas stations and filling stations have already been reported in the news, with fatalities. It has a variety of effects on the industry as well as the mental health of users. Take a look at Figure 2.

Perceptions of Residents on Danger Associated with Petrol Stations in Nigeria

Researchers continue to be interested in developing a sustainable way to maintain the natural environment. Construction field activities that can harm the environment have long been a source of worry. The structure of such places has the potential to cause significant environmental damage. A PFSs improves transporter and traveler convenience, but these stations are frequently dangerous [74,78]. Site selection is frequently cited as an important factor

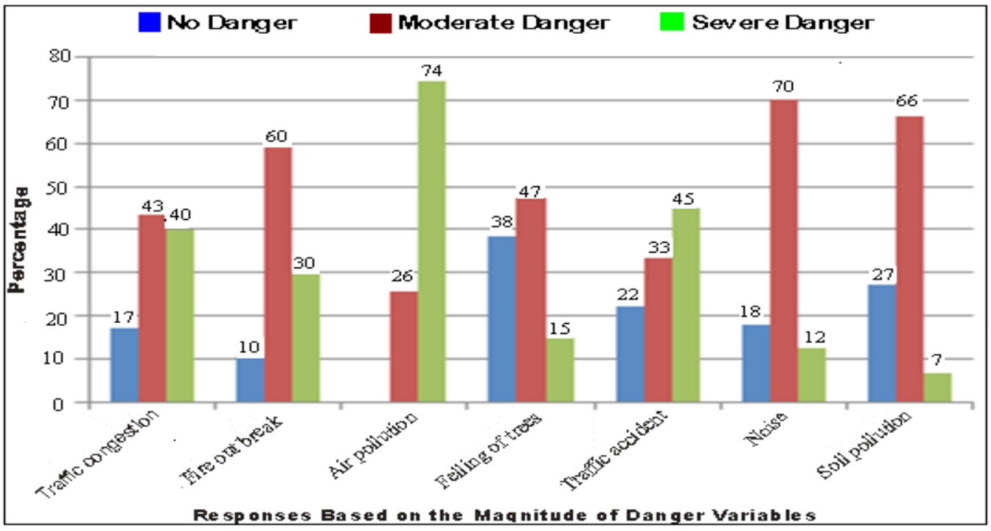

Figure 2. Perceptions of residents on danger of the presence PFSs [35].

in the success of any business venture. This industry has become increasingly concerned about major environmental issues and negative consequences around the world. Petroleum retail companies are attempting to implement sound and effective environmental policies for PFSs. The EIA was created as an effective instrument for better management of such assets for this aim. Using regression and GIS, the PFS's position is determined by traffic volume counts [79].

The amount of clients who visit per day determines the site's potentiality, which is critical for business growth. A study was carried out in the Kano Metropolitan Area in Northern Nigeria to ascertain the concern of businesses in the sector of petrol retailing for taking physical planning requirements into consideration [80]. The requirements stated for planned construction were found to be ignored by eight (8) stations (4%) out of 192 stations [78]. As illustrated in Figures 3a and 3b. It is said that building crews for petrol-filling stations prefer to choose a site based on personal preferences; however, for environmental protection and other preventive measures, a uniform method is required. Furthermore, it is noted that an EIA study is required prior to obtaining approval for the fuel site [81-84].

EIA entails the necessary examinations and analyses of a project's environmental viability. The methods and procedures involved in completing EIA reports take a significant amount of time, effort, and money [85,86]. The older approaches of site selection incorporate both qualitative and quantitative elements when deciding on a place. Because various factors are still involved in the EIA analysis of any facility, such as an FS, these studies lack factors considered in EIA assessment. And FS is a significant environmental liability since it poses a risk to the environment's well-being. As a result, a site study and general risk assessment are required before such facilities may be built [87].

Figures 3. Displaying PFSs with no setback to residential buildings in Delta and Imo State.

Source: Researchers' Fieldwork, 2021.

The level of awareness of risks and safety precautions among PFSs, as well as the existing safety practices in Petrol Filling Stations in Minna, Niger State, Nigeria was investigated. According to the statistics, 45% of PFSs in Minna do not meet Department of Petroleum Resources (DPR) siting requirements, with setbacks from the road and residential areas of less than 30 meters [88]. Independent Petroleum Marketers are unconcerned about people selling gallon-sized petroleum products in front of their stations. When opposed to those run by individual marketers, conglomerate-owned stations, such as the Nigeria National Petroleum Cooperation (NNPC) Retail Outlets-(State-owned), have stronger safety procedures and orientations.

GIS was used to conduct a location analysis of PFSs in Ilorin, Kwara State, Nigeria. The coordinates of the stations were recorded using a handheld Global Positioning System (GPS) device, and other data were gathered by presenting questionnaires to the owners and workers in each PFSs. During their investigation, they determined that the majority of the stations were near buildings, with 10 (3%) being near a school, 226 (76%) near retailers, 192 (65%) near residential houses, and 11 (4%) being near hospitals [61]. The study reveals that PFSs are overly packed throughout the metropolis, resulting in cluster patterns that pose a major hazard to the town's heavily populated districts and are not constructed in compliance with existing norms. In Malaysia, a similar study was carried out to determine suitable land parcels for the installation of new PFSs [89]. According to them, the Ipoh Mapping and Surveying Department provided the geographic data, while the Ipoh City Planning Department provided the norms used in practice for site selection for PFSs. They prepared a questionnaire to get feedback on the PFSs location choices from stakeholders. During their investigation, they revealed that the vast majority of PFSs failed to meet the specified guidelines for position and distance from residential residences, which served as the foundation for future PFSs construction as shown in Figures 4a and 4b.

4. Conclusions

As a result of the foregoing, it is clear that PFSs are forming in Nigeria without consideration for existing physical planning norms, putting the environment, as well as human and public health, in jeopardy. The majority of inhabitants, unfortunately, were unaware of the health risks associated with the petrol stations' infractions of planning requirements. As a result, the DPR must ensure that planning standards are properly enforced in Nigeria in order to protect public health and encourage healthy urban expansion. The relevant authorities also demand that fuel stations, as well as any other physical developments, be installed throughout the country, as well as public awareness campaigns about the environmental and health risks involved with such developments. These kinds of campaigns can be carried out with the help of the media and collaboration with traditional rulers and local groups.

Recommendation

In light of the study's findings, the following recommendation was made:

i. The law should empower the planning officer (s) to

Figures 4. Showing PFSs close to residential buildings in FCT and Rivers State.

Source: Researchers' Fieldwork, 2021.

investigate all instances of illegal development, as well as plans submitted by non-planners without the planner's permission.

ii. Public participation is important because landowners can band together and say that a facility that is poorly located cannot be built.

iii. A campaign should be initiated to increase awareness among filling station owners and other developers of the dangers of non-compliance with set requirements.

iv. All violators of the established criteria should face open punishment in order for others to learn from their mistakes.

Conflict of Interest

The authors declare no conflict of interest.

References

[1] Steinemann, A.C., 2008. Fragranced consumer products and undisclosed ingredients. Environmental Impact Assessment Review. 29, 32e38.

[2] Ott, M.G., Townsend, J.C., Fishbeck, W.A., et al., 1978. Mortality among workers occupationally exposed to benzene. Archives of Environmental Health. 33, 3e10.

[3] Lynge, E., Andersen, A., Nilsson, R., et al., 1997. Risk of cancer and exposure to gasoline vapors. American Journal of Epidemiology. 145(5), 449-458.

[4] Uren, S., 1997. A pilot study to assess benzene concentrations in the vicinity of petrol stations.

[5] Ohlrogge, K., Wind, J., Hassel, D. (editors), 2000. New technology for emission reduction at petrol stations. Conference Proceedings of the 12th Regional Central European Conference IUAPPA and 4th International Conference on Environmental Impact Assessment. p. 418e425.

[6] Brugnone, F., Perbellini, L., Romeo, L., et al., 1997. Environmental exposure and blood levels of benzene in gas station attendants. Comparison with the general population. Medicinadel Lavoro. 88, 131e147.

[7] Periago, J.F., Prado, C., 2005. Evolution of occupational exposure to environmental levels of aromatic hydrocarbons in service stations. Annals of Occupational Hygiene. 49, 233e240.

[8] Gonzalez-Flesca, N., Vardoulakis, S., Cicolella, A., 2002. BTX concentrations near a stage II implemented petrol station. Environmental Science and Pollution Research. 9, 169-174.

[9] Palmgren, F., Hansen, A.B., Berkowicz, R., et al., 2001. Benzene emission from the actual car fleet in relation to petrol composition in Denmark. Atmospheric Environment. 1, S35eS42.

[10] Srivastava, A., Joseph, A.E., More, A., et al., 2005. Emissions of VOCs at urban petrol retail distribution centers in India (Delhi and Mumbai). Environmental Monitoring and Assessment. 109, 227e242.

[11] Fernández-Villarrenaga, V., López-Mahía, P., Muniategui-Lorenzo, S., et al., 2005. Possible influence of a gas station on volatile organic compounds levels in the ambient air of an urban area. Fresenius Environmental Bulletin. 14, 368e372.

[12] Periago, J.F., Prado, C., 2005. Evolution of occupational exposure to environmental levels of aromatic hydrocarbons in service stations. Annals of Occupational Hygiene. 49(3), 233-240.

[13] Terrés, M., Minarro, D., Ferradas, G., et al., 2010. Assessing the impact of petrol stations on their immediate surroundings. Journal of Environmental Management. 91, 2754-2762.

[14] Patroescu, M., Nita, M.R., Ioja, I.C., et al., 2009. New residential areas in Bucharest metropolitan area location, type and characteristics. 767-772. Available from: https://corp.at/archive/CORP2009_153.pdf

[15] Official Journal of the European Communities. European Parliament and Council Directive 94/63/EC [Internet] [cited 2011 Nov 18]. Available from: http://eur-lex.europa.eu/LexUriServ/LexUriServ.do?uri=OJ:L:1994:365:0024:0033:EN:PDF

[16] Ioja, I.C., Onose, D., Cucu, A., et al., 2010. Changes in water quality in the lakes along Colentina River under the influence of the residential areas in Bucharest. Selected Topics in Energy. Environment, Sustainable Development and Landscaping. 164-169.

[17] DeRoos, A., Davis, S., Colt, S., et al., 2010. Residential proximity to industrial facilities and risk of non-Hodgkinlymphoma. Environmental Research. 110, 70-78.

[18] Ioja, I.C., 2008. Methods for evaluating the quality of the environment in the metropolitan area of Bucharest. University of Bucharest Publishing House: Bucharest.

[19] Joseph, P., Riva, J.R., 2010. The history of the words petroleum industry. New York Publisher: New York.

[20] Timothy, P.M., 2006. Health and environment effect of air pollution. EPA Publications: US. pp. 23-25.

[21] Isabel, M.C., Graciela, A., Monica, R.C., 2010. Evaluating emission from gas stations. Journal of Environmental Management. 6, 42-50.

[22] Amakiri-whyte, B.H., Aselemi, A.E., Akpabio, M.U.A., 2021. Causes and environmental problems of petrol filling stations in residential domain of Nigeria Town. International Journal of Research and

Scientific Innovation. 8(1), 2321-2705.

[23] Ulakpa, R.O.E., Ulakpa, W.C., 2021. A review on the effects of fumes from tricycles (Keke) on health and environment, Nigeria. An International Scientific Journal. 40, 49-64.

[24] Nuhu, G.O., 2019. Geology and mineral resources of Nigeria. Springer: Berlin.
DOI: https://doi.org/10.1007/978-3-540-92685-6

[25] Eyankware, M.O., Igwe, E.O., Ulakpa, R.O.E., 2020. Achieving sustainable use and management of water resources for irrigation in Nigeria: Review. Journal of Environment and Earth Sciences. 2(2), 47-55.

[26] Okonkwo, U.C., Orji, I.N., Onwuamaeze, I., 2014. Environmental impact assessment of petrol and gas filling stations on air quality in Umuahia, Nigeria. 13(1), 12-20.

[27] Mohammed, M.U., Musa, I.J., Jeb, D.N., 2014. GIS-based analysis of the location of filling stations in metropolitan Kano against the physical planning standards. American Journal of Engineering Research. 3(9), 147-158.

[28] Olapeju, O. (editor), 2017. Assessing the location and spatial distribution of petrol filling stations in Ilaro, Ogun State. National Environmental Conference of the School of Environmental Studies, Ilaro.

[29] Iojă, C.I., Tudor, C.A., 2012. Temporal analysis of incompatible land-use and land-cover: the proximity between residential areas and gas stations in Bucharest Suburban Area. Procedia Environmental Sciences. 14, 49-58.

[30] Sulaiman, Y., 2019. Analysis of locational compliance and fire safety preparedness among petrol filling stations in Dutse Town, Jigawa State. Yunus Confluence Journal of Environmental Studies. 13(1), 107-118.

[31] Ulakpa, R.O.E., Iyi E.A., Okwu, V.U.D., et al., 2016. Impact of telecommunication masts on environmental planning in Enugu Urban Area of Enugu State. International Journal of Science and Healthcare Research. 1(1), 1-17.

[32] Olusegun, A., Folakemi, O., Omotayo, S., et al., 2011. Assessment of safety practices in filling stations in Ile-Ife, South Western Nigeria. Journal of Community Medicine and Primary Health Care. 23, 9-15.

[33] Ayodele, S.J., 2011. Spatial Distribution of Petroleum Filling Station in Kaduna North.

[34] Ehinomen, C., Adeleke, A., 2012. An assessment of the distribution of petroleum products in Nigeria. E3 Journal of Business Management and Economics. 3(6), 232-241.

[35] Mshelia, A.M., John, A., Emmanuel, D.D., 2015. Environmental effects of petrol stations at close proximities to residential buildings in Maiduguri and Jere, Borno State, Nigeria. Journal of Humanities and Social Science. 20(4), 1-8.

[36] Arokoyu, S.B., Ogoro, M., Jochebed, O., 2015. Petrol filling stations' location and minimum environmental safety requirements in ObioAkpor LGA, Nigeria. International Journal of Scientific Research and Innovative Technology. 2(11), 19.

[37] Karakitsios, S.P., Delis, V.K., Kassomenos, P.A., et al., 2007. Contribution to ambient benzene concentrations in the vicinity of petrol stations: Estimation of the associated health risk. Atmospheric Environment. 41, 1889e1902.

[38] Afolabi, O.T., 2011. Assessment of safety practices in filling stations in Ile-Ife, South Western Nigeria. Journal of Community Medicine and Primary Health Care. 23(1-2), 9-15.

[39] Ogundahunsi, D.S., 2019. Locational analysis of fuel stations, in Ilesa, Osun State, Nigeria. International Journal of Development Strategies in Humanities, Management and Social Sciences. 4(2), 1-15.

[40] Boison, D.K., Asamoah, H.Y., Addison, L., et al., 2018. Assessing factors influencing sales performance and siting of a fuel station projects: Study of Spintex Road, Accra Ghana. International Journal of Social Science and Humanities Research. 6(4), 1268-1279.

[41] Joan, A., Ismail, W., 2020. Urban spatial risk assessment of fire from fueling stations on buildings case study: Lubaga Division, Kampala City, Uganda. Journal of Building Construction and Planning Research. 8, 57-72.

[42] Ulasi, J.O., Uwadiegwu, B.O., Okoye, C.O., 2020. Assessment of the level of compliance of petroleum filling stations to development control standards on land space/size and setbacks in Anambra State. International Institute for Science, Technology and Education (IISTE): E-Journals. 12(2), 2224-5790.

[43] Dispensing Petrol as a Fuel: Health and Safety Guidance for Employees [Internet] [cited 2014 Mar 20]. Available from: https://www.hse.gov.uk/pubns/indg216.htm

[44] Tatrai, E., Ungavry, G., Cseh, I.R., et al., 1981. The effect of long-term whole body exposure to orthoxylene on liver. Springer-Verlag: Berlin. pp. 161-168.

[45] Zahlsen, K., Nielson, A.M., Eide, I., et al., 1993. Inhalation kinetics of C8 to C10 1-alkenes and iso-alkanes in the rat after repeated exposures. Pharmacology & Toxicology. (73), 163-168.

[46] Onwurah, I.N.E., 1999. Lipid peroxidation and protein oxidation in Azotobactervinelandii exposed to mercury, silver, crude oil and fenton reagent. Journal of Toxic Substances. 18(4), 167-176.

[47] Khan, A.A., Coppock, R.W., Schuler, M.M., et al., 2002. Biochemical changes as early stage systemic biomarkers of petroleum hydrocarbon exposure in human. Toxicolology Letters. 134(1-3), 195-200.

[48] World Health Organization (WHO), 2012. Available from: https://www.who.int/

[49] Nwanjo, H.U., Ojiako, O.A., 2007. Investigating the potential health hazards of the petrol station attendants in Owerri Nigeria. Journal of Applied Science and Environmental Management. 11(2), 1-5.

[50] Oladele, E.A., Michael, A.O., 2021. Health implication on residents close to petrol station in Ife Central, Nigeria. Urban and Regional Planning. 6(2), 79-86. DOI: https://doi.org/10.11648/j.urp.20210602.13

[51] Alam, R., Zafar, A., Ghafoor, A., et al., 2014. Lung function abnormalities among fuel filling workers in Karachi, Pakistan. Pinnacle Environmental and Earth Sciences. 1(1), 183-187.

[52] Wallace, L.A., 1987. The Total Exposure Assessment Methodology (TEAM) Study: Summary and Analysis, Volume I [Internet]. Available from: https://nepis.epa.gov/Exe/ZyNET.exe/2000UC5T.TXT?ZyActionD=ZyDocument&Client=EPA&Index=1986+Thru+1990&Docs=&Query=&Time=&EndTime=&SearchMethod=1&TocRestrict=n&Toc=&TocEntry=&QField=&QFieldYear=&QFieldMonth=&QFieldDay=&IntQFieldOp=0&ExtQFieldOp=0&XmlQuery=&File=D%3A%5Czyfiles%5CIndex%20Data%5C86thru90%5CTxt%5C00000013%5C2000UC5T.txt&User=ANONYMOUS&Password=anonymous&SortMethod=h%7C-&MaximumDocuments=1&FuzzyDegree=0&ImageQuality=r75g8/r75g8/x150y150g16/i425&Display=hpfr&DefSeekPage=x&SearchBack=ZyActionL&Back=ZyActionS&BackDesc=Results%20page&MaximumPages=1&ZyEntry=1&SeekPage=x&ZyPURL

[53] CONCAWE, 1994. Review of European Oil Industry benzene Exposure Data (1986-1992) [Internet]. Available from: https://www.concawe.eu/publication/report-no-794/

[54] Duarte-Davidson, R., Courage, C., Rushton, L., et al., 2001. Benzene in the environment: An assessment of the potential risks to the health of the population. Occupational and Environmental Medicine. 58(1), 2-13.

[55] Esteves, F.A., Pastor, A., Guaria, M., 2007. Assessing air quality inside vehicles and at filling stations by minitoring benzene, toluene, ethylbenzene and xylenes with the use of semipermeable devices. Analytica Chimica Acta. 593(1), 108-116.

[56] Majumdar, D., Dutta, C., Mukherjee, A.K., et al., 2008. Source apportionment of VOCs at the petrol pumps in Kolkata, India; exposure of workers and assessment of associated health risk. Transportation Research Part D: Transport and Environment. 13(8), 524-530.

[57] Karakitsios, S.P., Papaloukas, C.L., Kassomenos, P.A., et al., 2007. Assessment and prediction of exposure to benzene of filling station employees. Atmospheric Environment. 41(40), 9555-9569.

[58] Karakitsios, S.P., Delisa, V.K., Kassomenos P.A., et al., 2007. Contribution to ambient benzene concentrations in the vicinity of petrol stations: Estimation of the associated health risk. Atmospheric Environment. 41(9), 1889-1902.

[59] Terrés, I.M.M., Miñarro, M.D., Ferradas, E.G., et al., 2010. Assessing the impact of petrol stations on their immediate surroundings. Journal of Environmental Management. 91(12), 2754-2762.

[60] Fracasso, M.E., Doria, D., Bartolucci, G.B., et al., 2010. Low air levels of benzene: Correlation between biomarkers of exposure and genotoxic effects. Toxicology Letters. 192(1), 22-28.

[61] Odipe, O., Lawal, A., Adio, Z., et al., 2018. GIS-Based location analyses of retail petrol stations in Ilorin, Kwara State, Nigeria. International Journal of Scientific and Engineering Research. (9), 790-794.

[62] Olanrewaju, S.O., Raheem, W.A., Ola, A.B., et al., 2020. Spatial Distribution and Perceived Environmental Health Impacts of Petrol Filling Stations in Ede, Osun State, Nigeria [Internet]. Available from: https://www.researchgate.net/publication/341464312_SPATIAL_DISTRIBUTION_AND_PERCEIVED_ENVIRONMENTAL_HEALTH_IMPACTS_OF_PETROL_FILLING_STATIONS_IN_EDE_OSUN_STATE_NIGERIA

[63] Aguib, A., Garni, D.A., Smith, S., 2013. Application of Remote Sensing and GIS for Locating Suitable Mangrove Plantation Sites along the Saudi Arabian Red Sea Coast [Internet] [cited 2013 Jan 21]. Available from: http://sfrc.ufl.edu/faculty/ssmith/Sea_Coast.pdf

[64] Ali, Z., Khan, D., Hussain, R., 2012. Adaptation measures in EIA and risks management: An overview of the legal framework in Pakistan. TOJSAT. 2(3), 1-11.

[65] Appiah, D.O., Schröder, D., Forkuo, E.K., et al., 2015. Application of geo-information techniques in land use and land cover change analysis in a peri-ur-

ban district of Ghana. ISPRS International Journal of Geo-Information. 4(3), 1265-1289.

[66] Carrión, J.A., Estrella, A.E., Dols, F.A., et al., 2008. Environmental decision-support systems for evaluating the carrying capacity of land areas: Optimal site selection for grid-connected photovoltaic power plants. Renewable and Sustainable Energy Reviews. 12(9), 2358-2380.

[67] Arumaningrum, D.G., 2021. Environmental Impact Assessment Study Report for the Proposed Maseki Filling Station in Kitui on Plot, L.R. Lincolin Arsyad 2014, 3 [Internet] [cited 2021 Jun 1]. Available from: http://journal.stainkudus.ac.id/index.php/equilibrium/article/view/1268/1127

[68] Matori, A.N., Ulfa Aula, B., 2010. Suitability analysis of petrol filling station site using GIS. Malaysian Construction Research Journal. (70), 1-14.

[69] Choudhury, C., Das, S., 2012. GIS and remote sensing for landfill site selection-A case study on Dharmanagar Nagar Panchayet. Journal of Environmental Science, Toxicology and Food Technology. 1(20), 36-43.

[70] Darko, S., 2015. Ghana Petrol Station Inferno Kills about 150 in Accra-BBC News [Internet] [cited 2015 Jun 1]. Available from: https://www.bbc.com/news/world-africa-33003673

[71] Davoudi Moghaddam, D., Haghizadeh, A., Tahmasebipour, N., et al., 2020. Introducing the coupled stepwise areal constraining and Mahalanobis distance: A promising MCDM-based probabilistic model for landfill site selection. Environmental Science and Pollution Research. 27, 24954-24966.

[72] Boclin, A.D.S.C., de Mello, R., 2006. A decision support method for environmental impact assessment using a fuzzy logic approach. Ecological Economics. 58(1), 170-181.

[73] Deeb, R.A., Hu, H.Y., Hanson, J.R., et al., 2001. Substrate interactions in BTEX and MTBE mixtures by an MTBE-degrading isolate. Environmental Science & Technology. 35(2), 312-317.

[74] Ekanayake, L.L., Ofori, G., 2000. Construction material waste source evaluation. Proceedings: Strategies for a Sustainable Built Environment, Pretoria. 23-25.

[75] International Finance Corporation (IFC), 2007. Environmental, Health, and Safety Guidelines for Cement and Lime Manufacturing [Internet]. Available from: https://www.ifc.org/wps/wcm/connect/topics_ext_content/ifc_external_corporate_site/sustainability-at-ifc/policies-standards/ehs-guidelines

[76] Ghayoumian, J., Saravi, M.M., Feiznia, S., et al., 2007. Application of GIS techniques to determine areas most suitable for artificial groundwater recharge in a coastal aquifer in southern Iran. Journal of Asian Earth Sciences. 30(2), 364-374.

[77] Hassanain, M.A., Al-Mudhei, A., 2006. Fire safety evaluation of motor fuel dispensing facilities. Structural Survey. 24(1), 65-76.

[78] Kirby, R.S., 2003. GIS and public health. Annals of the American Association of Geographers. (93), 261-263.

[79] Malczewski, J., 2006. GIS-based multicriteria decision analysis: A survey of the literature. International Journal of Geographical Information Science. 20(7), 703-726.

[80] Hangula, L.M., Shagama, F.N., 2020. Environmental Impact Assessment for the Establishment and Operation of a Proposed Fuel Service StationProject at Omutshona Filling Station, Okatana, Oshana Region [Internet]. Available from: http://the-eis.com/elibrary/sites/default/files/downloads/literature/1283_EIA_Construction%20and%20operation%20of%20a%20fuel%20service%20station%20by%20Omushona%20Trading.pdf

[81] Pedersen, K., Przychodzka, M., Civiš, M., et al., 2003. Environmental impact assessment of petrol usage [Bachelor's thesis]. Aarhus, Denmark: Aarhus University.

[82] Mohammed, M.U., Musa, I.J., Jeb, D.N., 2014. GIS-based analysis of the location of filling stations in metropolitan Kano against the physical planning standards. American Journal of Engineering Research. 3(9), 147-158.

[83] Mulroy, P. (editor), 2012. Environmental site investigation and due diligence in current market. Proceedings of the Environmental APEA Petroleum Seminar, Cork, Ireland.

[84] Mundjulu, I., 2020. Environmental Scoping Report (ESR) for a Fuel Storage Facility [Internet]. Tortoise Environmental Consultants. Available from: http://the-eis.com/elibrary/sites/default/files/downloads/literature/1941_ESR_Construction%20and%20operation%20of%20a%20Diesel%20Depot%20on%20Erf%20163_Lafrenz_Windhoek.pdf

[85] Mwania, L.M., Kitengela, K., 2013. Proposed Construction of a Filling Station on Plot No.Makindu/Kiboko B/687 Makindu [Internet]. Available from: https://docplayer.net/45711982-Proposed-construction-of-a-filling-station-on-plot-no-makindu-kiboko-b-687-makindu-makueni-county.html

[86] Njoku, C.G., Alagbe, A.O., 2015. Site suitability assessment of petrol filling stations (PFSs) in Oyo Town, Oyo State, Nigeria: A geographic information

systems (GIS) approach. ISOR Journal of Environmental Science, Technology and food Technology (IOSR-JESTFT). (9), 8-19.

[87] O'Faircheallaigh, C., 2010. Public participation and environmental impact assessment: Purposes, implications, and lessons for public policy making. Environmental Impact Assessment Review. 30(1), 19-27.

[88] Ahmed, S., AbdulRahman, A.S., Kovo, A.S., et al., 2014. Health, risk and safety of petrol stations in Minna town: An overview. World Applied Sciences Journal. 32(4), 655-660. Available from: https://staff.futminna.edu.ng/MME/content/journal/PF1380/11.pdf

[89] Gonzalez-Flesca, N., Vardoulakis, S., Cicolella, A., 2002. BTX concentrations near a stage II implemented petrol station. Environmental Science and Pollution Research. 9, 169-174.

BILINGUAL PUBLISHING CO.
Pioneer of Global Academics Since 1984

Journal of Environmental & Earth Sciences
https://ojs.bilpublishing.com/index.php/jees

ARTICLE

Metamorphic Evolution of the Amphibolites from Bundelkhand Craton, Central India: *P-T* Constraints and Phase Equilibrium Modelling

Pratigya Pathak* **Shyam Bihari Dwivedi** **Ravi Ranjan Kumar**

Department of Civil Engineering, Indian Institute of Technology (BHU), Varanasi, India

ARTICLE INFO

Article history
Received: 24 January 2022
Accepted: 17 March 2022
Published Online: 6 April 2022

Keywords:
Bundelkhand craton
Amphibolite
P-T pseudosection
Subduction setting

ABSTRACT

The amphibolites from the Mauranipur and Babina regions are located in the central part of the Bundelkhand Craton (BuC), northern India. During the geodynamic evolution of the BuC, these amphibolites underwent medium-grade metamorphism. This study combines textural observations of amphibolites from two distinct regions (Mauranipur and Babina) with mineral chemistry and phase equilibrium modelling. Observations suggest that the amphibolites of both areas have gone through three stages of metamorphism. The pre-peak stage in the amphibolites from the Mauranipur and Babina regions is marked by the assemblages Ep-Amp-Cpx-Pl-Ilm-Ru-Qz and Ep-Amp-Cpx-Pl-Ab-Ilm-Qz respectively; the peak metamorphic stage is characterized by the mineral assemblages Amp-Cpx-Pl-Ilm-Ru-Qz and Amp-Cpx-Pl-Ilm-Qz-H_2O, which is formed during the burial process, and the post-peak stage is represented by the assemblages Amp-Pl-Ilm-Ru-Qz and Amp-Pl-Ilm-Qz-H_2O respectively, which is formed by exhumation event. By applying the phase equilibria modelling in the NCFMASHTO system, the *P-T* conditions estimated from pre-peak, peak to post-peak stages are characterized as 6.7 kbar/510 °C, 7.3 kbar/578 ºC and > 3.0 kbar/> 585 ºC, respectively, for the Mauranipur amphibolites; and 6.27 kbar/520 ºC, 5.2 kbar/805 ºC and > 3.0 kbar/> 640 ºC respectively for Babina amphibolites. The textural association and *P-T* conditions of both amphibolites suggest that these rocks were affected by burial metamorphism followed by an exhumation process during subduction tectonism in the BuC.

1. Introduction

Continental crust formation began in the Hadean ages (4.4 Ga-4.0 Ga), as reported by the Acasta gneisses of northwestern Canada [1-3]. However, the current continental crust was developed through multiple mechanisms and stages before 2.5 Ga [4-6]. The Archean cratons have been well-known for their ability to provide insight into Earth's earlier crustal history. These Archean cratons contain a

*Corresponding Author:
Pratigya Pathak,
Department of Civil Engineering, Indian Institute of Technology (BHU), Varanasi, India;
Email: pratigyapathak.rs.civ17@itbhu.ac.in

DOI: https://doi.org/10.30564/jees.v4i1.4397

variety of igneous rocks that exhibit structural indicators, as well as supracrustal rocks such as amphibolites, tonalite-trondhjemite-granodiorite gneisses (TTGs), and banded iron formations (BIFs) displaying various metamorphic stages [7]. Supracrustal rocks contributed significantly to the formation of microcontinents, supercontinents, continental evolution, and the stabilization of continents [8-10]. As a result, the metamorphic study of supracrustal rocks is tremendously beneficial and required for a better understanding of geodynamic evolution and stabilization of cratons and continental crust.

The Bundelkhand Craton (BuC) is located in the northern Indian Shield and is also the best example of an Archean craton for studying supracrustal rocks because it contains a record of geological events from the Archean (3.5 Ga-2.7 Ga; TTGs and gneisses) to the Paleoproterozoic (2.5 Ga-2.4 Ga; granitoid pulses) periods [11-13]. Despite that, the BuC experienced various metamorphic events, and it preserves medium to high-grade metamorphism in multiple rock types. *P-T* conditions of 5.4 kbar/730 °C and 6.2 kbar/720 °C have been reported from the Mauranipur metapelites [14,15]. Similarly, high-grade hornblende-biotite-plagioclase bearing gneisses of *P-T* = 6.5-8.5 kbar/630-720 °C has been reported in the Sukwan (Babina) area [16]. High to ultrahigh-pressure metamorphism is reported in chlorite-phlogopite-corundum schists with *P-T* condition as 11 kbar/630 °C and 18 kbar/630 °C respectively, from the Babina region [11]. The garnet-bearing BIF from the Mauranipur region reveals a peak temperature of ~500 °C at 0.1 GPa-0.2 GPa, suggesting lower amphibolite facies [17]. The peak metamorphic condition of garnet-biotite gneiss has been revealed as 6.35-6.75 kbar/755-780 ºC [18]. Several authors concluded that the mafic and ultramafic rocks of the BuC underwent greenschist to amphibolite facies metamorphism based on textural and mineralogical observations [19,20]. Field investigations imply that amphibolites are connected with multiple metamorphic Archean terrains, and hence, understanding the geological history of that terrain requires a complete understanding of amphibolites. Amphibolites have been reported from various cratons in the Indian shield. Amphibolites (hornblende-garnet-epidote-glaucophane-augite-chlorite) have been reported from the Nagaland Ophiolite Complex, with *P-T* conditions of 13.8 kbar-12.6 kbar and 625 °C-645 °C [21]. However, low-pressure amphibolites (amphibole-plagioclase-biotite-quartz-garnet-chlorite-epidote-magnetite) have also been delineated from the Western Dharwar Craton with *P-T* conditions of 5 kbar/600 °C [22].

One of the most contentious and exciting issues in metamorphic petrology has always been the origin of amphibolites. These rocks have a variety of origins and have been determined to be the most difficult in nature, as well as playing a significant role in revealing the history of Archean terrain crustal evolution [23]. Amphibolites are thought to be formed from igneous rocks of basic and tholeiitic magma that represent pieces of earlier oceanic crust. Amphibolites can also be produced by metasomatism of calcareous sediments [24]; some amphibolites can be formed from pre-existing rocks that have undergone a succession of mineral and chemical transformations as a result of metamorphism [21]. Most researchers believe that three processes, namely meta-igneous, meta-sedimentary, and metasomatism, are the most valid mechanisms for the production of amphibolites [25]. However, multiple mechanisms have been reported to give rise to amphibolites hence predicting the origin of different amphibolites is the most debated and intriguing subject in metamorphic petrology.

To better understand the metamorphic development of amphibolites from the BuC, we used petrographical study, mineral chemistry of numerous minerals, and phase equilibria modelling of amphibolites from the Mauranipur and Babina regions. The field evidence of amphibolites and textural relationship of existing minerals are explained in this study, as well as pseudosection modelling is used to create the *P-T* trajectory paths.

2. Geological Backgrounds

The Indian shield comprises two cratonic blocks, namely the northern cratonic block consisting of Aravalli and Bundelkhand cratons, and the southern cratonic block, which includes Dharwar, Bastar, and Singhbhum cratons [26] (Figure 1a). The BuC has a semi-circular shape and is located in the north-central section of the Indian subcontinent covering a 30,000 km^2 area [27]. It is separated from the southern cratonic block by the Central Indian Tectonic Zone (CITZ) [9]. The BuC is separated from the Aravalli Craton by the NE-SW trending Great Boundary Fault (GBF) and from the Himalaya by the Yamuna Fault. The BuC is covered by Indo-Gangetic alluvium in the north, by Vindhyan rocks in the east as well as south, and by Deccan basalts in the southwest [28] (Figure 1b). The Paleoproterozoic (2.0 Ga-1.8 Ga) peripheral sedimentary basins of Gwalior, Sonrai, and Bijawar border the BuC from the northwest, south, and southeast, respectively [29]. These basins are homotaxial, with clastic sedimentary rocks at the bottom and carbonate with banded iron formations (BIFs) at the top [30].

The BuC was primarily created throughout the Paleoarchean to Neoarchean periods, with the multistage crustal formation. The BuC is divided into two crustal segments

by an E-W trending Bundelkhand Tectonic Zone (BTZ) that runs roughly 200 kilometres from Mahoba to Babina (Figure 1b). The first segment is the central domain, known as the central Bundelkhand greenstone terrane (CBGT), and the second is the southern domain, known as the southern Bundelkhand greenstone terrane (SBGT) [30]. NW-SE trending mafic dykes of Proterozoic age (~1.98 Ga, 1.8 Ga, and 1.0 Ga) and NE-SW trending quartz veins of Palaeoproterozoic age (1.9 Ga-1.8 Ga) dissect the whole BuC.

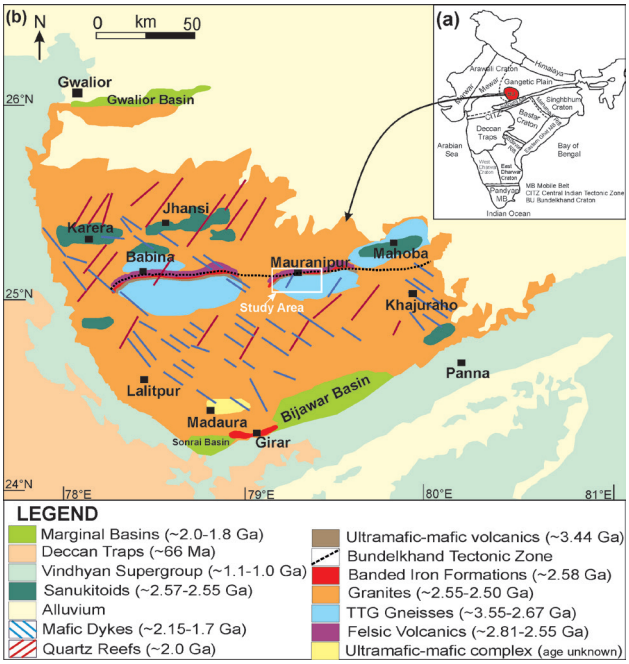

Figure 1. (a) Inset map showing the location of the Bundelkhand Craton in India. (b) The geological map shows different lithological units and tectonic elements of the Bundelkhand Craton [30].

The CBGT is mainly dominated by Tonalite-Trondhjemite-Granodiorite (TTG) gneisses of Mesoarchean age, greenstones of Neoarchean age, intrusive granites, quartz reefs, mafic dykes, BIFs, and metabasites [16,31]. The CBGT, mostly exposed in the Babina and Mauranipur regions, contains metamorphosed mafic rocks of the Paleo-Mesoarchean period [28], felsic volcanic rocks of the Mesoarchean period [32] and metasedimentary rocks (BIFs). Ultramafic-mafic volcanic rocks from the Babina and Mauranipur regions have been emplaced during the Paleoarchean age (3.44 Ga) [31]. This volcanism is likely to have occurred after the emplacement of TTGs (3.55 Ga-3.20 Ga) in a subduction scenario from a depleted mantle source. Pink granites and granodiorites (2.58 Ga-2.52 Ga) cross this belt in various directions, indicating an intrusive link with CBGT rocks [33]. According to available geochronological data [34], the CBGT has been formed during three stages of volcanic activity. Early felsic volcanic activity occurred in the Mauranipur region around 2.82 Ga, implying Mesoarchean subduction tectonics [34]. At 2.54 Ga, a new period of volcanic activity was identified in the Babina region [34], whereas the third stage has culminated during ~2.5 Ga by the accretion of massive continental chunks [31].

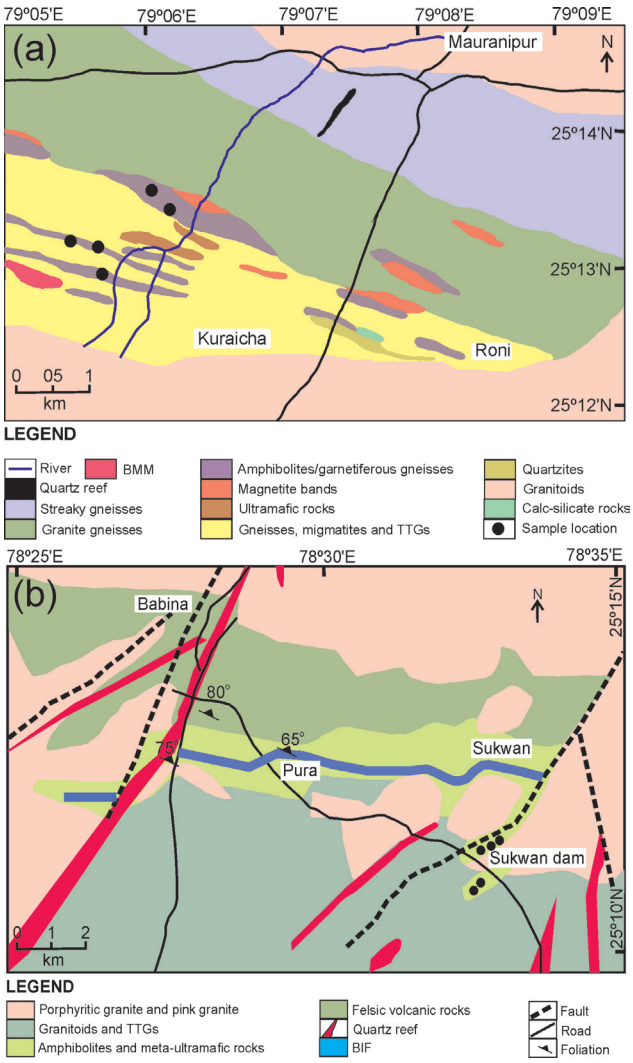

Figure 2. (a) Local geological map of the study area around Mauranipur region [19]. (b) Local geological map around the Babina region, elucidating various geological occurrences [47].

3. Field and Megascopic Description

The amphibolite samples were collected from a variety of locations in the Babina and Mauranipur regions. Amphibolites were exposed in the Mauranipur (Lattitude 25º11'54" N to 25º14'48" N, Longitude 79º05' S to 79º09'35" S; Figure 2a) as well as in the Babina region (Lattitude 25º09'45" N to 25º15' N, Longitude 78º25' S to 78º35'S; Figure 2b). Amphibolites are found as enclaves

within TTG gneisses and felsic granitoid (Figure 3a), but they have also been seen as intrusive dykes in TTG gneisses in the Mauranipur and Babina regions (Figure 3b). Amphibolites have been found associated with a variety of rock types, including BIF, calc-silicate rocks, white schists, quartzites, and metapelites. Mauranipur amphibolites are found with garnetiferrous gneisses, whereas Babina amphibolites are associated with meta-ultramafic rocks. Amphibolites from both sites have a nematogranoblastic texture that overwrites all previous textures and structures [32]. The amphibolites are primarily dark in colour and reveal a fractured nature in several areas of the research field (Figure 3b). Amphibolites from the Mauranipur region show a massive emplacement of felsic magmatism (Figure 3c) with folded and distorted structures (Figure 3d). Babina amphibolites (near the Sukwa-Dukwa dam) resemble Mauranipur amphibolites in appearance and are likewise intruded by felsic magma (Figure 3e,f).

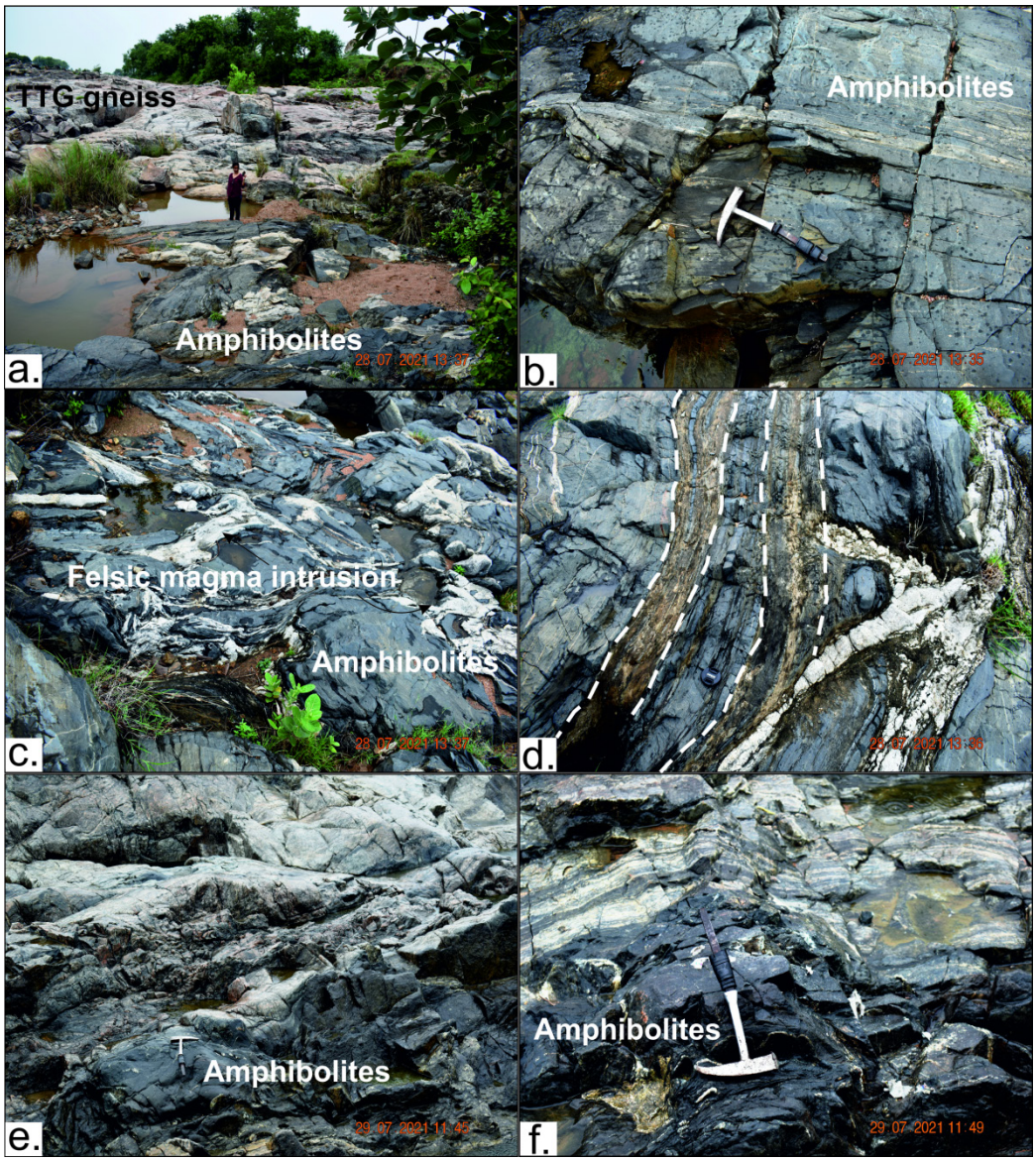

Figure 3. Field photographs of the amphibolites from the study area (a) Amphibolites exposed along with TTG gneisses in Mauranipur, (b) Small scale field photograph of amphibolites along with deformational features in Mauranipur, (c) Felsic magma intrusion in amphibolites of Mauranipur (d) Folding in the layers of amphibolites of Mauranipur (e,f) Amphibolites of Babina (near Sukwa-dukwa dam) intruded by felsic magma.

4. Petrography

The principal minerals in amphibolites from both regions are amphibole, clinopyroxene, and plagioclase, with K-feldspar, epidote, quartz, and opaque minerals (rutile, ilmenite, and magnetite) occurring as accessory phases. Table 1 shows the mineral assemblages and modal abundances of various amphibolite samples from the Mauranipur and Babina regions. The mineral assemblages' paragenesis is as follows:

a. Amphibole-clinopyroxene-plagioclase-rutile-epidote-ilmenite-quartz

b. Amphibole-clinopyroxene-plagioclase-albite-epidote-ilmenite-quartz

c. Amphibole-clinopyroxene-plagioclase-rutile-ilmenite-quartz

d. Amphibole-clinopyroxene-plagioclase-ilmenite-quartz

e. Amphibole-plagioclase-rutile-ilmenite-quartz

f. Amphibole-plagioclase-ilmenite-quartz

The petrographical investigation of amphibolites from both samples MM-1 and BB-1 has revealed three different modes of occurrence of amphiboles. These all three amphiboles have characteristics features and textural association, which are depicted in the following way; the inclusion-type amphibole (Amp1) enclosed in clinopyroxene, the porphyroblastic amphibole (Amp2) associated with clinopyroxene crystals, and the retrograde amphibole (Amp3) replacing clinopyroxene crystal. The first-generation amphibole (Amp1) is light brown to green color and occurs as inclusions within porphyroblast clinopyroxene, intergrown with plagioclase, a textural feature indicating that Amp1 is a result of the prograde metamorphism (Figure 4a,b). Porphyroblastic and subhedral grains of amphiboles are considered as the second generation of amphiboles (Amp2), closely associated with clinopyroxene porphyroblast; and textural features suggest that it would be a product of peak metamorphism (Figure 4c,d). The Amp2 has a green color and contains inclusions of discrete plagioclase, quartz, and ilmenite, representing sieve texture. Amphibole crystals are mainly medium to coarse-grained in nature as well as subhedral to anhedral in shape depicting two sets of cleavage, present with porphyroblasts of clinopyroxene (Figure 4c). Green to grey clinopyroxene up to 1 cm in length, intergrown with plagioclase, displays an ophitic texture (Figure 4d). The textural relationship of amphibole replacing clinopyroxene suggests retrograde metamorphism (Figure 4e,f). This petrographical evidence indicates that the third generation of amphibole (Amp3) is preserved in the studied amphibolites. Plagioclase is an essential mineral in amphibolites, and it records essential metamorphic information. The plagioclase is fine to medium-grained 0.1 mm-0.2 mm in size and anhedral shape and is characterized by colorless prismatic crystals and first-order grey color. In spite of the presence of the plagioclase as inclusion within clinopyroxene and amphibole, it also occurs as the dominant phase of the matrix (Figure 4g). Epidotes occur as < 50 µm rounded subhedral crystals associated with amphibole and plagioclase but mostly appeared as inclusion within amphibole and clinopyroxene crystals (Figure 4a,b). Plagioclase can also be found as an inclusion inside the amphibole and clinopyroxene matrix (Figure 4h). At the confluence of amphibole and plagioclase, Figure 4i displays a lengthy lath of ilmenite.

Table 1. Summary of approximate modal composition (in percentage) of the Amphibolites of Mauranipur (MM-1, MM-2, MM-3, MM-4, MM-5) and Babina (BB-1, BB-2, BB-3, BB-4, BB-5) samples observed under a petrological microscope through Lieca Qwin software.

Sample	Model %						
	Amp	Cpx	Pl	Kfs	Ep	Qz	Opq
MM-1	52	30	6	1	4	1	6
MM-2	49	32	8	-	3	2	6
MM-3	53	27	5	2	4	1	8
MM-4	50	33	7	1	4	1	4
MM-5	55	21	10	1	5	1	7
BB-1	48	33	8	2	3	1	5
BB-2	52	24	11	-	3	2	8
BB-3	51	29	9	1	5	1	4
BB-4	53	35	5	1	2	1	3
BB-5	54	31	9	1	2	1	2

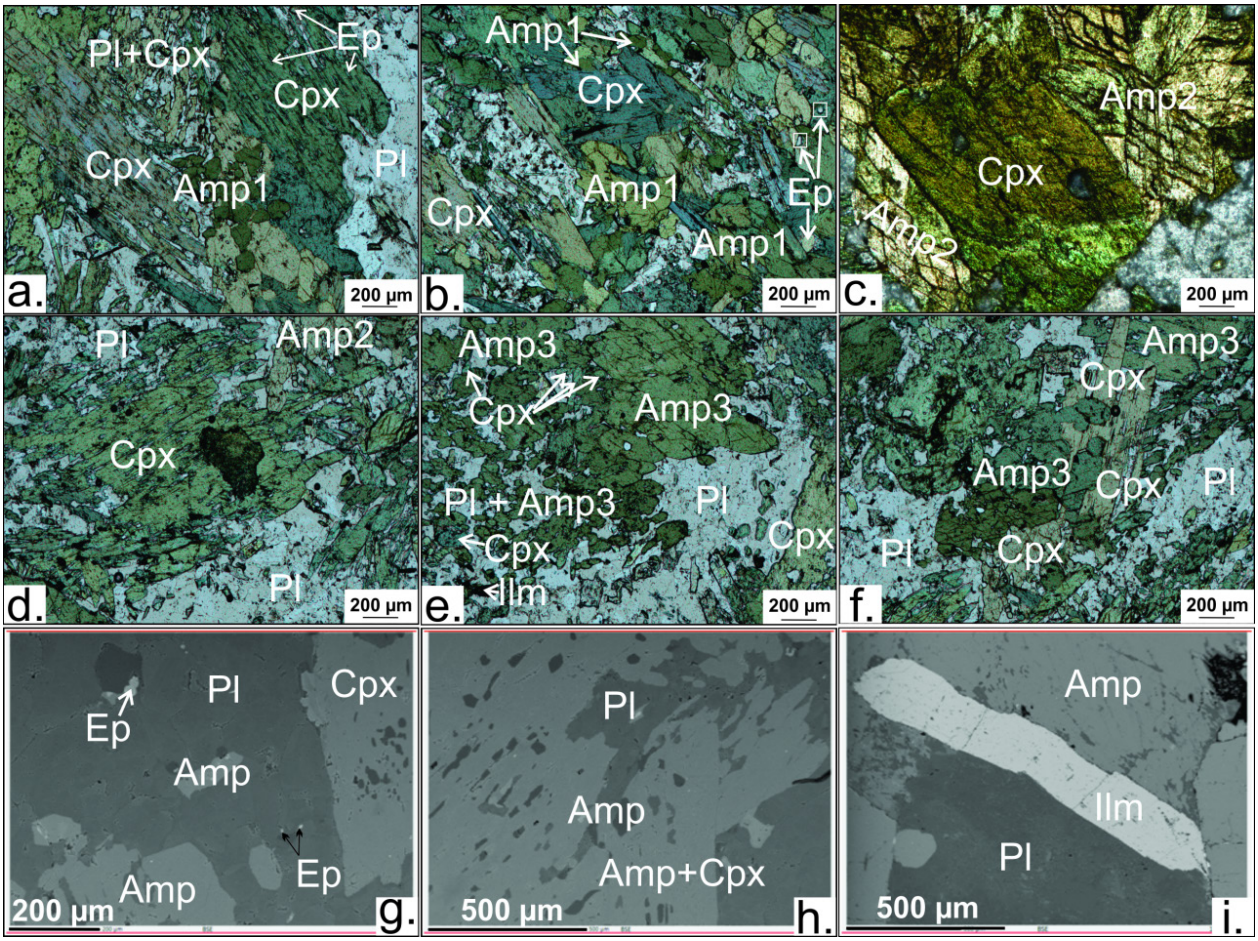

Figure 4. Photomicrographs (plane-polarized light, PPL) and back-scattered electron (BSE) images of the amphibolites (MM-1 and BB-1): (a & b) First generation Amp1 and Ep present as inclusions in Cpx with Pl, (c) Prismatic crystals Amp2 depicting two sets of cleavage with porphyroblastic Cpx, (d) Laths of Pl embedded within Cpx crystals depicting ophitic texture, (e) Third generation Amp3 contains inclusions of Cpx, (f) Cpx crystals partially replaced by third-generation Amp3, (g) Ep crystals occurring as inclusions within Amp and Pl, (h) Pl present as inclusion within the matrix of Amp and Cpx, (i) Long lath shaped grain of Ilm at a junction of Amp and Pl. Mineral abbreviations are taken from Whitney and Evans [49].

5. Mineral Chemistry

5.1 Analytical Method

Based on petrological interpretations, two amphibolite samples, namely MM-1 (from Mauranipur) and BB-1 (from Babina), were selected for the electron microprobe analysis (EPMA). The mineral chemical analysis was carried out using the EPMA (CAMECA SX five EPMA) at the Department of Geology, Banaras Hindu University, Varanasi, India, under operating conditions of 15 kV and the current 10 nA.

5.2 Amphibole

All the analysed amphiboles (sample MM-1 and BB-1) have (Na + K) < 0.50, Ti < 0.5, CaB > 1.5 pfu. Furthermore, according to Leak's, classification [35], these are Ca-amphibole groups in composition. When the analyzed amphiboles are plotted on the leaks classification diagram, they all occupy the tschermakite and Mgnesio-hornblende domains (Figure 5a). All the analyzed amphiboles (sample MM-1 and BB-1) based on 23 oxygens are presented in Table 2. Amp1 has a value of 0.75 for X_{Mg} [Mg/(Fe^{2+}+Mg)], Amp2 has a value of 0.78-0.79, and Amp3 has a value of 0.71-0.72 for the sample MM-1. The X_{Ca} values range from 0.31-0.33 for the amphiboles of MM-1. The sample BB-1 also includes three types of amphibole, compositionally distinct, and their X_{Mg} values are 0.71-0.74 for Amp1, 0.79-0.82 for Amp2 and 0.68-0.69 for Amp3.

Table 2. EPMA (wt%) and structural formula of amphibole, from the Amphibolites of Mauranipur and Babina (Sample MM-1 and BB-1).

Sample	**MM-1**						**BB-1**					
Domain	5/1	6/1	7/1	8/1	22/1	25/1	43/1	45/1	46/1	47/1	50/1	52/1
Position	Amp1		Amp2		Amp3		Amp1		Amp2		Amp3	
SiO_2	43.40	43.56	43.62	43.66	44.68	44.27	43.96	43.72	44.81	43.66	44.32	45.30
TiO_2	0.41	0.39	0.42	0.50	0.43	0.42	0.48	0.35	0.40	0.43	0.44	0.41
Al_2O_3	14.22	14.32	14.87	13.41	12.94	13.61	13.10	14.83	12.20	16.08	14.62	13.50
FeO	12.11	12.14	11.95	14.21	12.41	13.03	13.77	12.13	13.50	11.58	13.65	13.28
MnO	0.26	0.10	0.06	0.18	0.23	0.33	0.16	0.18	0.10	0.11	0.16	0.24
MgO	11.89	12.13	12.57	12.30	11.99	11.55	11.81	11.83	12.93	12.33	11.12	11.41
CaO	11.65	11.68	11.92	11.64	11.69	11.26	11.98	11.84	11.74	11.44	11.80	11.34
Na_2O	1.38	1.59	1.33	1.62	1.49	1.69	1.35	1.29	1.39	1.50	1.37	1.66
K_2O	0.18	0.17	0.20	0.18	0.21	0.18	0.25	0.21	0.17	0.19	0.23	0.20
Total	95.49	96.07	96.93	97.69	96.06	96.34	97.56	97.12	97.24	97.32	97.70	97.35
23 oxygens												
Si	6.37	6.36	6.28	6.29	6.55	6.46	6.42	6.36	6.46	6.23	6.40	6.56
Al^{IV}	1.63	1.64	1.72	1.71	1.45	1.54	1.58	1.64	1.54	1.77	1.60	1.44
Al^{VI}	0.83	0.82	0.81	0.57	0.78	0.81	0.67	0.90	0.54	0.94	0.89	0.86
Ti	0.05	0.04	0.05	0.05	0.05	0.05	0.05	0.04	0.04	0.05	0.05	0.05
Fe^{3+}	0.61	0.59	0.73	0.95	0.44	0.60	0.62	0.58	0.87	0.79	0.53	0.48
Fe^{2+}	0.87	0.89	0.71	0.76	1.08	0.99	1.06	0.90	0.76	0.59	1.11	1.13
Mn	0.03	0.01	0.01	0.02	0.03	0.04	0.02	0.02	0.01	0.01	0.02	0.03
Mg	2.60	2.64	2.70	2.64	2.62	2.52	2.57	2.57	2.78	2.62	2.39	2.46
Ca	1.83	1.83	1.84	1.80	1.84	1.76	1.88	1.84	1.81	1.75	1.83	1.76
Na	0.39	0.45	0.37	0.45	0.42	0.48	0.38	0.36	0.39	0.41	0.38	0.47
K	0.03	0.03	0.04	0.03	0.04	0.03	0.05	0.04	0.03	0.03	0.04	0.04
X_{Mg}	0.75	0.75	0.79	0.78	0.71	0.72	0.71	0.74	0.79	0.82	0.68	0.69

$X_{Mg} = Mg/(Fe^{2+} + Mg)$

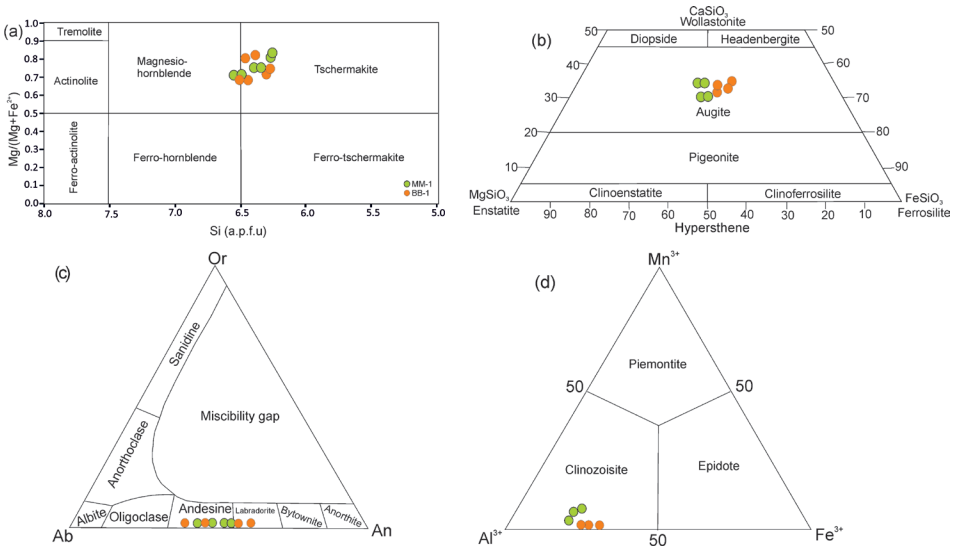

Figure 5. (a) Plots of the analyzed amphiboles obtained from the amphibolites of Mauranipur and Babina on classification diagram [35], (b) Pyroxene classification diagram showing the augite nature of the clinopyroxenes, from both amphibolites [36], (c) Plots of the orthoclase-albite-anorthite ternary diagram, showing andesine and labradoritic nature, (d) Plots of the ternary epidote diagram [37].

Table 3. EPMA (wt%) and structural formula of clinopyroxenes, from the Amphibolites of Mauranipur and Babina (Sample MM-1 and BB-1).

Sample	**MM-1**				**BB-1**			
Domain	11/1	12/1	13/1	14/1	23/1	44/1	45/1	88/1
SiO_2	49.22	49.55	48.89	47.45	48.25	48.74	47.24	48.56
TiO_2	0.14	0.12	0.16	0.1	0.10	0.15	0.18	0.16
Al_2O_3	0.49	0.55	0.77	0.5	0.60	0.99	0.55	0.47
Cr_2O_3	0.09	0.08	0.08	0.1	0.10	0.07	0.02	0.01
FeO	23.79	21.2	23.26	21.34	22.30	23.15	24.16	22.78
MnO	0.22	0.33	0.23	0.24	0.30	0.23	0.45	0.34
MgO	8.12	10.11	8.29	11.43	9.92	8.45	8.79	9.22
CaO	17.22	17.65	17.66	18.52	17.56	17.56	18.22	18.05
Na_2O	0.12	0.13	0.11	0.02	0.10	0.1	0.01	0.12
K_2O	0	0.02	0.01	0	0.00	0.01	0.02	0.01
Total	99.41	99.74	99.46	99.7	99.23	99.45	99.64	99.72
6 oxygens								
Si	1.96	1.95	1.95	1.89	1.92	1.94	1.90	1.93
Al	0.02	0.03	0.04	0.02	0.03	0.05	0.03	0.02
Cr	0.00	0.00	0.00	0.00	0.00	0.00	0.00	0.00
Ti	0.00	0.00	0.00	0.00	0.00	0.00	0.01	0.00
Fe^{3+}	0.07	0.11	0.09	0.29	0.18	0.10	0.23	0.17
Fe^{2+}	0.72	0.58	0.68	0.40	0.55	0.67	0.56	0.58
Mn	0.01	0.01	0.01	0.01	0.01	0.01	0.02	0.01
Mg	0.48	0.59	0.49	0.68	0.59	0.50	0.53	0.55
Ca	0.74	0.74	0.75	0.79	0.75	0.75	0.79	0.77
Na	0.01	0.01	0.01	0.00	0.01	0.01	0.00	0.01
K	0.00	0.00	0.00	0.00	0.00	0.00	0.00	0.00
X_{Mg}	0.40	0.51	0.42	0.63	0.52	0.43	0.48	0.48

$X_{Mg} = Mg/(Fe^{2+}+ Mg)$

5.3 Clinopyroxene

All the analyzed clinopyroxenes (sample MM-1 and BB-1) based on 6 oxygens are presented in Table 3. The calculated X_{Mg} value of clinopyroxene from amphibolites of the study area ranges from 0.40-0.63 (samples MM-1) and 0.43-0.52 (sample BB-1). The triangular plot [36] for the pyroxene end member shows clinopyroxenes from both sample plots in the augite composition field (Figure 5b). The Ca content of clinopyroxene ranged from 0.74 pfu to 0.79 pfu for sample MM-1 and from 0.75-0.77 pfu for sample BB-1, providing evidence of the high Ca content of clinopyroxene.

5.4 Plagioclase

Plagioclase in samples MM-1 and BB-1 has a wide range in anorthite content (Table 4). Plagioclases from both samples are dominated by anorthite and albite, with minor orthoclase. However, the plagioclase of sample MM-1 (An = 42.92 mol%-44.49 mol%, Ab = 55.06 mol%-56.67 mol%) has less content in anorthite and higher content in albite in comparison to sample BB-1, which has (An = 41.50 mol%-56.09 mol%, Ab = 43.55 mol%-58.32 mol%). Feldspar in both samples contains a small amount of total iron in the form of FeO (up to 0.47 in sample MM-1 and 0.16 in sample BB-1). The triangular plot for plagioclase end-members show that plagioclase is plotted in the andesine and labradorite composition fields from both samples (Figure 5c).

5.5 Other Minerals

Representative chemical compositions of the analyzed epidotes based on 25 oxygens for both the samples (MM-1 and BB-1) are listed in Table 5. As an inclusion within amphibole and clinopyroxene, epidote is present in both amphibolites (MM-1 and BB-1). Subtle variations are observed in the chemical composition of epidotes from both samples. The values of X_{Al} [X_{Al}= $Al/(Al+Fe^{3+})$] for

both representatives range from 0.84 to 0.85. All epidotes belong to the clinozoisite-epidote-piemontite series, and the triangular plot [37] (Figure 5d) shows that epidotes from both samples are dominated by clinozoisite composition (83.53 mol%-84.59 mol%) for sample MM-1, whereas it is 83.39 mol%-84.97 mol% for sample BB-1. Ilmenite reveals that TiO_2 content ranges between 49.87 wt%-50.15 wt% in sample MM-1 and 45.00 wt%-45.46 wt% in sample BB-1 (Table 6). Ilmenite minerals did not show zoning as analyses on different points on the same grain showed almost identical values supported by BSE images (Figure 4i).

Table 4. EPMA (wt%) and structural formula of plagioclase from Amphibolites (MM-1 and BB-1).

Sample	**MM-1**				**BB-1**			
Domain	37/1	38/1	39/1	40/1	144/1	142/1	149/1	150/1
SiO_2	56.53	56.13	56.24	55.38	55.08	54.38	55.39	56.82
Al_2O_3	25.17	27.24	27.31	27.38	27.58	27.78	26.70	25.69
FeO	0.47	0.00	0.00	0.00	0.00	0.00	0.13	0.16
CaO	9.92	9.58	9.24	9.87	11.41	12.10	9.44	9.82
Na_2O	6.92	6.65	6.74	6.75	5.53	5.19	7.33	6.47
K_2O	0.06	0.04	0.07	0.08	0.02	0.06	0.03	0.02
Total	99.07	99.63	99.60	99.47	99.61	99.52	99.03	98.98
8 Oxygens								
Si	2.58	2.53	2.54	2.51	2.50	2.47	2.53	2.58
Al	1.35	1.45	1.45	1.46	1.47	1.49	1.44	1.38
Fe^{2+}	0.02	0.00	0.00	0.00	0.00	0.00	0.00	0.01
Ca	0.48	0.46	0.45	0.48	0.55	0.59	0.46	0.48
Na	0.61	0.58	0.59	0.59	0.49	0.46	0.65	0.57
K	0.00	0.00	0.00	0.00	0.00	0.00	0.00	0.00
Total	5.05	5.03	5.03	5.05	5.01	5.01	5.08	5.01
An	44.06	44.24	42.92	44.49	53.21	56.09	41.50	45.54
Ab	55.63	55.56	56.67	55.06	46.67	43.55	58.32	54.36
Or	0.32	0.20	0.41	0.45	0.12	0.35	0.18	0.09

Table 5. EPMA (wt%) and structural formula of epidote, from the Amphibolites of Mauranipur and Babina (Sample MM-1 and BB-1).

Sample no.	**MM-1**			**BB-1**		
Domain	45/1	46/1	47/1	48/1	49/1	54/1
SiO_2	35.04	36.44	35.37	36.30	36.54	36.52
TiO_2	0.09	0.10	0.11	0.12	0.10	0.03
Al_2O_3	23.52	23.73	24.47	23.69	23.36	24.13
Fe_2O_3	13.89	13.90	13.74	12.85	14.11	13.20
MnO	0.28	0.15	0.10	0.12	0.21	0.11
CaO	23.31	22.47	22.55	23.05	22.77	23.11
Total	96.42	96.80	96.35	96.13	97.10	97.12
25 oxygens						
Si	6.14	6.31	6.16	6.29	6.33	6.27
Al	4.86	4.84	5.021	4.84	4.77	4.88
Ti	0.01	0.01	0.01	0.02	0.01	0.00
Fe^{3+}	0.92	0.91	0.90	0.84	0.92	0.85
Mn	0.04	0.02	0.01	0.02	0.03	0.02
Ca	4.38	4.17	4.21	4.28	4.22	4.25
Total	16.42	16.26	16.32	16.28	16.28	16.28
Cz	83.53	83.93	84.59	84.97	83.39	84.89
Ep	15.75	15.69	15.17	14.71	16.08	14.83
Pie	0.72	0.37	0.24	0.31	0.53	0.28
X_{Al}	0.84	0.84	0.85	0.85	0.84	0.85

$X_{Al} = Al/(Fe^{3+} + Al)$

Table 6. EPMA (wt%) and structural formula of rutile and ilmenite, from the Amphibolites of Mauranipur and Babina (Sample MM-1 and BB-1).

Sample no.	**MM-1**			**BB-1**		
Position	Rt	Ilm		Rt	Ilm	
Domain	51/1	14/1	20/1	56/1	21/1	27/1
SiO_2	0.09	0.23	0.01	0.09	0.03	0.00
TiO_2	99.46	49.87	50.15	99.46	51.15	51.10
FeO	0.49	45.31	44.82	0.49	45.46	45.00
MnO	0.05	0.89	1.08	0.05	1.20	0.50
CaO	0.44	0.05	0.09	0.44	0.09	0.15
V_2O_3	0.00	2.31	2.32	0.00	2.33	2.53
Total	100.54	98.87	98.55	100.54	100.38	100.04
3 oxygens						
Si	0.00	0.01	0.00	0.00	0.00	0.00
Ti	0.99	0.96	0.97	0.99	0.97	0.97
Fe^{3+}	0.00	0.03	0.02	0.00	0.02	0.00
Fe^{2+}	0.01	0.94	0.94	0.01	0.94	0.95
Mn	0.00	0.02	0.02	0.00	0.03	0.01
Ca	0.01	0.00	0.00	0.01	0.00	0.00
V	0.00	0.05	0.05	0.00	0.05	0.05
Total	1.01	2.00	2.00	1.01	2.00	2.01

6. Phase Equilibria Modelling

6.1 Analytical Method

The bulk rock chemical compositional analysis for the major oxides of the representative amphibolite samples of Mauranipur (MM-1) and Babina (BB-1) was performed at the Birbal Sahni Institute of Palaeosciences (BSIP), Lucknow, India. Major oxides were analyzed by X-ray fluorescence (XRF) using a wavelength dispersive (WD-XRF AXIOS MAX) machine with a power of 4 KW, 60 kV-160 mA analytical, on a pressed powder pellet machine using 'kameyo' at a pressure of 15-20 tones with a 4 mm pallet thickness.

6.2 *P-T* Pseudosection

Phase equilibria modelling was done by constructing *P-T* pseudosections for the representative amphibolites from the Mauranipur and Babina of the specific mineral assemblages. For this purpose, Perple_X ver.6.9.0 software [38,39] was used with an end-member thermodynamic dataset [40,41]. Various solution models were used for the pseudosection construction, such as clinopyroxene [42], amphibole [43], plagioclase [44], epidote [41] and ilmenite [45].

Pseudosections are generally constructed to decipher the equilibrium relationship among the various mineral phases in rocks at different metamorphic *P-T* conditions. Here, the *P-T* pseudosections for both amphibolites (MM-1 and BB-1) were calculated in the NCFMASHTO (Na_2O-CaO-FeO-MgO-Al_2O_3-SiO_2-H_2O-TiO_2-O_2) system, where P_2O_5 and MnO were removed due to their negligible amounts, and quartz was taken as a ubiquitous phase (Figures 6 and 7). Furthermore, because the sample contains no biotite, muscovite, or K-feldspar, the influence of K_2O on the T-X(H_2O) and *P-T* pseudosection diagrams was ignored. The measured whole-rock composition of MM-1 and BB-1 was normalized in mol%, represented in Tables 7 and 8, respectively. The H_2O content for both samples was derived with the help of T-X(H_2O) pseudosection; however, the O_2 was evaluated by the composition of mineral phases and their modal abundance present in the rock.

6.3 Sample MM-1

T-X(H_2O) diagram of sample MM-1 was built in order to specify the probable water content in stable constraints to distinct metamorphic stages and associated *P-T* requirements at 7.5 and 4.0 kbar, respectively. The H_2O content is determined by the variation of H_2O from 0.0 mol% to 6.0 mol% in the bulk rock composition (Figure 6a,b). In the NCFMASHTO system, the appropriate mole ratios of oxides are normalized to 100%, as shown in Table 7. As illustrated in Figures 6a and 6b, the epidote is unstable at lower H_2O values before breaching the Ep entry line

Table 7. Major element concentration (wt%) and calculated effective composition (mol%) of Amphibolites of Mauranipur (Sample MM-1).

Composition	(wt%)		$X(H_2O)=C_0$	$X(H_2O)=C_1$	(mol%)
SiO_2	50.27	SiO_2	52.52	49.83	50.42
Al_2O_3	15.50	Al_2O_3	9.54	8.98	9.16
CaO	8.36	CaO	9.35	8.80	8.98
MgO	7.90	MgO	12.30	11.81	11.81
FeO	11.27	FeO	9.84	9.26	9.45
Na_2O	3.78	Na_2O	3.83	3.61	3.68
TiO_2	1.33	TiO_2	1.04	0.98	1.0
LOI	1.60	H_2O	0	6	4.0
		O_2	1.56	1.47	1.50
Total	100.00	Total	100	100.0	100
Data used for figure			Figure 6a,b		Figure 6c,d

Table 8. Major element concentration (wt%) and calculated effective composition (mol%) of Amphibolites of Babina (Sample BB-1).

Composition	(wt%)		$X(H_2O)=C_0$	$X(H_2O)=C_1$	(mol%)
SiO_2	50.40	SiO_2	52.90	49.78	50.78
Al_2O_3	16.14	Al_2O_3	9.98	9.39	9.58
CaO	8.86	CaO	9.96	9.37	9.56
MgO	7.17	MgO	11.22	10.56	10.77
FeO	11.26	FeO	9.89	9.30	9.49
Na_2O	3.86	Na_2O	3.93	3.70	3.77
TiO_2	0.73	TiO_2	0.57	0.54	0.55
LOI	1.59	H_2O	0.00	6.00	4.00
		O_2	1.56	1.47	1.50
Total	100.00	Total	100	100.0	100
Data used for figure			Figure 7a,b		Figure 7c,d

(yellow line). The solid red line indicates the appearance of H_2O as the temperature increases. The pre-peak stage mineral assemblage Ep-Amp-Cpx-Pl-Ilm-Ru-Qz is stable in $X(H_2O)$ values of 0.72-0.85 (long dashed black line). The observed mineral assemblage of the peak stage, Amp-Cpx-Pl-Ilm-Ru-Qz, is stable for $X(H_2O)$ values 0.61-0.65, while the mineral assemblage of the post-peak stage Amp-Pl-Ilm-Ru-Qz does not appear at a higher pressure of 7.5 kbar, this is most likely due to the pressure value chosen being too high (Figure 6a). When the T-$X(H_2O)$ diagram is calculated at lower pressure values of 4.0 kbar, the post-peak stage mineral assemblage appears (Figure 6b). Hence, we chose an $X(H_2O)$ value of 4.00, which was calculated on the basis of effective composition (Table 7) and then normalized to 100% by considering stable fields of mineral assemblages for pre- peak, peak and post-peak, which is marked by a black dash line and is also used to construct the *P-T* pseudosection diagram (Figure 6c,d).

The mineral assemblages identified in the petrographic observations include clinopyroxene, amphibole, plagioclase, epidote, quartz, ilmenite, and rutile. A *P-T* pseudosection for the sample MM-1 is constructed in the *P-T* range of 3-8 kbar and 400 ºC-800 ºC in the NCFMASHTO system (Figure 6c). Clinopyroxene in the pseudosection is pressure-dependent and continuously increases with pressure, and it becomes stable under higher temperature conditions. Amphibole is ubiquitous and stable in approximately all *P-T* fields. Plagioclase also mostly appears in the pseudosection. The significant occurrence of amphibole and plagioclase is supported by the presence of amphibole and plagioclase in petrographic thin sections. The epidote is present at higher pressures (4.5 kbar-8.0 kbar) and lower temperatures (400 ºC-600 ºC). To acquire the appropriate *P-T* conditions for metamorphism of the significant mineral assemblage, the isopleths of amphibole, clinopyroxene, and epidote are delineated on the pseudosection (Figure 6d). During pre-peak metamorphism, clinopyroxene grains contain epidote, amphibole, plagioclase, ilmenite, and rutile, as represented by the mineral assemblage Ep-Amp-Cpx-Pl-Ilm-Ru-Qz, which is stable at a *P-T* range of

5.5 kbar-8.0 kbar and 450 ºC-600 ºC. Amphibole, clinopyroxene, and epidote isopleths further narrow down the *P-T* conditions of the pre-peak metamorphic stage at 6.7 kbar and 510 ºC. The mineral assemblage of Amp-Cpx-Pl-Ilm-Ru-Qz characterizes the peak metamorphic stage. The epidote becomes unstable with increasing temperatures. This assemblage is stable in a *P-T* range of 7.2 kbar-8.0 kbar and 560 ºC-580 ºC. Isopleths of amphibole and clinopyroxene defined the *P-T* conditions for the peak metamorphic stage at P = 7.3 kbar and T = 578 ºC.

Later, the post-peak metamorphic stage is characterized by the mineral assemblage of Amp-Pl-Ilm-Ru-Qz, which acquires a Cpx free field. Due to a lowering in pressure, clinopyroxene is no longer stable at the post-peak metamorphic stage. This assemblage is stable under a *P-T* range of 3.0-5.0 kbar and 580 ºC-700 ºC. Isopleths of amphibole reveal the *P-T* conditions of the post-peak metamorphic stage at P = > 3.0 kbar and T = > 585 ºC.

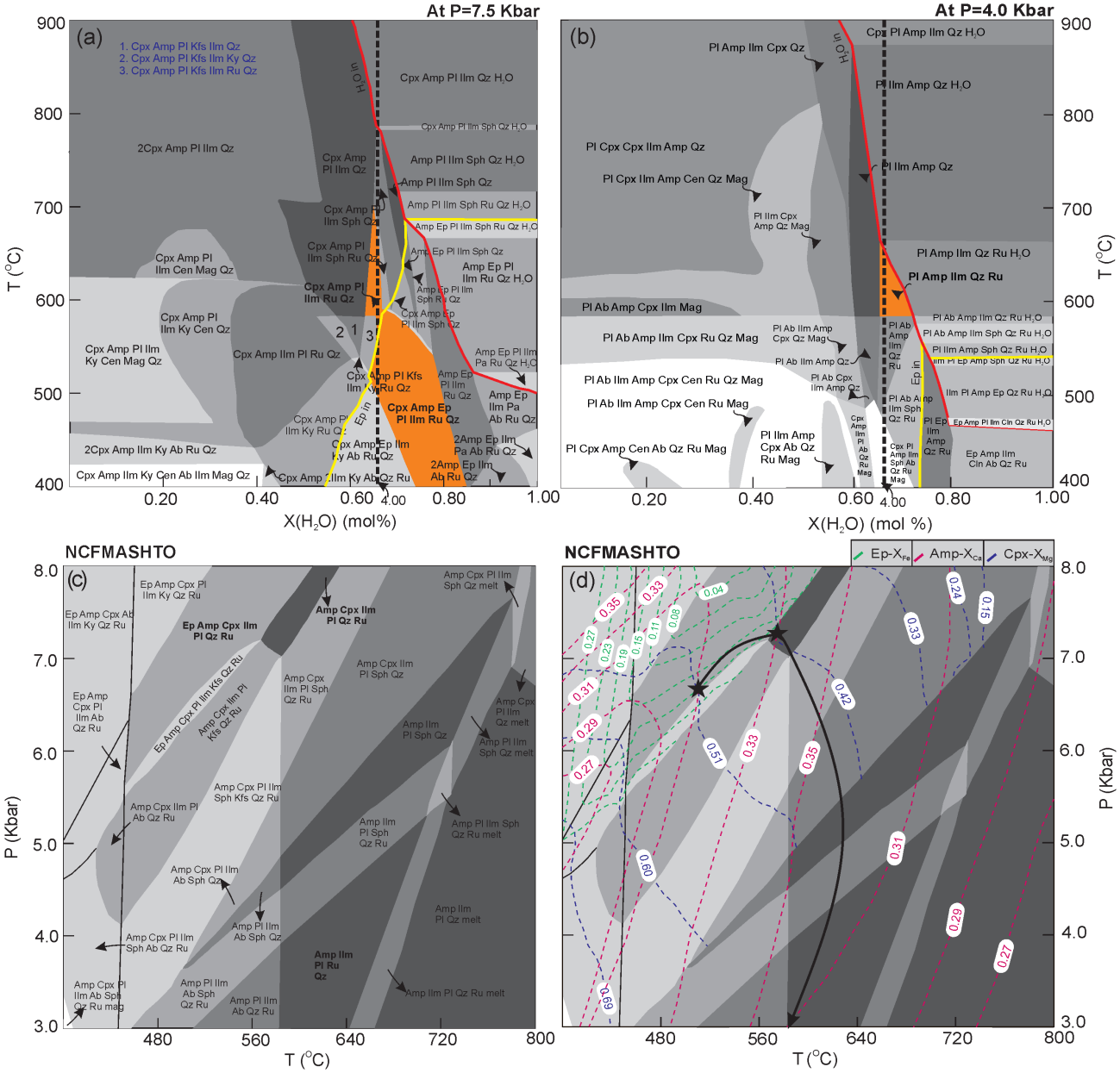

Figure 6. (a) T-X(H_2O) pseudosection at 7.5 Kbar, and (b) at 4.0 kbar, showing the effects of varying the molar proportions of bulk-rock H_2O (in MM-1). The black dashed line is the modelled composition of H_2O (4.00%). (c) *P-T* pseudosection showing pre-peak, peak and post-peak assemblages. (d) Isopleths X_{Ca} of Amp, X_{Mg} Cpx and X_{Fe} of Ep.

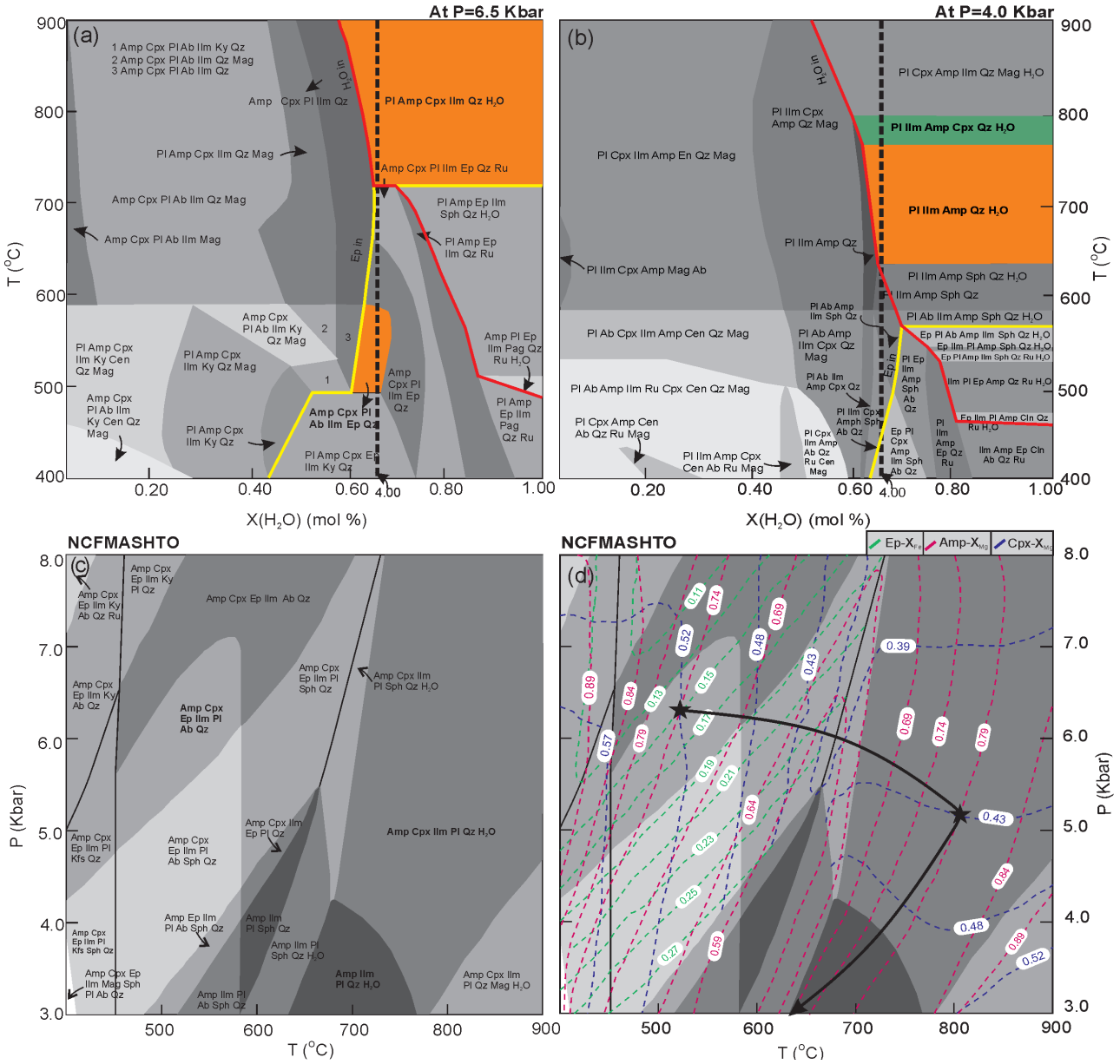

Figure 7. (a) T-X(H_2O) pseudosection at 6.6 Kbar and (b) at 4.0 Kbar, showing the effects of varying the molar proportions of bulk-rock H_2O in amphibolite (sample BB-1). The black dashed line is the modelled composition of H_2O (4.00%). (c) *P-T* pseudosection (sample BB-1) of amphibolites showing pre-peak, peak and post-peak metamorphic assemblages in the NCFMASTHO system. (d) Isopleths X_{Mg} of amphibole, X_{Mg} of clinopyroxene and X_{Fe} of epidote contouring *P-T* pseudosection.

6.4 Sample BB-1

The same process of computing H_2O values was repeated for sample BB-1. Table 8 shows how the necessary mole ratios of oxide are normalized to 100% in the NCFMASHTO system. At 6.5 and 4.0 kbar, a T-X(H_2O) pseudosection was also displayed (Figure 7a,b). The epidote is unstable at lower H_2O concentrations before breaching the Ep entry line, as seen in Figures 7a and 7b. As the temperature rises, the solid red line represents the emergence of H_2O. In X(H_2O) values of 0.60-0.65, the pre-peak mineral assemblage Ep-Amp-Cpx-Pl-Ab-Ilm-Qz remains stable (long dashed black line). While the mineral assemblage of the peak stage Amp-Cpx-Pl-Ilm-Qz-H_2O is stable for X(H_2O) values of 0.61-1.00, the mineral assemblage of the post-peak stage Amp-Pl-Ilm-Qz-H_2O does not appear in Figure 7a at a higher pressure of 6.5 kbar, and this is most likely owing to the pressure value chosen to be high. The post-peak and peak stage mineral assemblages became visible when the T-X(H_2O) diagram is calculated

at lower pressures of 4.0 kbar (Figure 7b). As a result, we chose an X(H_2O) value of 4.00, which was calculated using effective composition (Table 8) and then normalized to 100% in the NCFMASHTO system by considering stable fields of mineral assemblages for pre-peak, peak and post-peak, which is marked by a black dash line and is also used to construct the *P-T* pseudosection diagram (Figures 7c and 7d).

In the NCFMASHTO model system, a specific *P-T* pseudosection for the representative amphibolite sample (BB-1) has been generated in the *P-T* range of 3 kbar-8 kbar and 400 °C-900 °C (Figure 7c). In the pseudosection, clinopyroxene shows a pressure-dependent character and is stable at higher temperatures with other mineral phases such as amphibole, plagioclase, ilmenite, quartz, and H_2O. Amphibole is ubiquitous in all phases and is stable over a wide *P-T* range. Plagioclase is also found mostly in the pseudosection. Epidote can be found at high and low pressures (3.0 kbar-8.0 kbar), but only at much lower temperatures (> 680 °C). The most common Ti-bearing phases are ilmenite and magnetite. This rock is devoid of rutile. The *P-T* pseudosection of the BB-1 sample revealed three stages of metamorphism. The first is the pre-peak metamorphic stage, which is characterized by epidote, amphibole, plagioclase, and ilmenite inclusions inside clinopyroxene grains. This stage produces the mineral assemblage Ep-Amp-Cpx-Pl-Ab-Ilm-Qz, stable in the pseudosection at *P-T* ranges of 4.8 kbar-7.0 kbar and 450 °C-580 °C. *P-T* conditions of the pre-peak metamorphic stage at P = 6.27 kbar and T = 520 °C are further constrained by isopleths of amphibole, clinopyroxene, and epidote (Figure 7d). The peak metamorphic stage is defined by the mineral assemblage Amp-Cpx-Pl-Ilm-Qz-H_2O. With the rising temperature, the epidote becomes unstable, and H_2O forms at a higher temperature. This assemblage obtains a field with a *P-T* of 3.0 kbar-8.0 kbar and a temperature of 680-900 °C. The *P-T* conditions of the peak metamorphic stage at P = 5.2 kbar and T = 805 °C are further narrowed by isopleths of amphibole and clinopyroxene. Finally, the mineral assemblage Amp-Pl-Ilm-Qz-H_2O denotes the post-peak metamorphic stage. At the post-peak metamorphic stage, clinopyroxene is no longer stable. This assemblage acquires a field with a *P-T* of 3.0 kbar-4.2 kbar and a temperature of 620 °C-780 °C and is further defined as > 3.0 kbar and > 640 °C by the isopleths of amphibole.

7. Discussion

The Mauranipur and Babina amphibolites were chosen for this investigation because they demonstrate medium to high-grade metamorphism in the BuC. The BuC amphibolites are primarily found in the Mauranipur-Babina region as enclaves within the TTGs. The mineralogical assemblage of amphibolites is Hbl + Cpx + Pl ± Qz ± Ep [46]. The geochemistry of amphibolites from the CBGT was also previously studied. According to their findings, tholeiitic magma is the primary source of amphibolites [34]. The Nd isotopic values of amphibolites provide two model ages: one for the protolith of amphibolites, 4.9-4.2 Ga, and the other for amphibolites metamorphism, 3.4-3.3 Ga [31]. Based on the Nd levels, the amphibolites were generated in a subduction-related environment. Many researchers have postulated a subduction zone context for the evolution of the BuC based on the analysis of TTGs, granitoids, amphibolites, basaltic, and komatiitic rocks [34]. A geodynamic model for the evolution of the CBGT based on observations of exposed mafic-ultramafic rocks in the Babina and Mauranipur regions was also explained earlier [31]. The presence of mafic-ultramafic rocks, metabasic rocks, amphibolites, BIFs, and meta-sediments in CBGT shows that they are remains of earlier oceanic crust. At 2.7 Ga, the oceanic plate subducted, causing the melting of mafic rocks containing garnet and water, which reacted with the mantle, forming the TTGs [47].

Three metamorphic stages have been identified based on mineral assemblages, textural correlations, and *P-T* pseudosections. The creation of isopleths on the *P-T* pseudosection defines the *P-T* conditions of these three metamorphic stages. For amphibolites from the Mauranipur and Babina regions, they have set up a clockwise *P-T* path. Figures 6d and 7d demonstrate the *P-T* pathways of Mauranipur and Babina amphibolites, respectively. The *P-T* routes of both amphibolites follow a similar pattern, although the *P-T* conditions of the different metamorphic stages differ significantly. Mauranipur amphibolites reach a pre-peak metamorphic stage at a lower pressure and temperature (6.7 kbar, 510 °C) than Babina amphibolites (6.27 kbar, 520 °C). Peak metamorphism occurs in Babina amphibolites at 5.2 kbar/805 °C, substantially higher in temperature and pressure than the peak metamorphic *P-T* conditions in Mauranipur amphibolites (7.3 kbar/578 °C). Due to the availability of rutile, these differences may be conceivable. Similarly, Mauranipur amphibolites' post-peak metamorphic stage is defined by a *P-T* condition of > 3.0 kbar/ > 585 °C, which is similar in pressure but lower in temperature than Babina amphibolites (> 3.0 kbar/ > 640 °C). Ep-Amp-Cpx-Pl-Ilm-Ru-Qz and Ep-Amp-Cpx-Pl-Ilm-Ab-Qz mineral assemblages characterize the pre-peak stage of Mauranipur and Babina amphibolites, respectively. In the Mauranipur region, rutile is found in both a pre-peak and a peak metamorphic state, but it is rare in amphibolites from the Babina region. Rutile is a stable mineral in medium- to high-grade metamorphic belts and serves as a clue material for subduction tectonic environments [48].

Following that, both locations were further buried, resulting in a constant rise in pressure and temperature, and amphibolites underwent peak metamorphism, generating mineral assemblages of Amp-Cpx-Pl-Ilm-Ru-Qz and Amp-Cpx-Pl-Ilm-Qz-H_2O in the Mauranipur and Babina regions, respectively. Under a decompression procedure, a post-peak stage followed this peak stage, with a reduction in pressure conditions. The presence of the mineral assemblages Amp-Pl-Ilm-Ru-Qz (MM-1) and Amp-Pl-Ilm-Qz-H_2O (BB-1) in the post-peak stage indicates that it was formed by the decompression and subsequent exhumation of amphibolites on the surface.

8. Conclusions

1) *P-T* pseudosections for amphibolites from both regions are plotted in the NCFMASHTO system and characterized by three metamorphic stages.
2) The pre-peak, peak, and post-peak stages of amphibolites of the Mauranipur are designated by the presence of mineral assemblages Ep-Amp-Cpx-Pl-Ilm-Ru-Qz, Amp-Cpx-Pl-Ilm-Ru-Qz, and Amp-Pl-Ilm-Ru-Qz, respectively. However, the pre-peak, peak, and post-peak stages of amphibolites of the Babina are demarcated by the mineral assemblage Ep-Amp-Cpx-Pl-Ab-Ilm-Qz, Amp-Cpx-Pl-Ilm-Qz-H_2O, and Amp-Pl-Ilm-Qz-H_2O, respectively.
3) The *P-T* condition of the pre-peak stage is 6.7 kbar/510 ºC, the peak stage is 7.3 kbar/578 ºC, and the post-peak stage is > 3.0 kbar/> 585 ºC in the Mauranipur amphibolites. Similarly, the *P-T* condition of the pre-peak stage is 6.27 kbar/520 ºC, the peak stage is 5.2 kbar/805 ºC, and the post-peak stage is > 3.0 kbar/> 640 ºC in the Babina amphibolites.
4) Amphibolites of both regions show a clockwise *P-T* path, suggesting burial followed by exhumation.

Authors' Contributions

Pratigya Pathak: Field sampling, Conceptualization, Analysis, Investigation, Writing-original draft. **Shyam Bihari Dwivedi:** Supervision, Reviewing and Editing. **Ravi Ranjan Kumar:** Conceptualization, Writing-original draft.

Conflicts of Interest

On behalf of all authors, the corresponding author would like to declare that this manuscript does not have any conflict of interest whatsoever following the Policy of the Journal of Environment and Earth Sciences.

Acknowledgements

The authors thank the Director, Indian Institute of Technology (BHU), for providing the infrastructure to carry out our work. We are grateful to the Ministry of Human Resource Development (MHRD) Fellowship Scheme for providing financial support. The author expresses her gratitude to Prof. R.K. Srivastava and Dr. G.C. Gautam from the Department of Geology, Banaras Hindu University (India), for facilitating the Microscopy Laboratory.

References

[1] Iizuka, T., Horie, K., Komiya, T., et al., 2006. 4.2 Ga zircon xenocryst in an Acasta gneiss from northwestern Canada: Evidence for early continental crust. Geology. 34, 245-248.
[2] Wilde, S.A., Valley, J.W., Peck, W.H., et al., 2001. Evidence from detrital zircons for the existence of continental crust and oceans on the Earth 4.4 Gyrago. Nature. 409, 175-178.
[3] Zeh, A., Stern, R., Gerdes, A., 2014. The oldest zircons of Africa—their U-Pb-Hf-O isotope and trace element systematics, and implications for Hadean to Archaean crust-mantle evolution. Precambrian Research. 241, 203-230.
[4] Armstrong, R.L., 1981. Radiogenic isotopes: The case for crustal recycling on a near steady-state-no-continental growth Earth. Philosophical Transactions Royal Society London. 301, 443-472.
[5] Dhuime, B., Hawkesworth, C.J., Cawood, P., 2011. When continents formed. Science. 331, 154-155.
[6] Guitreau, M., Blichert-Toft, J., Mojzsis, S.J., et al., 2014. Lu-Hf isotope systematics of the hadean–Eoarchean Acasta gneiss complex (northwest territories, Canada). Geochimica et Cosmochimica Acta. 135, 251-269.
[7] Pearce, J.A., 2014. Geochemical fingerprinting of the Earth's oldest rocks. Geology. 42, 175-176.
[8] Pearce, J.A., Peate, D.W., 1995. Tectonic implications of the composition of volcanic arc magmas. Annual Review on Earth Planet Sciences. 23, 251-285.
[9] Naqvi, S.M., 2005. Geology and evolution of the Indian plate (from Hadean to Holocene—4 Ga to 4 Ka). Capital Publishing Company: New Delhi. pp. 450.
[10] Condie, K.C., Davaille, A., Aster, R.C., et al., 2015. Upstairs-downstairs: Supercontinents and large igneous provinces, are they related? International Geology Review. 57, 1341-1348.
[11] Saha. L., Pant, N.C., Pati, J.K., et al., 2011. Neo-

archean high-pressure margarite-phengitic muscovite-chlorite corona mantled corundum in quartz-free high-Mg, Al phlogopite-chlorite schists from the BundelkhandCraton, north-central India. Contribution to Mineralogy and Petrology. 161, 511-530.

[12] Kumar, S., Raju, S., Pathak, M., et al., 2010. Magnetic susceptibility mapping of felsic magmatic litho units in the central part of Bundelkhand massif, central India. Journal of Geological Society of India. 75, 539-548.

[13] Joshi, K.B., Bhattacharjee, J., Rai, G., et al., 2017. The diversification of granitoids and plate tectonic implications at the Archaean-Proterozoic boundary in the Bundelkhand Craton, central India. Geological Society Special Publication. 449, 123-157.

[14] Singh, S.P., Dwivedi, S.B., 2009. Garnet-sillimanite-cordierite-quartz-bearing assemblages from early Archean supracrustal rocks of Bundelkhand massif, Central India. Current Science. 97, 103-107.

[15] Singh, S.P., 2012. Archean geology of Bundelkhand craton, Central India: An overview. Gondwana Geological Magzine. 13, 125-140.

[16] Nasipuri, P., Saha, L., Hangqiang, X., et al., 2019. Paleoarchean crustal evolution of the Bundelkhand Craton, north Central India. Earth's Oldest Rocks. 31, 793-817.

[17] Raza, M.B., Nasipuri, P., Saha, L., et al., 2021. Phase relations and in-situ U-Th-Pb total monazite geochronology of Banded Iron Formation, Bundelkhand Craton, North-Central India, and their geodynamic implications. International Journal of Earth Sciences. 1-29.

[18] Pathak, P., Dwivedi, S.B., Kumar, R.R., 2022. Geochemistry and Phase equilibrium modelling of garnet-biotite gneiss from Mauranipur, Bundelkhand Craton, Northern India; implication for tectonic setting and metamorphism. Journal of Geosciences Research. Under Review.

[19] Singh, S.P., Dwivedi, S.B., 2015. High-grade metamorphism of the Bundelkhand massif and its implications for crustal evolution of the middle archean crust of central India. Journal of Earth System Science. 124, 197-211.

[20] Slabunov, A., Singh, V., 2019. Meso-Neoarchean crustal evolution of the BundelkhandCraton, Indian Shield: New data from greenstone belts. International Geology Review. 61, 1409-1428.

[21] Bhowmik, S.K., Ao, A., 2016. Subduction initiation in the Neo-Tethys: Constraints from counterclockwise P-T paths in amphibolite rocks of the Nagaland Ophiolite Complex, India. Journal of Metamorphic Geology. 34(1), 17-44.

[22] Somesha, G.S., Govindaraju, M.V., Govindaiah, S., 2019. Petrochemistry and pt condition of amphibolites associated with pegmatites of holenarasipura and karighatta schist belts of Western Dharwar Craton, Karnataka, India. International Journal of Science Technology and Research. 8, 570-580.

[23] Meshram, T., Shukla, D., Behera, K., et al., 2017. Petrography and geochemistry of the Amphibolites from the southeastern part of Yerapalli schist belt, Eastern Dharwar Craton, India. Journal of Indian Geophysical Union. 21, 391-400.

[24] Rajendran, S., Thirunavukkarasu, A., Poovalinga, B., et al., 2007. Petrological and geochemical studies of amphibolites in parts of Salem District, Tamil Nadu, India. Indian Mineralogist. 41, 169-175.

[25] Fanka, A., Sutthirat, C., 2018. Petrochemistry, mineral chemistry, and pressure-temperature model of corundum-bearing amphibolite from Montepuez, Mozambique. Arabian Journal for Science and Engineering. 43, 3751-3767.

[26] Kumar, R.R., Kawaguchi, K., Dwivedi, S.B., et al., 2022. Metamorphic evolution of the pelitic and mafic granulites from Daltonganj, Chhotanagpur Granite Gneiss Complex, India: Constraints from zircon U–Pb age and phase equilibria modelling. Geological Journal. 57(3), 1284-1310.
DOI: https://doi.org/10.1002/gj.4340

[27] Basu, A.K., 1986. Geology of parts of the Bundelkhand Granite massif Central India. Record of Geological Survey of India. 117, 61-124.

[28] Bhattacharya, A.R., Singh, S.P., 2013. Proterozoic crustal scale shearing in the Bundelkhand massif with special reference to quartz reefs. Journal of the Geological Society of India. 82, 474-484.

[29] Absar, N., Raza, M., Roy, M., et al., 2009. Composition and weathering conditions of the Paleoproterozoic upper crust of Bundelkhand craton, Central India: records from the geochemistry of clastic sediments of 1.9 Ga Gwalior Group. Precambrian Research. 168, 313-329.

[30] Singh, P.K., Verma, S.K., Singh, V.K., et al., 2021. Geochronology and petrogenesis of the TTG gneisses and granitoids from the Central Bundelkhand granite-greenstone terrane, BundelkhandCraton, India: Implications for Archean crustal evolution and cratonization. Precambrian Research. 359, 106-210.

[31] Singh, P.K., Verma, S.K., Moreno, J.A., et al., 2019. Geochemistry and SmNd isotope systematics of mafic-ultramafic rocks from the Babina and Mauranipur greenstone belts, Bundelkhand Craton, India: Impli-

cations for tectonic setting and Paleoarchean mantle evolution. Lithos. 330, 90-107.

[32] Singh, V., Slabunov, A., Svetov, S., et al., 2018. Occurrence of archean iron bearing rocks from Babina, Mauranipur and Girar Area of the Bundelkhand Region: As potential reserves. Archaeology Anthropology Open Access. 3, 108-113.

[33] Pandey, U.K., Bhattacharya, D., Shastry, D.V.L.N., et al., 2011, Geochronology Rb-Sr, Sm-Nd and Pb-Pb, isotope geochemistry and evolution of the granites and andesites hosting Mohar Cauldron, Bundelkhand Granite Complex, Shivpuri district, Central India. Exploration Research on Atomic Minerals. 21, 103-116.

[34] Singh, V.K., Slabunov, A., 2015. The Central Bundelkhand Archaean greenstone complex, Bundelkhand craton, central India: Geology, composition, and geochronology of supracrustal rocks. International Geology Review. 57(11-12), 1349-1364.

[35] Leake, B.E., Woolley, A.R., Arps, C.E.S., et al., 1997. Nomenclature of amphiboles: Report of the subcommittee on amphiboles of the international mineralogical association, commission on new minerals and mineral names. Canadian Mineral. 35, 219-246.

[36] Morimoto, N., 1988. The nomenclature of pyroxenes. Mineral Magzine. 52, 425-433.

[37] Tarantola, A., Voudouris, P., Eglinger, A., et al., 2019. Metamorphic and metasomatic kyanite-bearing mineral assemblages of Thassos Island (Rhodope, Greece). Minerals. 9(4), 252.

[38] Connolly, J.A.D., 2005. Computation of phase equilibria by linear programming: A tool for geodynamic modelling and its application to subduction zone decarbonization. Earth Planet Science Letters. 236, 524-541.

[39] Connolly, J.A.D., 2009. The geodynamic equation of state: What and how. Geochemical Geophysical Geosystems. 10(10), 1-19.

[40] Holland, T.J.B., Powell, R.T.J.B., 1998. An internally consistent thermodynamic data set phases of petrological interest. Journal of Metamorphic Geology. 16(3), 309-343.

[41] Holland, T.J.B., Powell, R., 2011. An improved and extended internally consistent thermodynamic dataset for phases of petrological interest, involving a new equation of state for solids. Journal of Metamorphic Geology. 29, 333-383.

[42] Green, E.C.R., White, R.W., Diener, J.F.A., et al., 2016. Activity-composition relations for the calculation of partial melting equilibria in metabasic rocks. Journal of Metamorphic Geology. 34(9), 845-869.

[43] Diener, J.F.A., Powell, R., White, R.W., et al., 2007. A new thermodynamic model for clino- and orthoamphiboles in the system Na_2O-CaO-FeOMgO-Al_2O_3-SiO_2-H_2O-O. Journal of Metamorphic Geology. 25(6), 631-656.

[44] Holland, T.J.B., Powell, R., 2003. Activity-composition relations for phases in petrological calculations: an asymmetric multi-component formulation. Contribution to Mineralogy and Petrology. 145, 492-501.

[45] White, R.W., Powell, R., Holland, T.J.B., et al., 2000. The effect of TiO_2 and Fe_2O_3 on metapelitic assemblages at greenschist and amphibolite facies conditions: Mineral equilibria calculations in the system K_2O-FeO-MgO-Al_2O_3-SiO_2-H_2O-TiO_2-Fe_2O_3. Journal of Metamorphic Geology. 18, 497-511.

[46] Pati, J.K., 2020. Evolution of Bundelkhand craton. Episodes. 43(1), 69-87.

[47] Verma, S.K., Verma, S.P., Oliveira, E.P., et al., 2016. LA-SF-ICP-MS zircon U-Pb geochronology of granitic rocks from the central Bundelkhand greenstone complex, Bundelkhand craton, India. Journal of Asian Earth Science. 118, 125-137.

[48] Meinhold, G., 2010. Rutile and its applications in earth sciences. Earth-Science Reviews. 102, 1-28. DOI: https://doi.org/10.1016/j.earscirev.2010.06.001

[49] Whitney, D.L., Evans, B.W., 2010. Abbreviations for names of rock-forming minerals. American Mineralogist. 95, 185-187.

BILINGUAL PUBLISHING CO.
Pioneer of Global Academics Since 1984

Journal of Environmental & Earth Sciences
https://ojs.bilpublishing.com/index.php/jees

ARTICLE

Spatial Distribution of Black Soot and Its Health Effects in Port Harcourt Metropolis, Nigeria

Miebaka Oriasi[1*] Eteh Desmond Rowland[2] Ayowei Alvin Harry[3]

1. University of Port Harcourt, River State, Nigeria
2. Niger Delta University, Wilberforce Island, Amassoma, Bayelsa State, Nigeria
3. University of Salford, London, UK

ARTICLE INFO

Article history
Received: 7 January 2022
Accepted: 4 March 2022
Published Online: 29 April 2022

Keywords:
Black soot
Port harcourt
Air polluion
WHO
$PM_{2.5}$
PM_{10}
PAHs

ABSTRACT

This research presents a novel approach to assessing the health implications of black soot using a MiniVol air sampler. The MiniVol air sampler was used to collect PM from the ambient air at six monitoring sites in Port Harcourt, Nigeria. Sampling was conducted every day for seven days, for 24 hours. $PM_{2.5}$ concentrations at Uniport Junction, GRA Junction, Slaughter Roundabout, Abuloma Jetty, Rumuomasi Roundabout, and New Road Borokiri were 38.6 g/m^3, 28.3 g/m^3, 93.7 g/m^3, 72.9 g/m^3, 30.6 g/m^3, and 31.3 g/m^3, respectively. PM_{10} concentrations ranged from 71.2 g/m^3 to 60.6 g/m^3, with 103.3 g/m^3, 85.5 g/m^3, 40.1 g/m^3, and 35.2 g/m^3 being the highest. The level of $PM_{2.5}$ and PM_{10} pollution in the ambient air was high across the six sampling sites, with mean $PM_{2.5}$ and PM_{10} concentrations exceeding the WHO (2011) guideline. The flame atomic absorption spectrometry (FAAS) technique was used. The presence of heavy metals, such as mean metal concentrations of lead, cadmium, chromium, mercury, and nickel, ranged from 0.009 g/m^3-0.532 g/m^3, 0.002 g/m^3-0.544 g/m^3, 0.002 g/m^3-0.338 g/m^3, 0.001 g/m^3, and 0.001 g/m^3-0.432 g/m^3, across the six sampling sites. The GC-MS was used to determine the presence of PAHs in particulate matter. Correlation results revealed a strong positive correlation between $PM_{2.5}$ and PM_{10}. The findings also revealed a positive relationship between the metals as well as between the metals and PAHs, resulting in asthma, lung cancer, breathing difficulties, and miscarriages among pregnant women, which have affected the health implications of the people living in the environment.

*Corresponding Author:
Miebaka Oriasi,
University of Port Harcourt, River State, Nigeria;
Email: desmondeteh@gmail.com

DOI: https://doi.org/10.30564/jees.v4i1.4340

1. Introduction

As residents of Port Harcourt and its environs deal with the latest atmospheric threat, black soot, experts warn that long-term exposure to soot poses serious health risks, including cancer and other critical health problems that could lead to premature death. Soot produced as a byproduct of incomplete combustion of organic (carbon-containing) materials such as wood, fuel oil, plastics, and household waste contributes to air pollution, which is a major environmental health risk [1]. Carcinogens such as arsenic, cadmium, and chromium have been found in soot, a fine black or brown powder. In the last ten years, a large and well-documented literature on the effects and severity of air pollution on human health has emerged. The elderly and young infants are more vulnerable to illness as a result of air pollution. Air pollution has been linked to a variety of health effects, including eye, nose, and throat irritation, pneumonia, bronchitis, lung cancer, heart disease, brain, nerve, liver, and kidney disease [2]. According to Wikipedia, Port Harcourt is the capital of Rivers State, located within the southern region of Nigeria. Port Harcourt has a population of over 1.8 million people as of 2016, a 3 square mile coastline, and an elevation of 468 meters (Latitude 4.78N, Longitude 7.01E). Because of the presence of oil and gas, it is assumed that oil and gas-related businesses are the primary source of income for the majority of people, followed by farming and trading. This huge focus on oil and gas in the city has affected the city both positively and negatively. Air pollution, water pollution, and land pollution are among the negative effects it has on the environment and the people. From exhaust fumes to gas flaring, black soot, and oil spills on land and water bodies. This paper will be focusing on air pollution, chief among which is black soot.

A work on Satellite Determination of Particulate Load over Port Harcourt during Black Soot Incidents carried out by Ede and Edokpa [3] suggested that the black soot in Port Harcourt is a result of hydrocarbon combustion. 0.000035 mg/m^3 was the minimum and 0.18 mg/m^3 (0.035 g/m^3-180 g/m^3) was the maximum dispersed emission concentration found. He further inferred that the above-mentioned concentrations exceeded the national annual average limits, which is 40 g/m^3-60 g/m^3.

Black soot is a carbon constituent produced as a result of incomplete combustion of hydrocarbons. It is a climate forcer [4]. Generally, black soot is regarded as a very dangerous air pollutant. Black soot in Port Harcourt, Rivers State, was significantly noticed in the last quarter of the year 2016 and has carried on to date. Many residents suggest that the origin of the soot is a result of the burning of crude oil illegally with the use of various illegal refineries, the burning of tyres, gas flaring, and asphalt burning. Black soot has no doubt increased the amount of cardiovascular disease in the city.

The most visible air pollution within Port Harcourt, Rivers State and its environs is black soot, which is emitted daily with little or no strict rules and mitigating actions from the responsible bodies. Exposure to black soot in low or high concentrations frequently results in serious health issues and, in some cases, death. This underscores the dire need to understand the entirety of the problem (black soot) to enable the possibility of concrete, reliable solutions. Understanding the characteristics of black soot is a key step forward in getting to a concrete solution.

Study Area

The Port Harcourt is situated in the Niger Delta region of Nigeria and is the capital of Rivers state (Figure 1). Port Harcourt is located on latitude 4.91°N and longitude 7.09°E, 4.74°N and 6.89°E meters elevation above sea level with a population of 1,382, 592 according to Nigerian census [5]. It occupies an area of 1811.6 square kilometres and shares boundaries with the Gulf of Guinea along Bonny River. The city lies in the tropical monsoon climate with lengthy and heavy rainy season and very short dry season. The rainy season starts in March and ends in October while the dry season starts in November to February. December is the driest month of the year with an average rainfall of 20 mm while September is the month with the highest rainfall of about 367 mm. The average temperature is between 25-28 °C in the city with numerous hydrocarbon flow stations owned by the SPDC Total E& P and Agip Oil Company. In Port Harcourt and other Niger Delta states, gas flaring is a major environmental and public health issue. The human health consequences are diverse, encompassing a wide range of morbidities and fatalities [6]. The six monitoring sites include Uniport Junction, GRA, Slaughter round about, Rumuomasi round about, Abuloma Jetty and New Road Borokiri. The choice of the roundabout and junction is the area which experiences heavy vehicular traffic most often. The monitoring locations cover the traffic, residential and commercial areas in line with National Ambient Air Quality stipulations that monitoring must be undertaken where people may be exposed. Other factors considered in selecting the locations include accessibility, security, distance, cost and availability of electricity.

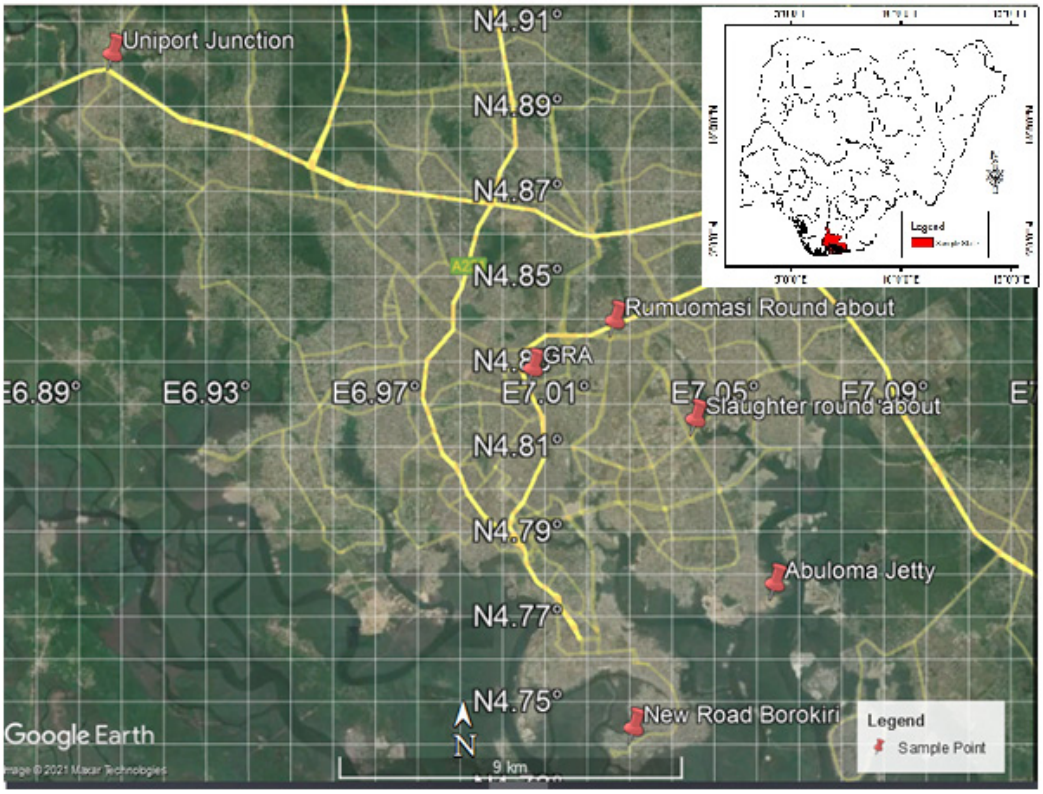

Figure 1. Map of the study area.

2. Literature Review

2.1 Sources of Air Pollution

Air pollution is the introduction of substances into the air that is not originally there or is above the standard concentration and it is harmful to the environment and living things within a short or long period of time. Pollution of air is hugely due to anthropogenic, geogenic and biogenic emissions [7]. Anthropogenic source of pollution is pollution caused by the activities of man, examples of such are gas flaring, black soot, chlorofluorocarbons. Geogenic source of pollution is air pollution that occurs naturally without any active influence by human beings but still has the potential to cause harm examples of such are volcanoes, the emission of sand by wind. Biogenic source of pollution is natural sources like plants and vegetation. These are temperature dependent mostly.

Weli [8] carried out research that included an in-depth quantitative analysis of the spatial and seasonal atmospheric levels of PM_{10} in Port Harcourt, as well as the environmental health implications of their presence at measured concentrations. Relative quantities of the pollutant were compared in various areas based on land use and time of year, including commercial, high-density residential, low-density residential, industrial, and rural. PM_{10} samples and analyses were collected and analyzed during the dry, transition, and wet seasons. The findings suggest that land use and seasons influence PM_{10} concentrations in the atmosphere. The seasonal trend in PM_{10} levels was dry > transition > wet for all land use types. During the dry season, the commercial and industrial areas had the highest values in terms of land use. The lowest PM_{10} value was found in low-density residential areas. The seasonal total atmospheric loading was 3436.1 g/m^3, 8573.12 g/m^3, and 16,148.87 g/m^3 for the wet, transition, and dry seasons, respectively. According to the study, there is also a statistically significant difference. There is a seasonal variation in PM_{10} concentrations across land use types. People who live and work in areas with high levels of PM are more likely to contract respiratory diseases. This includes densely populated areas.

Nwachukwu et al. [9] discovered that all of the criteria air pollutants were significantly higher in Rivers State than the WHO specification. They discovered that air pollution was linked to air-related morbidities and deaths in the state. Among the air-related morbidities studied, which included cerebrospinal meningitis (CSM), chronic bronchitis, measles, pertussis, pulmonary tuberculosis, pneumonia, and upper respiratory tract infection (URTI),

pneumonia was the most common for all of the years studied and was responsible for the most deaths in 2005.

2.2 Black Soot

Black soot produced by the incomplete combustion of hydrocarbon [10] is considered as an airborne environmental contaminant, which is very toxic to the environment and human beings. It is also considered to have a composition of particulate matter (PM), carbon mono oxide (CO), nitrogen oxides (NO_x) and sulphur dioxide (SO_2). It has a typical size ranging from 10 nm to 1 mm and the carbon content level is less than 60% of the particle [10]. We are all affected by these emissions, and the difference is our susceptibility which varies with health or age. Coarse particulates between 2.5 μm and 10 μm are said to be emissions of mechanical processes and dust. While finer particulates of 2.5 μm or less originate from a combustion source [11]. In most urban settlements, a mixture of both is observed but the ratio determines the dominant factor.

2.3 Black Soot in Port Harcourt

Due to the city's heavy reliance on oil exploration, this has not been mitigated to date; however, the ratio varies seasonally. During the dry season, it seemed to be more pronounced than during the rainy season. The major sources of black soot in Port Harcourt are mostly anthropogenic activities. Examples are gas flaring by the oil and gas industry, burning of crude by illegal refineries, burning of tyres, bombing of illegal refineries, and burning of asphalt. However, a paper by the National Environmental Standards and Regulations Enforcement Agency (NESREA) [12] on the "Impact of air pollution on the environment in Port Harcourt" inferred that the most likely reason for the prevalent soot is due to poorly maintained public transport diesel buses within the city, thermal power stations, and industrial enterprises. The black soot in Port Harcourt is more potent during the early hours of the day, which suggests that it is highly due to illegal refineries and the destruction of illegal refineries, which is done at that time of the day.

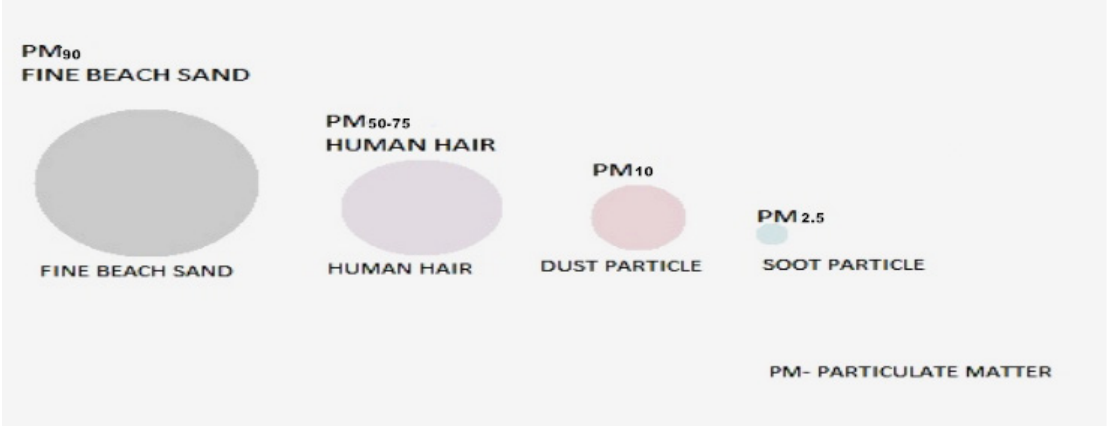

Figure 2. Sizes of particulate matter.

Figure 3. Depicting black soot in Port Harcourt.

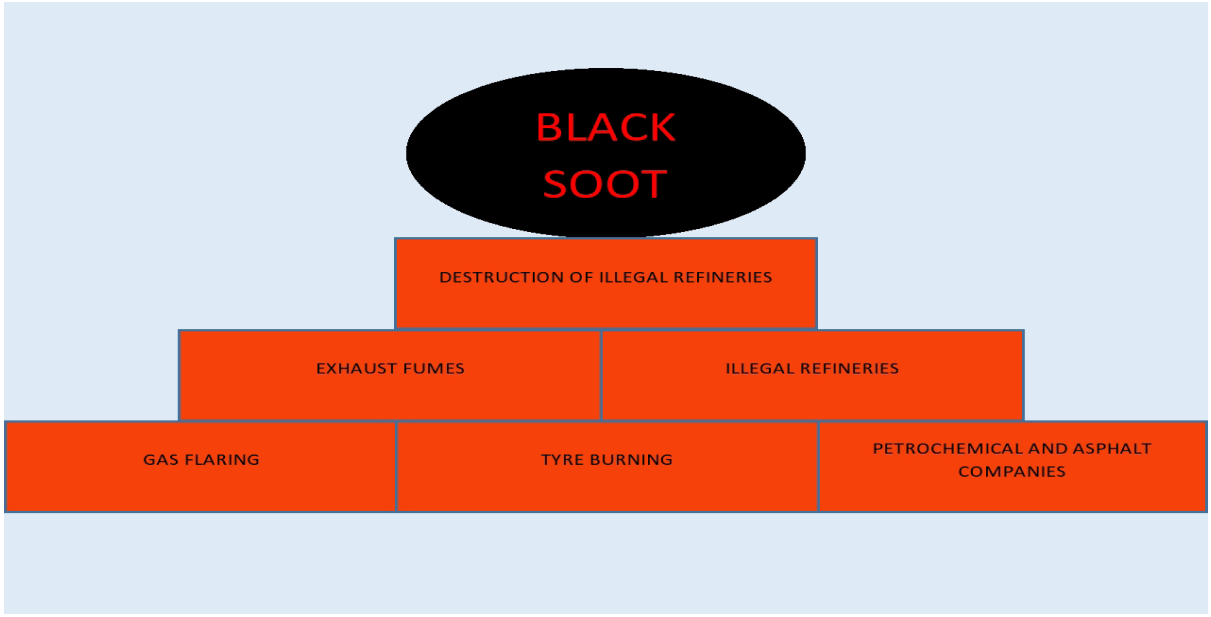

Figure 4. Sources of black soot.

2.4 Health Implications of Black Soot

Exposure to black soot can lead to a generation of cancerous cells in different body tissues by DNA methylation and histone modification, which provokes a lack of control over cell growth, changes in nuclear factor kappa B (this regulates cellular differentiation in the body) and trigger C-FOS activation (production of oncogene which overly expresses in many cancers).

Black soot can lead to an alteration in the expression of endothelia molecules or VCAM (vascular cell adhesion molecule). This can trigger various forms of cardiovascular malformation such as coronary heart disease, cardio myopathes and ischemic changes.

Black soot can also affect the respiratory system by affecting the eosinophyl and mast cell infiltration which leads to fibroblast activation, epithelial cell hyperplasia and deposition of extracellular matrix proteins which disintegrates into loss of lung functions or malformation of lung tissues.

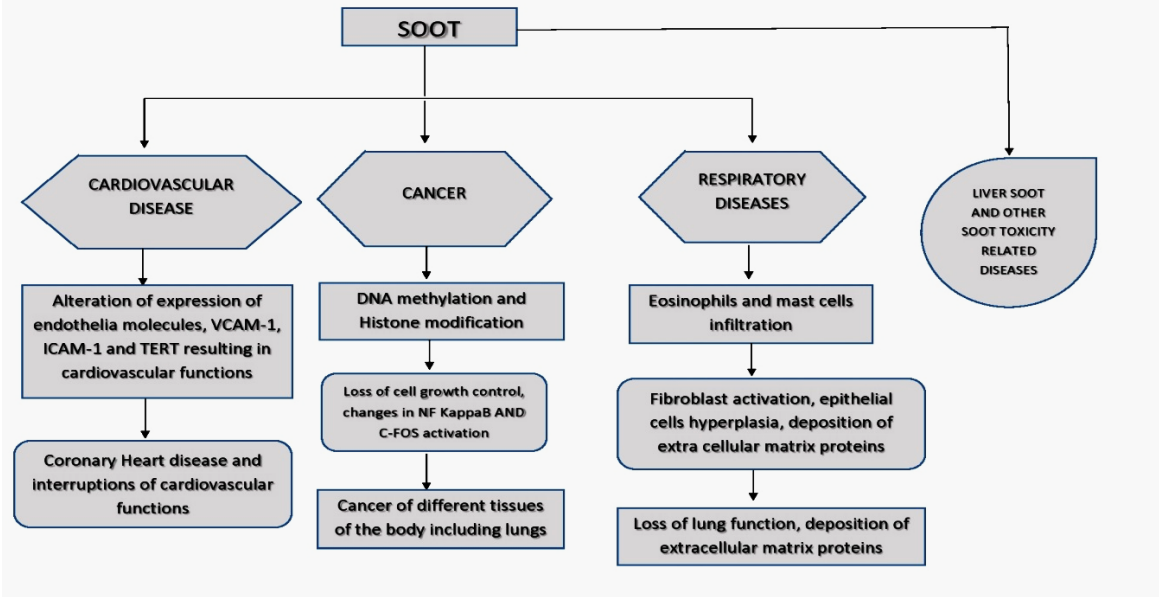

Figure 5. Implications of black soot by Niranjan et al. [10].

Table 1. Health effects of black soot components.

S/N	CHEMICALS FOUND IN THE "BLACK SOOT"	KNOWN HEALTH ADVERSE EFFECT
1.	THE PARTICULATE MATTER (PM)	Particulate Matter particles are >2.5 microns as such can and often do travel deep into the human body and sometimes are absorbed into the blood vessels. They are carcinogenic and often result in hypertension, lung liver and heart diseases. On the skin it is often an irritant, that causes allergic reactions to the eyes, nose, skin diseases.
	THE POLYAROMATIC HYDROCARBONS (PAH)	These are hydrocarbons found in black soot, they are persistent in nature, if introduced into the body system. they tend to remain in the system for a very long time without significant degrading which causes cancer in almost every part of the body.
2.	**GASES**	
	CARBON OXIDES	Heart and Respiratory diseases are common due to exposure to a certain limit of carbon oxide exposure. Dizziness and asphyxiation in extreme cases are also observed.
	SULPHUR OXIDES	Respiratory and heart diseases are generally observed including asthma.
	NITROGEN OXIDES	Hypertention and respiratory diseases often occur.
3.	**METALS**	
	NICKEL	The nickel itch is a common effect of nickel, respiratory, cardiovascular and stomach diseases are common also.
	LEAD	In acute cases shut down of nervous system, impairment of the brain also occurs.
	COBALT	Carcinogenic, causes ulcers and lung disease.
	COPPER	Kidney and liver disease, carcinogenic.
	CHROMIUM	Cardiovascular diseases are carcinogenic and often causes infertility.

Over 2 million deaths yearly are credited to air pollution [10], due to small particulate nature of black soot it travels deep into the human body, some consisting of PAH (poly aromatic Hydrocarbon) which is carcinogenic [10].

3. Material and Method

3.1 Measurement of TSP

Mini Vol Air Samplers were used to collect particulate matter (PM_{10} & $PM_{2.5}$) from the air at six different locations (East-West Road Uniport Junction, GRA Junction, Trans Amadi Slaughter roundabout, Rumuomasi Roundabout, Abuloma Jetty, and New Road Borokiri). To trap the particles, quartz filter papers with a diameter of 47 mm and high purity and efficiency were used. Prior to and after sampling, the Whatman quartz fiber filter papers on which the particles were trapped were stabilized in a desiccator for at least 24 hours to remove any moisture. The quartz filter papers were weighed before and after sampling, and the difference in weight (W2–W1) was used to calculate particulate matter concentrations in g/m^3 using the USEPA method for calculating PM10 (USEPA, 1999).

$$(\text{TSP})\ \mu g/m^3 = \frac{W_2 - W_1}{Q \times T} \times 10^6 \times 10^3$$

where:
W_1 = the initial weight of clean filter paper (g)
W_2 = the final weight of the exposed filter paper (g)
Q = average sampling rate (flow rate), m^3/min
T = Time (hours)
10^6 = g to g/m^3 conversion
10^3 = L to m^3 conversion

"The miniVol samplers' flow rates were set to 5.0 L/min." On each monitoring site, sampling was carried out over a twenty-four-hour period (Figure 6). During the sampling period, six (6) samples were collected from six monitoring locations for particulate matter characterization. Each sampling site received a sample identification in order to identify samples collected from each site. The sample identifications were created using the first letter of each sampling site's name, followed by the date of sampling (in subscript). For example, U17/09/18 identifies a sample collected on February 17th, 2020 at East West Road Uniport Junction.

Heavy metal analyses were performed at the Century Laboratory in Port Harcourt.

Figure 6. MiniVol air sampler.

3.2 TSP Extraction and Determination of Heavy Metals

Shimadzu Atomic absorption spectrophotometer was used to determine heavy metal concentrations in TSP (model AA-6650 Series Agilent Technologies). For the extraction process, the USEPA method IO-3.1 (USEPA, 1999) was used.

To remove heavy metals, the TSP-loaded filters were extracted in an acid mixture. This acid mixture was composed of hydrochloric acid and nitric acid in a 3:1 ratio. Each filter paper was carefully placed in a Teflon tube, and 10 mL of the acid mixture was added slowly to cover the samples. The Teflon tubes were sealed and placed in stainless steel bombs, which were then heated at 150 °C for 6 hours on a hot plate.

After allowing the digested samples to cool to room temperature, they were filtered and transferred into polypropylene graduated tubes. The Teflon tubes were rinsed three times with deionized water, filtered, and the contents were mixed with the digested sample in the polypropylene tubes. The resulting solution was diluted to 30 mL with deionized water. The flame atomic absorption spectrophotometer was then used to analyze heavy metals (FAAS). The same method as described for the exposed filter paper was used to prepare an unexposed filter paper as a blank. FAAS detection limits for cadmium and nickel were 0.002 gm^{-3} and 0.001 gm^{-3}, respectively. The detection limits for lead and mercury were 0.009 gm^{-3} and 0.001 gm^{-3}, respectively.

The following equation was used to convert metal concentration units from mg/L to g/m^3:

$$\text{Metal concentrations } (\mu g/m^3) = \frac{(C_1 - C_2) \times v}{W_t} \times 10^{-6}$$

where:
C_1 = metal concentration in the sample solution (mg/L)
C_2 = metal concentration in the blank filter solution (mg/L)
V = sample solution volume (mL)
W_t = particle weight on quartz filter paper (g)
10^{-6} = grams (g) to cubic meters (m^3) conversion

PAHs Analysis

The air filter particulate samples were extracted using USEPA 355 °C standard method. The filter paper was shredded and weighed into a 100 mL beaker made of borosilicate material and 5 mL of dichloromethane was added to the sample. The beaker and the content were placed in a sornicator to extract the hydrocarbons for 20 minutes. The extract was filtered into an extraction bottle, and the process was repeated to recover any adherent hydrocarbon content that was left during the first extraction. The total extract obtained was concentrated to 1 mL prior to GC/FID analysis I in accordance with USEPA 8015C standard method. The GC/FID was calibrated using 35 components TPH standards, manufactured by ACUU standard USA. The model of the Agilent GC/FID is 6890N series. The concentration of TPH was calculated as follows:

The air volume is calculated from the periodic flow reading taken during sampling using the following equation:

$$QXT = V$$

where:
Q denotes the average flow rate of sampling in m^3/minutes
T = sampling time in minutes
V = total sample volume in m^3 at ambient conditions

C (g/m^3 = Cs*Ve/V_1*Vs) gives the concentration of TPH compound in g/m^3 in the air sampled.
Where Cs concentration of TPH in g/mL is recorded by capital GC in the sample extract.

3.3 Data Analysis

Correlation, time series analysis and scatter plot will be used in the analysis of the data.

4. Results and Discussion

4.1 Results

4.1.1 PM_{10} Concentrations

Figure 7 compares the mean $PM_{2.5}$ and PM_{10} concentrations at the various sampling sites to WHO guideline values.

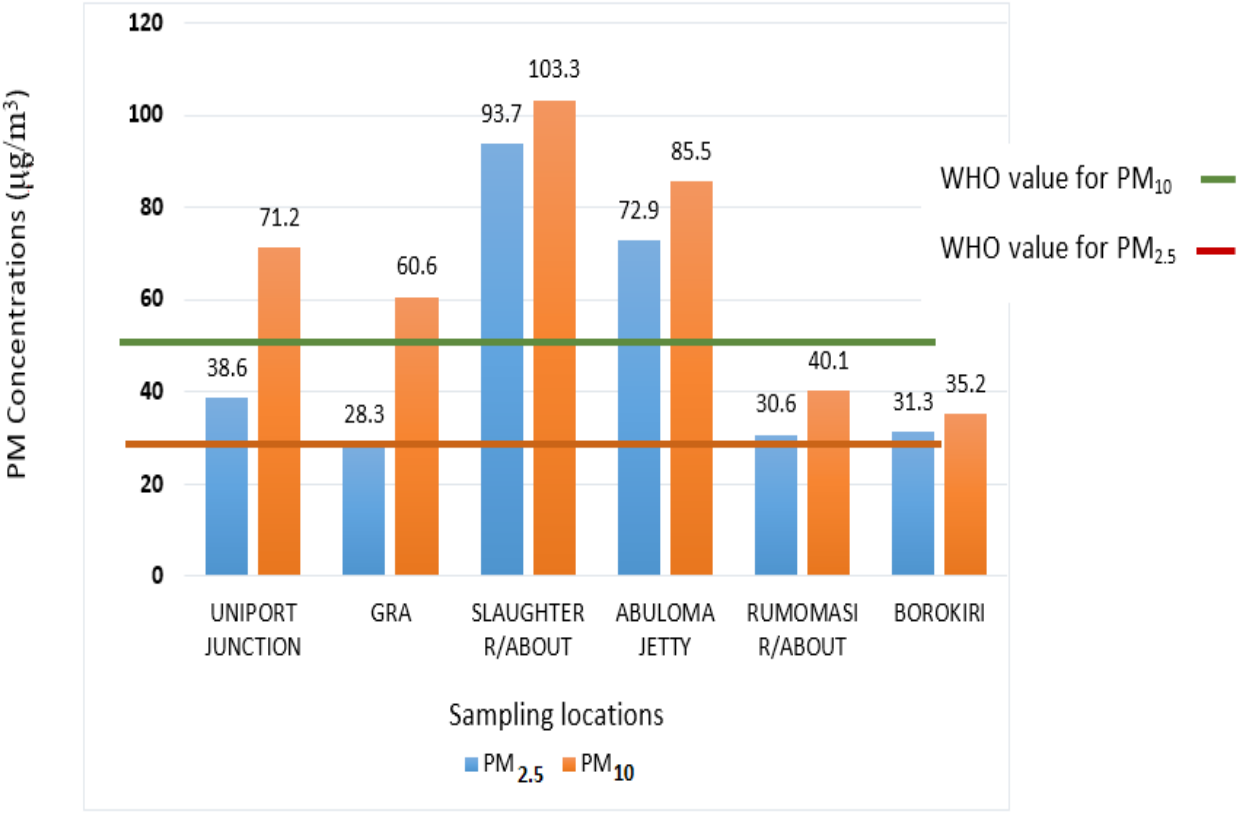

Figure 7. Mean $PM_{2.5}$ and PM_{10} concentrations at the sampling sites.

$PM_{2.5}$ and PM_{10} values recorded at all six sampling sites exceeded the 24-hour guideline values of 25 µg/m^3 and 50 µg/m^3 respectively from WHO. Slaughter roundabout recorded the highest mean PM_{10} concentrations (103.30 µg/m^3) followed by Abuloma jetty (85.50 µg/m^3), Uniport Junction (71.2 µg/m^3) , GRA(60.60 µg/m^3) , Rumomasi R/about (40.10 µg/m^3) and New road Borokiri (35.2 µg/m^3). For $PM_{2.5}$, Slaughter roundabout recorded the highest mean concentrations (93.70 µg/m^3) while New road Borokiri recorded the least mean concentration (31.3 µg/m^3).

$PM_{2.5}$ & PM_{10} concentrations recorded at Slaughter roundabout are the highest probably due to heavy vehicular traffic and mass burning in the slaughter while the least PM concentration is at GRA possibly due to low industrial activity. Meanwhile the overall mean $PM_{2.5}$ and PM_{10} concentration for the six sites respectively are 49.23 µg/m^3 and 65.98 µg/m^3.

Table 2. Daily $PM_{2.5}$ & PM_{10} concentrations at the sampling sites.

SAMPLING SITE	$PM_{2.5}$ MEAN (µg/m^3)	PM_{10} MEAN (µg/m^3)
UNIPORT JUNCTION	38.6	71.2
GRA	28.3	60.6
SLAUGHTER R/ABOUT	93.7	103.3
ABULOMA JETTY	72.9	85.5
RUMOMASI R/ABOUT	30.6	40.1
NEW ROAD BOROKIRI	31.3	35.2

4.1.2 Metal Concentrations at Different Sampling Locations

Metal concentrations measured at various sampling sites were compared to EPA cancer target risk (1 in one million) and European Union air quality standards.

As shown in Table 3, the highest concentration of lead is 0.532 g/m^3 at Abuloma jetty, which is slightly higher than the European Union AQS guideline value of 0.5 g/m^3 and also higher than the EPA cancer target risk of 0.03 g/m^3.

Table 3. The lead (Pb) concentrations in g/m^3 at the various sampling sites.

Sampling Site	Mean	Reference guideline/value
UNIPORT JUNCTION	<0.009	
GRA	<0.009	
SLAUGHTER R/ABOUT	0.490	0.5 µg/m^3 (EU AQS)
ABULOMA JETTY	0.532	0.03 µg/m^3 (EPA cancer TR)
RUMOMASI R/ABOUT	0.021	
BOROKIRI	0.017	

The mean Concentrations of Mercury for the six sampling locations were below 0.001 µg/m^3 which is below 0.014 µg/m^3 (US EPA National Ambient levels at urban sites) as shown in Table 4 below.

Table 4. Mercury (Hg) concentrations in µg/m^3 at the various sampling sites.

Sampling Site	Mean	Reference guideline/value
UNIPORT JUNCTION	0.001	
GRA	0.001	
SLAUGHTER R/ABOUT	0.001	0.014 µg/m^3 (US EPA National ambient Air concentration for urban environment)
ABULOMA JETTY	0.001	
RUMOMASI R/ABOUT	0.001	
BOROKIRI	0.001	

From Table 5 shown below, the highest mean Concentration of cadmium is 0.544 µg/m^3 at slaughter roundabout which is below 0.6 µg/m^3 (US EPA National Ambient levels at industrial sites) but above EPA cancer target risk (1 in one million) of 0.0014 µg/m^3.

Table 5. Cadmium (Cd) concentrations in µg/m^3 at the various sampling sites.

Sampling Site	Mean	Reference guideline/value
UNIPORT JUNCTION	0.002	
GRA	0.002	0.6 µg/m^3 (US EPA National ambient Air concentration for industrial environment) 0.0014 µg/m^3 (EPA (cancer TR)
SLAUGHTER R/ABOUT	0.544	
ABULOMA JETTY	0.41	
RUMOMASI R/ABOUT	0.011	
BOROKIRI	0.011	

From Table 6 below, the highest mean concentration of chromium is 0.338 µg/m^3 at slaughter roundabout which is below 0.4 µg/m^3 (US EPA National Ambient levels at industrial sites).

Table 6. Chromium (Cr) concentrations in µg/m^3 at the various sampling sites.

Sampling Site	Mean	Reference guideline/value
UNIPORT JUNCTION	0.012	
GRA	0.01	0.4 µg/m^3 (US EPA National ambient Air concentration for industrial environment)
SLAUGHTER R/ABOUT	0.338	
ABULOMA JETTY	0.274	
RUMOMASI R/ABOUT	0.002	
BOROKIRI	0.009	

From Table 7 below, the highest mean Concentration of Nickel is 0.407 µg/m^3 at Abuloma jetty which is above 0.17 µg/m^3 (US EPA National Ambient levels at industrial sites) and 0.01 µg/m^3 (EPA cancer target risk for 1 in one million).

Table 7. Nickel (Ni) concentrations in µg/m^3 at the various sampling sites.

Sampling Site	Mean	Reference guideline/value
UNIPORT JUNCTION	0.017	
GRA	0.001	0.17 µg/m^3 (US EPA National ambient Air concentration for industrial environment) 0.01 µg/m^3 (EPA cancer TR)
SLAUGHTER R/ABOUT	0.432	
ABULOMA JETTY	0.407	
RUMOMASI R/ABOUT	0.005	
BOROKIRI	0.016	

4.1.3 Heavy Metals in Particulate Matter Fraction

From Figure 8 below, it could be observed that the total PM concentration recorded across the six sampling sites constitutes 30% lead, 27% cadmium, 25% Nickel, 18% Chromium and 0% mercury. The most abundant metal in PM fraction is lead.

The pie chart shows the percentage composition of heavy metals in the PM fraction across the six sampling sites.

4.1.4 Correlation between Particulate Matter Concentration and Meteorological Parameters

From Figure 9 below, we can see a strong positive relationship between $PM_{2.5}$ and PM_{10} (r = 0.87) which can also be seen in Figure 9 straight line. We can see that $PM_{2.5}$ and PM_{10} have a weak but positive correlation with relative humidity and wind speed respectively. Meanwhile $PM_{2.5}$ and PM_{10} (r = –0.19, r = –0.20) have a weak and negative correlation with temperature respectively.

4.1.5 Correlation between Heavy Metals and Meteorological Parameters

Figure 10 below shows there is a strong positive correlation between heavy metals and PAHs. We can also see a weak and positive correlation between relative humidity, wind speed and heavy metals. While there exists a weak and negative relationship between heavy metals and temperature. Important to state is also the negative relationship that exists between wind speed, temperature and PAHs. But relative humidity is positively correlated with Poly Aromatic Hydrocarbons (PAHs).

4.1.6 Trend Analysis Concentration of $PM_{2.5}$ & PM_{10} Varies with Meteorological Parameters

Figure 11 shows that high particulate matter concentration occurs at a wind speed of 0.6 m/s to 0.62 m/s while the least PM concentration occurred at a wind speed range of 2.34 m/s to 2.86 m/s.

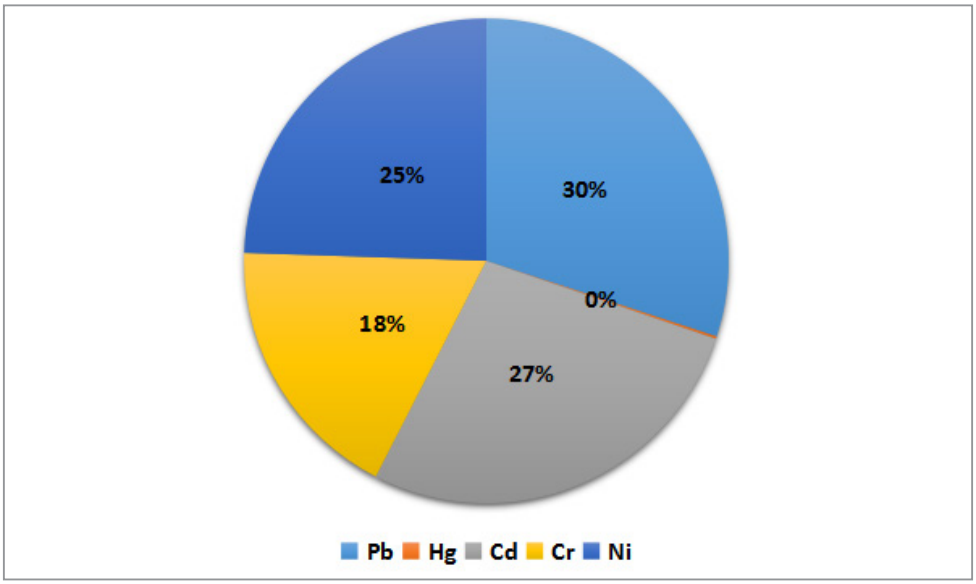

Figure 8. Percentage concentrations of heavy metals in PM fraction.

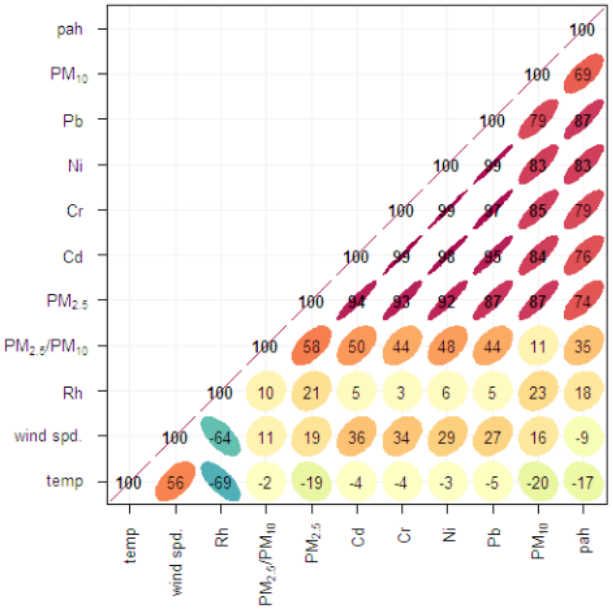

Figure 9. Correlation plot showing the relationship between pollutant and meteorological parameters.

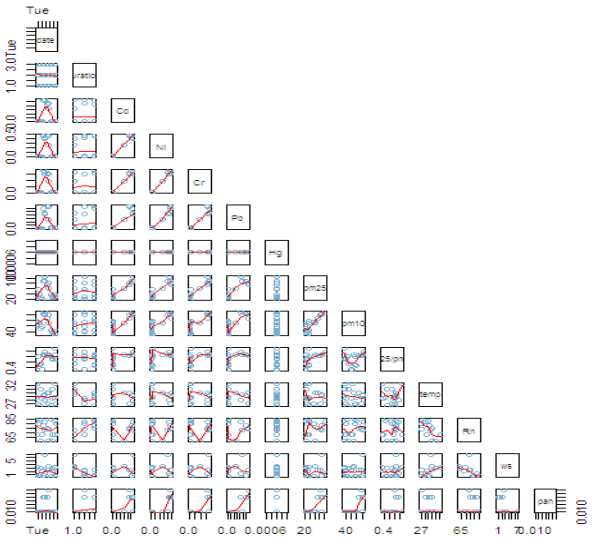

Figure 10. Pair plot showing correlation between heavy metals and meteorological parameters.

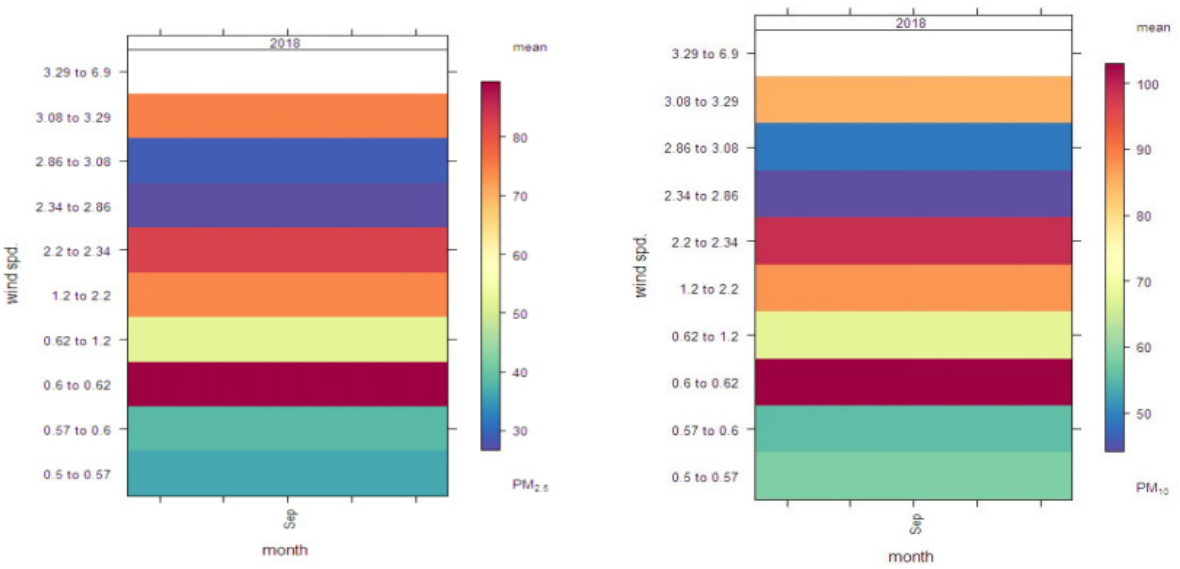

Figure 11. Trend plot showing variation in $PM_{2.5}$ & PM_{10} against wind speed.

Figure 12 shows that high particulate matter concentration occurs at a temperature range of 27.1 °C to 28.5 °C while the least PM concentration occurred at a temperature range of 30.6 °C to 31.5 °C.

Figure 13 shows that high particulate matter concentration occurs at a relative humidity range of 78.5% to 80.1% while the least PM concentration occurred at a relative humidity range of 61.5% to 68.1%.

4.1.7 Trend Analysis Concentration of $PM_{2.5}$ & PM_{10} Varies with Time

The diurnal (hourly) plot shows that $PM_{2.5}$ and PM_{10} concentrations are highest in the evening and lowest in the afternoon. Meanwhile, the day of the weak plot shows that the highest PM concentration was on Wednesday at the slaughter roundabout monitoring location. The calendar plot in Figures 14 and 15 equally confirmed that Wednesday 19th September experienced the highest particle pollution at Slaughter roundabout.

Figure 16 shows a ratio of 0.79 in the morning, 0.63 in the afternoon and a ratio of 1.1 in the evening depicting predominance of $PM_{2.5}$ fraction in all the areas in the day. But the mean $PM_{2.5}/PM_{10}$ ratio is 0.74.

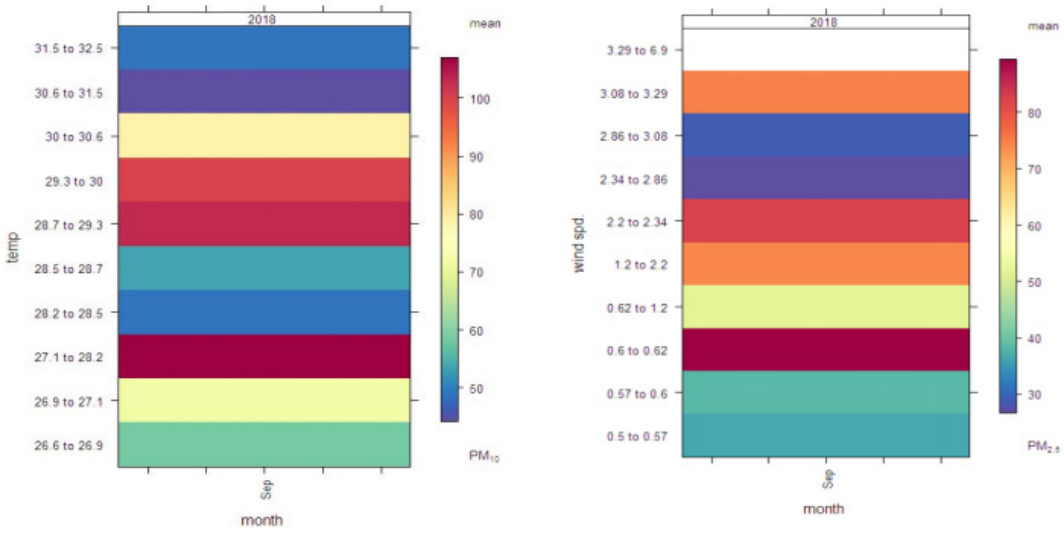

Figure 12. Trend plot showing variation in $PM_{2.5}$ & PM_{10} against temperature.

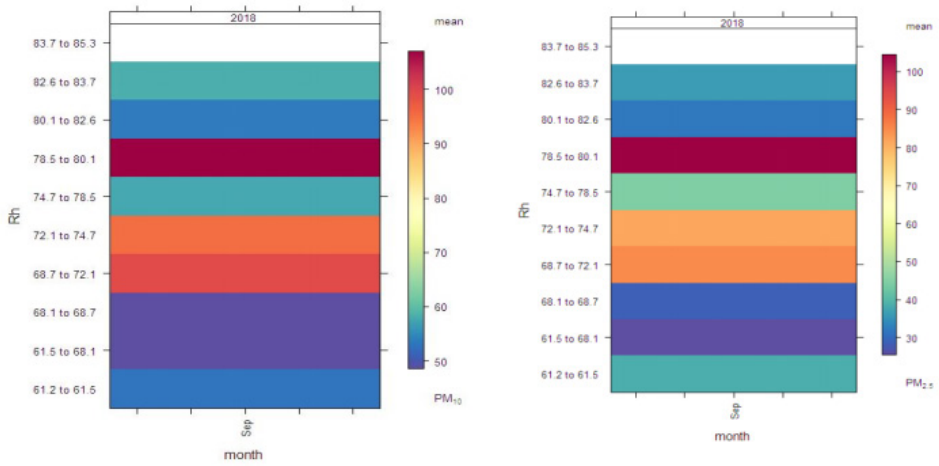

Figure 13. Trend plot showing variation in $PM_{2.5}$ & PM_{10} against relative humidity.

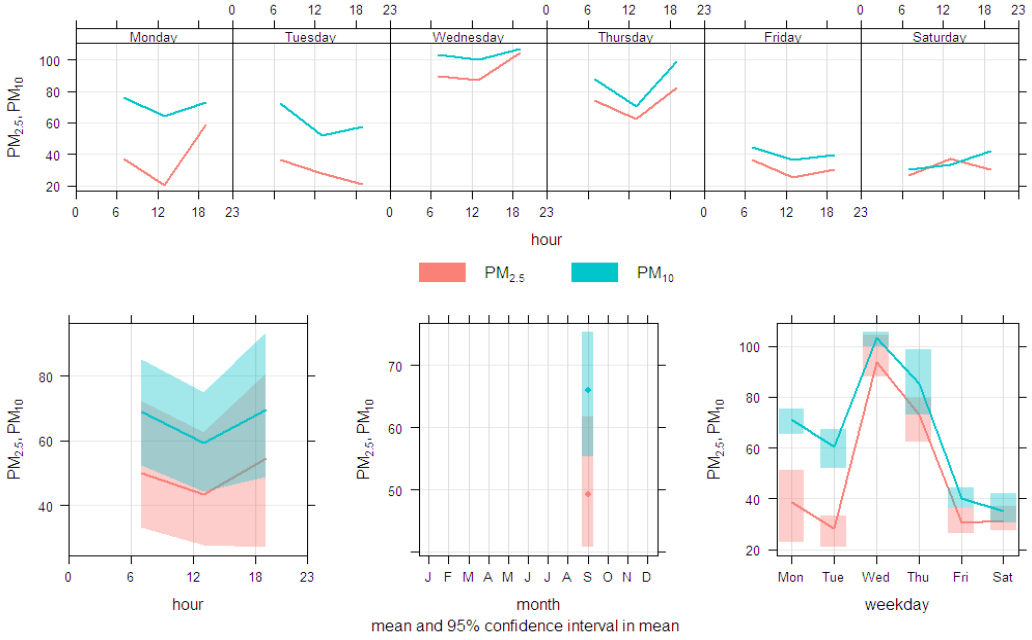

Figure 14. Time variation plot showing how $PM_{2.5}$ & PM_{10} varies with time at the monitoring sites.

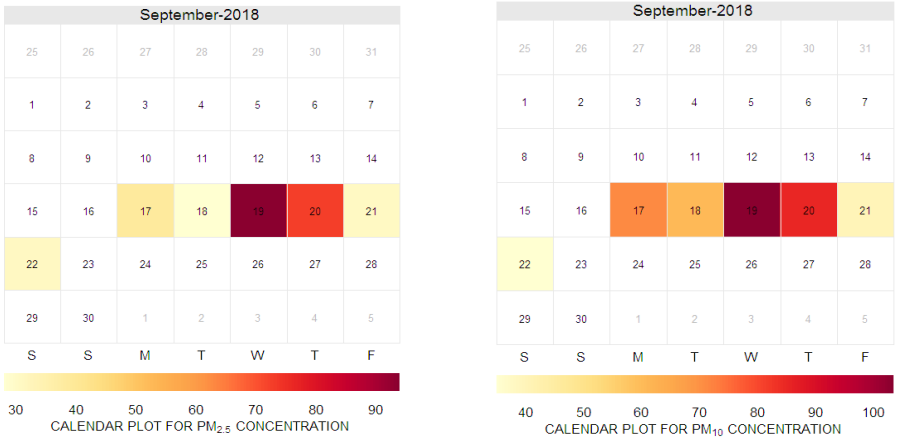

Figure 15. Calendar plot for $PM_{2.5}$ & PM_{10} concentration.

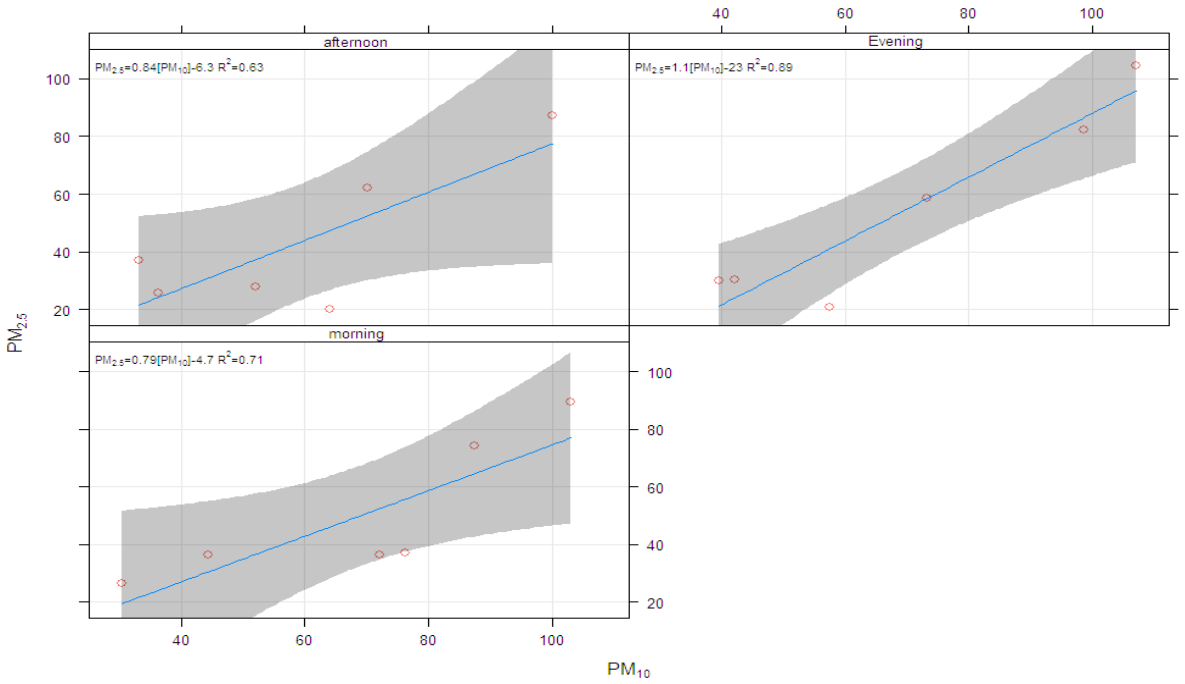

Figure 16. Scatter plot showing $PM_{2.5}/PM_{10}$ ratio.

4.2 Discussion

4.2.1 Particulate Matter

From Figure 7, it could be deduced that Slaughter roundabout had the highest mean $PM_{2.5}$ and PM_{10} concentrations of 103.3 µg/m^3 and 93.7 µg/m^3 respectively. GRA monitoring recorded the least $PM_{2.5}$ (28.3 µg/m^3). From Figure 7 it could be seen that $PM_{2.5}$ and PM_{10} concentrations for the six locations are above the WHO recommended value of 25 µg/m^3 and 50 µg/m^3 in 24 hours. It then means that these locations are non-attainment areas with particle pollution.

4.2.2 Heavy Metals Concentration in Particulate Mater

From Figure 8 above, it could be observed that the total PM concentration recorded across the six sampling sites constitutes 30% lead, 27% cadmium, 25% Nickel, 18% Chromium and 0% mercury. The most abundant metal in PM fraction is lead.

From Table 3, the highest concentration of lead is 0.532 g/m^3 at Abuloma jetty, which is slightly above the European Union AQS guideline value of 0.5 g/m^3 and also above the EPA cancer target risk of 0.03 g/m^3. All the sites have a value below the reference value except for Slaughter junction, which has the highest value. The high value of lead at the location can be attributed to the burning of oil and leaded waste. It is a serious public health concern because, at a high exposure level, most organs and systems, such as the kidneys and central nervous system, are injured.

According to Table 5, the highest mean concentrations of cadmium are 0.544 g/m^3 at the slaughter roundabout, which is less than 0.6 g/m^3 (US EPA National Ambient levels at industrial sites) but greater than the EPA cancer target risk (1 in one million) of 0.0014 g/m^3. According to the USEPA, it is carcinogenic to humans. Prolonged exposure to cadmium may cause renal dysfunction which may in turn lead to devastating bone disease in people with risk factors like poor nutrition. People who live in cadmium-polluted areas are more likely to develop diseases such as osteoporosis and have a higher risk of fractures. Vehicle exhaust emissions, including tyre abrasion; open burning of municipal waste containing Ni-Cd batteries; and plastics containing cadmium pigments are all potential sources of cadmium.

According to Table 4, the mean Mercury concentrations for the six sampling locations were less than 0.001 g/m^3, which is less than 0.014 g/m^3 (US EPA National Ambient levels at urban sites). Except for regional "hot spots", mercury levels in outdoor air are typically in the order of 0.005 g/m^3-0.010 g/m^3 and thus are marginal when compared to exposure from dental amalgam, according to WHO guidelines. At these air levels, exposure to mercury from outdoor air is not expected to have a direct impact on human health. However, to avoid potential health effects in the near future, mercury levels in the ambient air should be kept as low as possible.

According to Table 7, the highest mean concentration

of nickel is 0.407 g/m^3 at Abuloma jetty, which is higher than 0.17 g/m^3 (US EPA National Ambient levels at industrial sites) and 0.01 g/m^3 at other locations (EPA cancer target risk for 1 in one million). Nickel exposure has been linked to chronic bronchitis, reduced lung function, lung cancer, and nasal sinusitis. The EPA has determined that nickel refinery dust and nickel subsulfide are carcinogens to humans. The primary source of anthropogenic nickel emissions is oil combustion, which could explain the high concentration at Abuloma jetty.

According to Table 6, the highest mean concentration of chromium is 0.338 g/m^3 at the slaughter roundabout, which is less than 0.4 g/m^3 (US EPA National Ambient levels at industrial sites).

Chromium (III) is a trace element that is required by both humans and animals. Chromium(VI) compounds are toxic and carcinogenic, but the potencies of the various compounds vary greatly. Because the bronchial tree is the primary target organ for the carcinogenic effects of chromium (VI) compounds, and cancer is primarily caused by inhalation exposure, uptake in the respiratory organs is extremely important in terms of cancer hazard and subsequent risk of cancer in humans. According to the IARC, there is sufficient evidence of carcinogenicity in humans for chromium and certain chromium compounds.

4.2.3 Correlation between Particulate Matter Concentration and Meteorological Parameters

From Figure 9 we can see a strong positive relationship between $PM_{2.5}$ and PM_{10} (r = 0.87) which can also be seen in Figure 10 straight line. We can see that $PM_{2.5}$ and PM_{10} have a weak but positive correlation with relative humidity and wind speed respectively. Meanwhile $PM_{2.5}$ and PM_{10} (r = –0.19, r = –0.20) have a weak and negative correlation with temperature respectively. It therefore shows that wind speed and relative humidity slightly increases particulate matter concentration while increase in temperature slightly reduces PM concentration. However, increase in $PM_{2.5}$ gives rise to a corresponding increase in PM_{10} concentration.

4.2.4 Correlation between Heavy Metals and Meteorological Parameters

Figures 10 and 9 show there is a strong positive correlation between heavy metals and PAHs. We can also see a weak and positive correlation between relative humidity, wind speed and heavy metals. While there exists a weak and negative relationship between heavy metals and temperature. Important to state is also the negative relationship that exists between wind speed, temperature and PAHs. But relative humidity is positively correlated with Poly Aromatic Hydrocarbons (PAHs). It shows that PAHs increase as heavy metals increase in particulate matter showing a possibility of related origin. Also, relative humidity and wind speed slightly increase concentration of heavy metals in PM while temperature does not allow heavy metals to bond with PM. Relative humidity increases the concentration of PAHs in particulate matter.

4.2.5 Trend Analysis Showing How Concentration of $PM_{2.5}$ & PM_{10} Varies with Meteorological Parameters

Figure 11 shows that high particulate matter concentration occurs at a wind speed of 0.6 m/s to 0.62 m/s while the least PM concentration occurred at a wind speed range of 2.34 m/s to 2.86 m/s. This indicates that at low wind speed when the atmosphere is relatively stable, they tend to be more PM concentration due to lack of dispersion.

Figure 12 shows that high particulate matter concentration occurs at a temperature range of 27.1 ºC to 28.5 ºC while the least PM concentration occurred at a temperature range of 30.6 ºC to 31.5 ºC. It explains the fact that high temperature aids in air turbulence which consequently disperses the particulate matter.

Figure 13 shows that high particulate matter concentration occurs at a relative humidity range of 78.5% to 80.1% while the least PM concentration occurred at a relative humidity range of 61.5% to 68.1%. It clearly shows that high relative humidity does not support air dispersion instead it encourages suspension of PM in the air.

4.2.6 Trend Analysis Showing How Concentration of $PM_{2.5}$ & PM_{10} Varies with Time

The diurnal (hourly) plot shows that $PM_{2.5}$ and PM_{10} concentrations are highest in the evening and lowest in the afternoon. Meanwhile, the day of the weak plot shows that the highest PM concentration was on Wednesday at slaughter roundabout monitoring location. The calendar plot in Figure 15 equally confirmed that Wednesday 19th September experienced the highest particle pollution at Slaughter roundabout. The reason for high PM concentration in the evening and morning could be attributed to peak hours that entail high vehicular movement. There is a lot of human activities happening at slaughter roundabouts such as vehicular movement, mass burning and other commercial activities which gave rise to high PM concentrations.

4.2.7 PM Ration

According to WHO guidelines $PM_{2.5}/PM_{10}$ ratio within

the range of 0.5-0.8 shows predominance of $PM_{2.5}$ fraction while ratios below show dominance of PM_{10}. Figure 16 shows a ratio of 0.79 in the morning, 0.63 in the afternoon and a ratio of 1.1 in the evening depicting predominance of $PM_{2.5}$ fraction in all the areas in the day. But the mean $PM_{2.5}/PM_{10}$ ratio is 0.74 which is within the WHO range for developing countries. This high $PM_{2.5}/PM_{10}$ ratio is an indication that we have a predominance of $PM_{2.5}$ in the ambient air.

5. Conclusions

The result of the investigation shows the ambient air at the six monitoring sample stations was heavily polluted with $PM_{2.5}$ and PM_{10}. The PM concentrations exceeded the WHO (2010) guideline value, which could be the cause of the current PM episode in Port Harcourt, resulting in asthma, lung cancer, breathing difficulties, and miscarriages among pregnant women, which have affected the health implications of the people living in the environment. However, the constituents of PM contain heavy metals in extremely low concentrations that are unlikely to endanger human health due to their short half-life. Despite the fact that the PM concentrations recorded in this study were extremely high, the metal constituents have a low lifetime risk.

Recommendation

The need for more research to be conducted during both the wet and dry seasons to determine both seasonal and temporal variability, as well as long-term studies to determine the effects of PM on public health.

Conflict of Interest

There is no conflict of interest.

References

[1] WHO, 2010. Health and Environment in Europe: Progress Assessment. Copenhagen: WHO Regional Office for Europe.

[2] Alberini, A., Krupnick, A.,1998. Air quality and episodes of acute respiratory illness in Taiwan cities: Evidence from survey data. Journal of Urban Economics. 44, 68-92.

[3] Ede, P.N., Edokpa, D.O., 2017. Satellite determination of particulate load over Port Harcourt during black soot incidents. Journal of Atmospheric Pollution. 5(2), 55-61. Available from: https://pubs.sciepub.com/jap/5/2/3/index.html

[4] Durdina, L., Lobo, P., Trueblood, M.B., et al., 2016. Response of real-time black carbon mass instruments to mini-CAST soot. Aerosol Science and Technology. 50(9), 906-918.

[5] Report of Nigeria's National Population Commission on the 2006 Census [Internet]. Population and Development Review. 33(1), 206-210. Available from: http://www.jstor.org/stable/25434601

[6] Gobo, A.E., Richard, G., Ubong, I.U., 2010 Health impact of gas flares on Igwuruta/Umuechem communities in Rivers State. Journal of Applied Sciences & Environmental. 13, 27-33.

[7] Swemgba, H., Ahiarakwem Cosmas, A., Nwankwor Godwin, I., et al., 2019. Air quality index assessment in some parts of Porthacourt Metropolis, Nigeria. International Journal of Environment and Pollution Research. 7(4), 1-20.

[8] Weli, E.V., 2014. Atmospheric concentration of particulate pollutants and its implications for respiratory health hazard management in Port Harcourt metropolis, Nigeria. Civil Environmental Research. 9, 11-17.

[9] Nwachukwu, A.N., Chukwuocha, E.O., Igbudu, O., 2012. A survey on the effects of air pollution on diseases of the people of Rivers State, Nigeria. African Journal of Environmental Science & Technology. 6, 371-379.

[10] Niranjan, R., Thakur, A.K., 2017. The toxicological mechanisms of environmental soot (black carbon) and carbon black: Focus on oxidative stress and inflammatory pathways. Frontiers in Immunology. 8, 763.
DOI: https://doi.org/10.3389/fimmu.2017.00763

[11] WHO, 2005. Air Quality Guidelines for Particulate, Matter, Ozone, Nitrogen Dioxide and Sulfur Dioxide: Global Update 2005.

[12] National Environmental Standards and Regulations Enforcement Agency (Establishment), 2007 [Internet]. Available from: https://www.placng.org/lawsofnigeria/laws/nesrea.pdf

BILINGUAL PUBLISHING CO.
Pioneer of Global Academics Since 1984

Journal of Environmental & Earth Sciences
https://ojs.bilpublishing.com/index.php/jees

ARTICLE

Promoting Pedestrian Transportation to Reducing Air Pollution from Urban Transport

Emre Kuşkapan[1*] Muhammed Yasin Çodur[2]

1. Civil Engineering Department, Faculty of Architecture and Engineering, Erzurum Technical University, Erzurum, Turkey
2. College of Engineering and Technology, American University of the Middle East, Kuwait

ARTICLE INFO

Article history
Received: 29 March 2022
Accepted: 26 April 2022
Published Online: 5 May 2022

Keywords:
Air pollution
Urban transport
Pedestrians

ABSTRACT

Increasing air pollution around the world causes many problems, especially in the field of health. Air pollution affects not only human health but also other living things' health. The factors that cause air pollution the most are heating, industry, and transportation. Many countries in the world carry out various studies to reduce the effect of these factors on air pollution. Especially in the field of transportation, studies have been done quite a lot in recent years. In this study, air pollution caused by transportation in Erzurum, Turkey has been investigated. Emission amounts of NO_X, PM_{10}, and SO_2 values have been calculated according to the types of vehicles in the city. Then, the amount of emissions from transportation in the total sector has been revealed. The transportation structure of the city has examined in general terms and the missing aspects in terms of pedestrian transportation have been revealed. Finally, some solution proposals aiming to encourage the use of pedestrian transportation and micro mobility vehicles in order to reduce motor land vehicles are presented.

1. Introduction

Air pollution is the presence of foreign substances in the air in the form of solids, liquids and gas in the atmosphere in an amount, density and for a long time that will harm human health, living life and ecological balance. The air layer is polluted with the wastes generated during the production and consumption activities that occur as a result of various activities of people, negatively affecting the living life on earth. There are natural and artificial factors affecting air pollution. While natural factors usually occur with natural events, artificial factors emerge with the effect of humans. The three biggest artificial factors affecting air pollution are heating, industry and transportation sectors [1].

Air pollution originating from these sectors may differ according to the region. In regions where industrial facilities are very concentrated, air pollution originating from

*Corresponding Author:
Emre Kuşkapan,
Civil Engineering Department, Faculty of Architecture and Engineering, Erzurum Technical University, Erzurum, Turkey;
Email: emre.kuskapan@erzurum.edu.tr

DOI: https://doi.org/10.30564/jees.v4i1.4570

the industrial sector is high. Air pollution in the heating sector is high in regions where the winter period is long and coal-derived fuels are used frequently. In areas where road vehicles using fossil fuels are heavily used, air pollution from transportation is higher [2,3].

Air pollution from transportation is affected by driving patterns, speed and traffic congestion, altitude, meteorological conditions, vehicle type, size, age, technical inspection, exhaust inspection and most importantly, emission control equipment and its maintenance. Especially old motor vehicles, vehicles that do not have periodic maintenance and repair, vehicles with carburetors, vehicles carrying loads above the limit, bad roads and traffic congestion cause an increase in air pollution [4,5].

Due to the increase in air pollution caused by transportation in the world, many studies are carried out in this field. A significant part of the studies carried out by considering the effect of the transportation sector on air pollution reveals the necessity of making some changes in this sector [6-8]. Some studies examine the negative effects of air pollution from transportation on human health and the environment [9,10]. Harmful gases in the air can significantly damage people's respiratory systems [11]. Problems that occur in the respiratory system can progress seriously enough to cause cancer later on. Harmful gases in the air can adversely affect animals and plants as well as humans. In areas with intense air pollution, some animal species may become uninhabitable. Similarly, intense air pollution can cause vegetation to change [12,13].

Especially in the city centers, the high number of road vehicles and the traffic jams in these regions increase the air pollution that may occur. Therefore, in studies dealing with transportation-related air pollution, city centers are generally examined. For example, due to the COVID-19 epidemic, which has been affecting the world since 2019, lockdowns occurred at certain times in various parts of the world. In these periods, it has been observed from the studies that air pollution has decreased significantly, especially in urban centers. Because in these periods, people did not feel the need to go to work or school because they stayed at home. For this reason, since they do not provide transportation to any place by vehicles, harmful gas emissions in cities have decreased [14-16].

Some of the studies affecting the air pollution of transportation deal with the economic costs caused by this air pollution. Because it is necessary to apply some treatments in order to improve the health problems caused by air pollution. These treatments can also be provided with serious costs. In addition, the cleaning of particles released from transportation incurs certain costs [17,18].

There are many studies examining the transportation sector and air pollution [19,20]. These studies provide readers with important information to reduce air pollution. In addition, the results obtained from these studies can offer important ideas to policy makers or local governments. In addition to the existing studies in this field, new studies are being conducted every day that examine the relationship between transportation and air pollution.

In this study, motor road vehicles in Erzurum province have been examined separately according to their types and fuel types. Annually released NO_X, PM_{10} and SO_2 gas amounts have been calculated for each species. Then, the gas emissions from the transportation sector and the gas emissions from the industry and heating have been compared and the share of transportation in air pollution has been revealed. Finally, some suggestions have been made to reduce air pollution caused by transportation in the city. It has stated that some studies should be prioritized especially in order to encourage pedestrian transportation.

2. Materials and Methods

2.1 Study Area

The city of Erzurum, used as the study area, is located at an altitude of 1900 meters above sea level and in the eastern part of Turkey. The population of the city is approximately 750 thousand as of 2021. Road vehicles are used in urban transportation. The total number of motor road vehicles in the city is approximately 117 thousand. Cars and trucks cover a large part of this number of vehicles [21,22]. The location of Erzurum, the study area, is shown in Figure 1.

2.2 Data Processing

Most of the data used in the study have been obtained from the reports of the Provincial Directorate of Environment and Urbanization [23]. An inventory of traffic activity data has been created by the staff of the Provincial Directorate of Environment and Urbanization, in written and one-on-one interviews with the institutions. The length of roads and vehicle counts in Erzurum Province have been obtained from the Erzurum Metropolitan Municipality Presidency (Directorate of Transportation and Urban Planning), and the number of vehicles according to the motor types and fuel types in the traffic in the city have been obtained by the Turkish Statistical Institute and the Provincial Police Department (Traffic Registration Branch Directorate) [24-27]. From the records of Vehicle Maintenance Services operating in Erzurum province, the average annual fuel consumption and annual road distances have been determined according to vehicle types. Annual fuel amounts sold in Erzurum have been also obtained from the Energy Market Regulatory Authority and compared

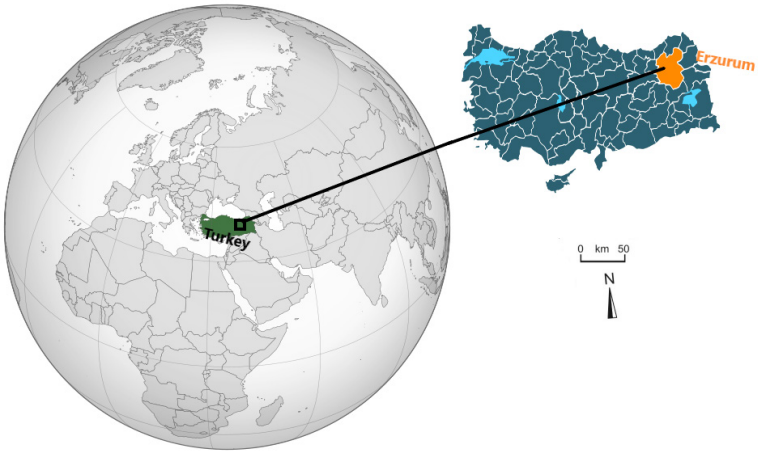

Figure 1. Location of study area.

with the fuel consumed by the vehicles. Defined fuel and vehicle subcategories: Air pollutant emissions can reach significant levels around main streets, intersections and highways where traffic is intense.

Table 1 below shows the statistics including the types of vehicles in Erzurum and the types of fuel they use.

The main emissions from vehicles are NO_2, CO, HC, SO_2, PM and lead in PM. Although PM emissions from exhaust gases are low, they should be carefully examined in terms of threatening human health and nature due to the lead they contain. These emissions from vehicles depend on parameters such as vehicle age, engine operating speed, operating temperature, ambient temperature, ambient pressure, fuel type and quality. In the study, different emission factors have been used according to each vehicle type and fuel type. These factors have been determined by the Ministry of Environment and Urbanization. Emission factors determined according to vehicle types are given in Table 2.

Table 1. Number of vehicles in Erzurum province.

Type of vehicle	Gasoline	Diesel	LPG	Total
Truck		5,878		5,878
Small truck		26,645		26,645
Minibus		2,990		2,990
Motorcycle	2,662			2,662
Bus		1,159		1,159
Automobile	15,031	20,917	22,318	58,266
Tractor		19,663		19,663
Total	17,693	77,252	22,318	117,263

Table 2. Emission factors determined by vehicle type.

Type of vehicle	Types of Fuel	Emission Factor (NO_X)	Emission Factor (PM_{10})	Emission Factor (SO_2)
Automobile	Gasoline	14.5	0.03	0.02
Automobile	Diesel	11	1.1	0.02
Automobile	LPG	15.5	0	0.1
Light Vehicle	Gasoline	24	0.02	0.02
Light Vehicle	Diesel	15	1.52	0.02
Light Vehicle	LPG	16	0	0.1
Heavy Vehicle	Gasoline	6.6	0	0.02
Heavy Vehicle	Diesel	37	0.94	0.02
Heavy Vehicle	CNG (Bus)	13	0.02	0.1
Motorcycle	Gasoline	9.5	2.2	0.02

*CNG: compressed natural gas.

3. Results

In order to calculate the amount of emissions from road vehicles in a year, the emission coefficient of each type of vehicle and the amount of fuel used in a year must be taken into account. Total NO_X, PM_{10} and SO_2 gas emissions in a year are given in Tables 3-5, respectively.

When all three tables are examined, the total NO_X emission amount in a year is 4,843.95 tons, the total PM_{10} emission amount is 212.87 tons and the total SO_2 emission amount is 7.70 tons. It is seen that NO_X emission amount is quite higher than PM_{10} and SO_2 emission amount. The reason for this is that the emission coefficient of NO_X is quite high. In order to determine the share of these three emission values in the city's air pollution, it is necessary to compare them with the emission values in the heating and industry sectors. The graph in Figure 2 below shows the sectoral distribution of one-year NO_X, PM_{10} and SO_2 emission values in Erzurum.

Table 3. Total NO_X emission amount in a year.

Traffic Total Emissions (NO_X)				
Type of vehicle	**Types of fuel**	**Emission factor (A)**	**Total fuel (Tons) (B)**	**Total emission (tons/year) (A)*(B)/1000**
Automobile	Gasoline	14.5	13,527.9	196.15
Automobile	Diesel	11	14,641.9	161.06
Automobile	LPG	15.5	40,172.4	622.67
Light Vehicle	Gasoline	24	0	0.00
Light Vehicle	Diesel	15	85,449.5	1,281.74
Light Vehicle	LPG	16	0	0.00
Heavy Vehicle	Gasoline	6.6	0	0.00
Heavy Vehicle	Diesel	37	69,781.84	2,581.93
Heavy Vehicle	CNG (Bus)	13	0	0.00
Motorcycle	Gasoline	9.5	399.3	0.40
Total			223,972.84	4,843.95

Table 4. Total PM_{10} emission amount in a year.

Traffic Total Emissions (PM_{10})				
Type of vehicle	**Types of Fuel**	**Emission Factor (A)**	**Total fuel (Tons) (B)**	**Total emission (tons/year) (A)*(B)/1000**
Automobile	Gasoline	0.03	13,527.9	0.41
Automobile	Diesel	1.1	14,641.9	16.11
Automobile	LPG	0	40,172.4	0.00
Light Vehicle	Gasoline	0.02	0	0.00
Light Vehicle	Diesel	1.52	85,449.5	129.88
Light Vehicle	LPG	0	0	0.00
Heavy Vehicle	Gasoline	0	0	0.00
Heavy Vehicle	Diesel	0.94	69,781.84	65.59
Heavy Vehicle	CNG (Bus)	0.02	0	0.00
Motorcycle	Gasoline	2.2	399.3	0.88
Total			223,972.84	212.87

Table 5. Total SO_2 emission amount in a year.

Traffic Total Emissions (SO_2)				
Type of vehicle	**Types of Fuel**	**Emission Factor (A)**	**Total fuel (Tons) (B)**	**Total emission (tons/year) (A)*(B)/1000**
All vehicles	Gasoline	0.02	13,927.2	0.28
All vehicles	Diesel	0.02	169,873.24	3.40
All vehicles	LPG	0.10	40,172.4	4.02
Total			223,972.84	7.70

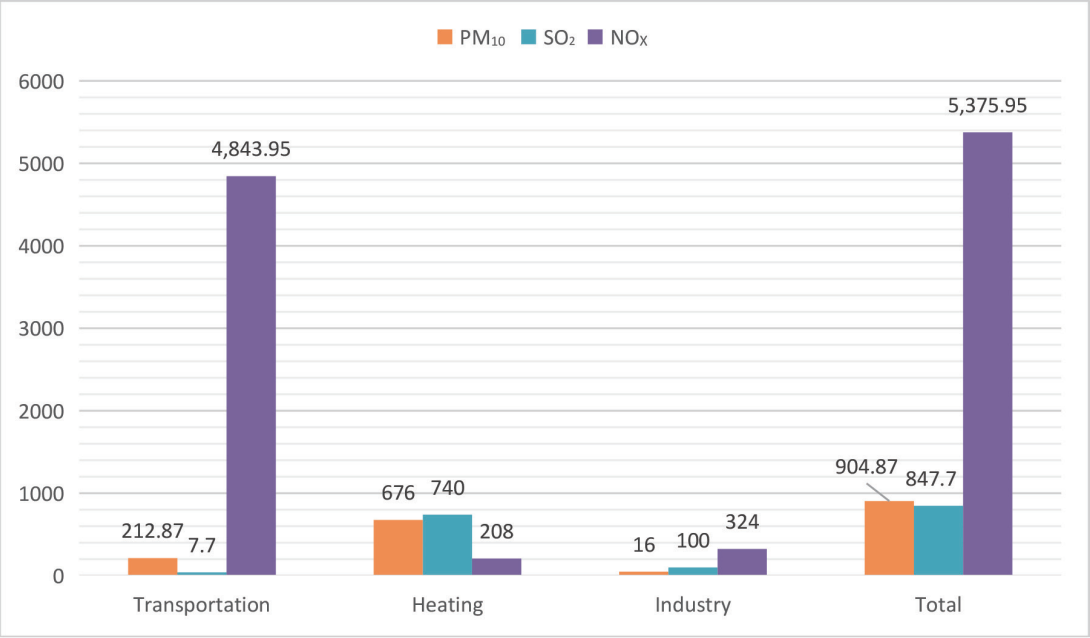

Figure 2. Sectoral distribution chart of NO_X, PM_{10}, SO_2 emissions.

When the sectoral distribution of emission values in the city is examined, it is seen that the transportation sector covers approximately 70% of the total emission values. A very large part of this amount is due to NO_X emissions. In addition to this situation, in the study, it has been determined that motor vehicles on the road increased between 07.00-09.00 in the morning and 17.00-20.00 in the evening. Particulate matter and emissions from motor vehicles reach significant levels, especially around main streets, intersections and highways. The amount of these emissions from vehicles depends on parameters such as the age of the vehicle, the operating speed of the engine, operating temperature, ambient temperature, ambient pressure, fuel type and quality. Although air pollution caused by heating occurs in the city due to cold weather, air pollution caused by transportation is much higher. It is seen that the share of the industrial sector in air pollution in the city is much lower. The reason for this is that the city is not an industrial city and the industrial facilities are generally located far from the city.

4. Discussion

The fact that the share of the transportation sector in the air pollution in the city is too high is an important problem. Because while interventions to air pollution originating from the heating and industry sector are quite difficult, it is easier to intervene in air pollution related to the transportation sector. For this reason, it is possible to significantly reduce air pollution related to the transportation sector with some regulations.

Although the use of hybrid and electric vehicles in the transportation sector is increasing day by day, air pollution caused by transportation is very high as the demands of individuals for automobile ownership are higher. In addition, although the province of Erzurum, which has been chosen as the study area, has a cold climate, the air

pollution caused by the heating of houses and workplaces is almost one third of the air pollution caused by transportation.

In this study, when the urban transportation structure is examined, it has been determined that individuals prefer individual automobile use rather than public transportation. In addition, it is seen that individuals travel by automobile even for very short distances. In order to prevent these and similar problems and to prevent air pollution in the city, some suggestions are presented below.

- Within the framework of the Transportation Master Plan, the pedestrian roads should be redesigned to reduce the traffic density in the city center.
- It is necessary that the pedestrian roads provide a connection between the important points of the city and the pedestrian crossings should be made suitable for this.
- A minimum number of safe pedestrian crossings are required, rather than a large number of pedestrian crossings. In this way, safe passage can be provided for pedestrians. In addition, air pollution can be reduced by reducing stops on the road.
- In order to reduce the use of individual vehicles, it is necessary to carry out studies to make public transportation services attractive.
- For the planning and management of traffic, green wave, smart signaling systems, traffic congestion pricing, different parking fees need to be implemented.
- It is necessary to limit the use of vehicles in the hours and regions where the traffic density increases and individuals should be directed to public transportation vehicles or pedestrian transportation.
- In order to increase micromobility in the city, bicycle lanes and similar alternative transportation should be increased and encouraged.

5. Conclusions

In this study, the problems caused by the increasing air pollution in the world have been mentioned. The transportation sector, which is one of the most important factors causing air pollution, has been discussed. For this reason, the air pollution caused by transportation has calculated for the province of Erzurum, which has determined as the study area. Emission factors determined for each vehicle type and each fuel type have been taken into account in the calculation process. NO_X, PM_{10} and SO_2 emissions have been calculated by taking into account the amount of vehicle fuel used in the city in a year. As a result of the calculations, it has been determined that the NO_X emission is particularly high. Accordingly, the amount of emissions originating from transportation and the amount of emissions originating from heating and industry have been compared. It has been determined that approximately 70% of the total amount of emissions in the city originates from transportation. In the discussion part, this situation has been examined and some suggestions have been made in order to reduce the use of vehicles in the city. In particular, the preference for public transportation vehicles, the increase in bicycle paths and the increase in pedestrian transportation have been mentioned. It has been mentioned that in order to spread pedestrian transportation, the pedestrian ways should be designed to connect the important points in the city, the pedestrian ways should be made more usable and the pedestrian crossings should be designed safely. In this direction, cleaner and healthier living conditions will be provided for living things.

This study revealed the effect of transportation on air pollution in cities. In order to reduce this air pollution, it has been stated that the use of motor vehicles should be reduced and measures should be taken to increase pedestrian transportation. Future studies can optimize the design of pedestrian roads that increase pedestrian access and public transport systems that will reduce the preference for motor vehicles.

Author Contributions

Emre Kuşkapan: Conceptualization; Data curation; Formal analysis; Investigation; Methodology; Resources; Software; Validation; Visualization; Writing - original draft. Muhammed Yasin Çodur: Conceptualization; Data curation; Formal analysis; Investigation; Methodology; Resources; Software; Validation; Visualization; Writing - original draft.

Conflict of Interest

There is no conflict of interest in this study.

Funding

This research received no external funding.

References

[1] Sun, J., Dang, Y., Zhu, X., et al., 2021. A grey spatio-temporal incidence model with application to factors causing air pollution. Science of the Total Environment. 759, 143576.

[2] Li, S., Feng, K., Li, M., 2017. Identifying the main contributors of air pollution in Beijing. Journal of Cleaner Production. 163, S359-S365.

[3] Van Fan, Y., Perry, S., Klemeš, J.J., et al., 2018. A review on air emissions assessment: Transportation.

Journal of Cleaner Production. 194, 673-684.

[4] Bera, B., Bhattacharjee, S., Shit, P.K., et al., 2021. Significant impacts of COVID-19 lockdown on urban air pollution in Kolkata (India) and amelioration of environmental health. Environment, Development and Sustainability. 23(5), 6913-6940.

[5] Xie, R., Zhao, G., Zhu, B.Z., et al., 2018. Examining the factors affecting air pollution emission growth in China. Environmental Modeling & Assessment. 23(4), 389-400.

[6] Ambarwati, L., Verhaeghe, R., van Arem, B., et al., 2016. The influence of integrated space–transport development strategies on air pollution in urban areas. Transportation Research Part D: Transport and Environment. 44, 134-146.

[7] Vafa-Arani, H., Jahani, S., Dashti, H., et al., 2014. A system dynamics modeling for urban air pollution: A case study of Tehran, Iran. Transportation Research Part D: Transport and Environment. 31, 21-36.

[8] Armah, F.A., Yawson, D.O., Pappoe, A.A., 2010. A systems dynamics approach to explore traffic congestion and air pollution link in the city of Accra, Ghana. Sustainability. 2(1), 252-265.

[9] Vallero, D., 2019. Air pollution calculations: Quantifying pollutant formation, transport, transformation, fate and risks. Elsevier: Amsterdam.

[10] Requia, W.J., Mohamed, M., Higgins, C.D., et al., 2018. How clean are electric vehicles? Evidence-based review of the effects of electric mobility on air pollutants, greenhouse gas emissions and human health. Atmospheric Environment. 185, 64-77.

[11] Eguiluz-Gracia, I., Mathioudakis, A.G., Bartel, S., et al., 2020. The need for clean air: The way air pollution and climate change affect allergic rhinitis and asthma. Allergy. 75(9), 2170-2184.

[12] Gatersleben, B., Uzzell, D., 2000. The risk perception of transport—generated air pollution. IATSS research. 24(1), 30-38.

[13] Krzyżanowski, M., Kuna-Dibbert, B., Schneider, J., 2005. Health effects of transport-related air pollution. WHO Regional Office: Europe.

[14] Sahraei, M.A., Kuşkapan, E., Çodur, M.Y., 2021. Public transit usage and air quality index during the COVID-19 lockdown. Journal of Environmental Management. 286, 112166.

[15] Ali Sahraei, M., Kuşkapan, E., Yasin Çodur, M., 2021. Impact of COVID-19 on public transportation usage and ambient air quality in Turkey. Promet-Traffic & Transportation. 33(2), 179-191.

[16] Chang, H.H., Meyerhoefer, C.D., Yang, F.A., 2021. COVID-19 prevention, air pollution and transportation patterns in the absence of a lockdown. Journal of Environmental Management. 298, 113522.

[17] Guo, X.R., Cheng, S.Y., Chen, D.S., et al., 2010. Estimation of economic costs of particulate air pollution from road transport in China. Atmospheric Environment. 44(28), 3369-3377.

[18] Yaduma, N., Kortelainen, M., Wossink, A., 2013. Estimating mortality and economic costs of particulate air pollution in developing countries: The case of Nigeria. Environmental and Resource Economics. 54(3), 361-387.

[19] Kuşkapan, E., Sahraei, M.A., Çodur, M.K., et al., 2022. Pedestrian safety at signalized intersections: Spatial and machine learning approaches. Journal of Transport & Health. 24, 101322.

[20] Kuşkapan, E., Çodur, M.Y., Atalay, A., 2021. Speed violation analysis of heavy vehicles on highways using spatial analysis and machine learning algorithms. Accident Analysis & Prevention. 155, 106098.

[21] Erzurum Clean Air Action Plan [Internet]. Erzurum Provincial Directorate of Environment and Urbanization [cited 2022 Jan 21]. Available from: https://erzurum.csb.gov.tr/

[22] Anenberg, S., Miller, J., Henze, D., et al. (editors), 2019. A global snapshot of the air pollution-related health impacts of transportation sector emissions in 2010 and 2015. International Council on Clean Transportation: Washington, DC, USA.

[23] Umar, M., Ji, X., Kirikkaleli, D., et al., 2021. The imperativeness of environmental quality in the United States transportation sector amidst biomass-fossil energy consumption and growth. Journal of Cleaner Production. 285, 124863.

[24] Number of Road Vehicles in Erzurum [Internet]. Erzurum Metropolitan Municipality [cited 2021 Dec 13]. Available from: https://www.erzurum.bel.tr/

[25] Annual Gas Emission Status of Road Vehicles [Internet]. Erzurum Metropolitan Municipality Department of Transportation [cited 2021 May 8]. Available from: https://ulasim.erzurum.bel.tr/

[26] Number of Road Vehicles by Fuel [Internet]. Erzurum Police Department [cited 2020 Sep 26]. Available from: https://www.erzurum.pol.tr/

[27] Fuel Types of Road Vehicles Registered in Erzurum Province [Internet]. Turkish Statistical Institute [cited 2022 Feb 11]. Available from: https://www.tuik.gov.tr/

BILINGUAL PUBLISHING CO.
Pioneer of Global Academics Since 1984

Journal of Environmental & Earth Sciences
https://ojs.bilpublishing.com/index.php/jees

ARTICLE

Soil Bunds Effect on Soil Properties under Different Topographies of Southwest Ethiopia

Wondimu Bekele Goba[1] Alemayehu Muluneh[2] Kebede Wolka[3*]

1. Gena Bosa Woreda Agriculture and Natural Resources Office, Dawuro Zone, Ethiopia
2. Faculty of Bio-systems and Water Resources Engineering, Hawassa University, Hawassa, Ethiopia
3. Wondo Genet College of Forestry and Natural Resource, Hawassa University, Shashemene, Ethiopia

ARTICLE INFO

Article history
Received: 3 January 2022
Accepted: 28 April 2022
Published Online: 8 May 2022

Keywords:
Soil erosion
Environmental problem
Soil fertility
Soil and water conservation
Intra-bund
Steep slope

ABSTRACT

Soil erosion is a major environmental problem affecting development endeavors. Physical soil and water conservation (SWC) measures such as soil bunds are implemented to mitigate soil erosion. However, information on the effects of soil bunds on soil fertility is limited. This study aimed to evaluate soil quality in fields with soil bunds and with no soil bunds in steep, middle and lower sloping cultivated lands as well as spatial variation of soil properties in between bunds in southwest Ethiopia. About 7-15 years old bunds and nearby cultivated fields lacking bunds were assessed. From 0 cm-20 cm soil depth, 36 soil samples were collected. Soil texture, soil organic carbon (SOC), total nitrogen (N_{tot}) and exchangeable potassium (K_{exch}) were analyzed. Soil bunds showed significantly (p<0.0.5) greater clay but less sand than adjacent no-bund fields. In steep, middle, and lower slopes, concentrations of SOC and K_{exch} were greater in fields with soil bunds than without. Lower slope fields showed greater clay, SOC and nutrients than steep slopes. In between soil bunds, soil was more fertile at bunds than below the bunds. In Fanta watershed, soil bunds are a vital conservation measure to retain soil fertility in cultivated mountainous areas.

1. Introduction

Food security for the increasing human population relies on the quality of environment and sustainability of soil and water resources. Across the world, erosion removes as high as 75 billion tons of soil per annum [1] and is an alarming environmental problem with far-reaching impact. Soil quality decline due to erosion is a problem resulting in nutrient depletion and constraining the development of the agricultural sector and attainment of food security. About 65% of the total area is regarded as degraded, Sub-Saharan Africa is among the regions highly affected by soil quality loss that emanates from poor land management and excessive removal by erosion [2,3]. The geographic distribution of quality loss varies due to differences in topography, climate and land management. For example, east African highland is a soil degradation hot spot due to high annual soil loss,

*Corresponding Author:
Kebede Wolka,
Wondo Genet College of Forestry and Natural Resource, Hawassa University, Shashemene, Ethiopia;
Email: kebedewolka@gmail.com

DOI: https://doi.org/10.30564/jees.v4i1.4322

e.g., 420 tons per hectare in Uganda [4-6].

Ethiopia is among the countries most affected by soil erosion. The traditional and fragmented -agriculture dominating landscape of Ethiopia has been affected by soil erosion [7,8]. In Ethiopia, about 50% of the highlands, landscapes with an elevation exceeding 1500 meters from sea level, suffer from sheet and rill erosion [6], which is a severe problem in sloping areas, mainly in the northern and central highlands having little permanent vegetation cover and shallow soils. Every year, about 1.4-2 billion tonnes of soil are removed by erosion, about 50% of which is from cereal-growing landscapes [6,7]. Soil formation in Ethiopia varies between 2 tonnes/hectare/year and 22 tonnes/hectare/year [9], but several studies across the country reported soil erosion that exceeded soil formation rate [10-13]. This implied that the Ethiopian highlands have been experiencing a decline in soil fertility due to severe soil erosion. The traditional conventional farming system on shallow soil and sloping topography, excessive removal of plants by livestock and wood material extraction, crop residue removal, and shortened fallow periods due to increasing population and land scarcity have aggravated soil erosion and degradation [14,15]. Soil degradation due to erosion significantly contributes to food insecurity among rural households and poses a real threat to the sustainability of existing subsistence agriculture [16].

Traditional soil and water management practices have existed in Ethiopia for centuries [13]. However, expert-based efforts for controlling soil erosion were started in the past about four decades after recognizing the adverse effects of severe soil degradation and drought, particularly in Tigray and Wollo areas of northern Ethiopia. The modern erosion controlling efforts were implemented by constructing physical soil and water conservation techniques such as soil and stone bunds through resource support of international organizations [7,17,18]. The earlier incentives for controlling erosion and soil degradation were followed by food for work schemes [19]. In the recent two decades, the government emphasized environmental rehabilitation and protection using a participatory watershed management approach mainly in highlands, where population density is high and land degradation challenges agricultural production [18]. The government programs and development partners implemented watershed-based soil and water conservation measures. Productive Safety Net Program (PSNP) is one of the government-supported programs, involved in watershed-based soil and water conservation activities. The PSNP was initiated as social protection scheme in 2005 and supports food security issues resulting from environmental degradation and prolonged drought [20]. In food insecure areas, the PSNP has a public work scheme in which the beneficiaries receive cash or grain for, e.g., construction of soil and stone bunds [21].

Soil bunds, the physical barriers with about 50 cm deep and wide ditch, are constructed along contour to reduce surface runoff and soil loss [12,22,23]. On sloping cultivated lands, without soil bunds or sufficient vegetation cover, erosion could adversely affect soil quality. Research reported that, in plots treated with soil bunds, soil organic carbon and total nitrogen were greater than in plots without bunds on Nitisol of northern Ethiopia [24]. Studies reported positive effect of soil bunds on reducing soil erosion [12,13,25]. However, studies are rare on the effects of soil bunds on soil properties under different topographic set up [22,26,27]. Available literature on other related cross-slope barrier techniques such as *Fanya juu* reported insignificant differences in plant nutrients such as nitrogen and potassium, e.g., in Anjeni watershed of northern Ethiopia [28]. Alemayehu et al. [29] reported greater soil organic carbon in plots treated with stone bunds than without any physical measures. The erosion and subsequent deposition in the intra-*Fanya juu* area as well as in intra-terrace area reported spatial variation of soil organic carbon and nutrients in Ethiopia [30] and Uganda [31]. Effects of bunds may differ with climate, soil, and management practices [15], and the effect of bunds on soil properties is not well understood.

To combat soil erosion and associated soil degradation effect on food security, physical soil and water conservation measures including soil bunds were introduced to the Fanta watershed of the Omo-Gibe River basin, southwest Ethiopia, by government-supported programs such as PSNP. Thus, in this area, in the past 15 years, the PSNP has been supporting soil and water conservation activities. The program covers construction costs to the rural community and provides expert support. In addition to the PSNP, conservation measures were also implemented through state-initiated public campaigns since 2010 [32]. Even though the soil and water conservation practice has been promoted and implemented in a large area, its effects on soil properties are not understood. This study was aimed: (1) to evaluate the effect of soil bunds on soil quality at steep (> 25%), middle (15%-25%) and lower (3%-15%) slope areas of the cultivated landscape, and (2) to assess relative locational difference in soil properties in between two soil bunds of about 7-15 years old on Nitisol.

2. Methods and Materials

2.1 Description of the Study Area

The study was conducted in the Fanta watershed of the

Omo-Gibe River basin, Southwest Ethiopia. The Fanta watershed, located at 7°17'30''-7°20'30''N latitude and 37°17'10''-37°19'40''E longitude (Figure 1), drains to Gibe III hydro-electric dam on Omo River. The Omo-Gibe River basin is well recognized in East Africa due to the cross-border Omo River and Mega dams. Fanta watershed is one of the typical and important agriculture-dominating landscapes in the basin and is characterized by a range of elevation (1000 m-2860 m above sea level) and topographies (mountains, valleys, and plateaus). The mean annual temperature and rainfall of the area are 15.1 °C-27.5 °C and 1400 mm, respectively. Crop growing season in the area is between March and September. Nitisols and Leptosol are dominant soil types [33]. Smallholder crop-livestock farming is a major livelihood of the community. Annual crops such as maize (*Zea mays*), teff (*Eragrostis tef*), sorghum *(Sorghum bicolor),* and barley (*Hordeum vulgare*) are commonly cultivated, while the plots around the homestead are covered with enset (*Ensete ventricosum*). Enset is a perennial plant and important staple food in the region [13]. Livestock production is an essential part of the farming system as nearly seed bed preparations are done with oxen-drawn plough. Agriculture has replaced most of the forest and woodlands.

2.2 Soil Sampling and Analysis

To understand the effect of soil bunds, soil analyses were conducted for fields with and without soil bunds. Croplands with 7-15 years-old soil bunds (Figure 2) were selected in the steep, middle, and lower slope areas of cultivated Fanta watershed. In each slope area, near conserved fields, fields without any physical soil and water conservation measures were selected. Plots treated with soil bunds and those lacking soil bunds had a similar history of farm management, and soil group. The steep, middle, and lower slope areas had slopes of > 25%, 15%-25%, and 3%-15%, respectively. In each slope category, three fields treated with soil bunds and other nearby three fields with no physical conservation measures were selected. In plots having soil bunds, soil samples were collected from three relative locations in between two bunds. That is, near soil bund at ~1 m downslope side of the bund, middle point, and above soil bund at ~1 m. This was replicated three times per field. The samples were collected from soil depth of 0 cm-20 cm. A total of twenty-seven soil samples (3 slope categories * 3 fields per slope category * 3 samples per field in between soil bunds) were collected from croplands with soil bunds. In fields lacking soil bunds, a

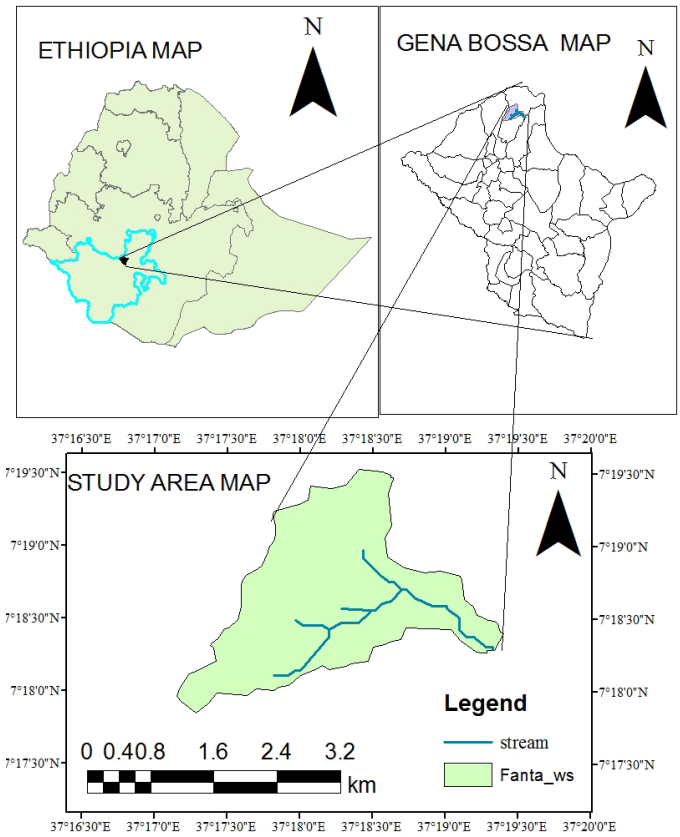

Figure 1. Location map of the Fanta watershed in Southwest Ethiopia.

Figure 2. Soil bunds on cultivated lands of the Fanta watershed, Southwest Ethiopia.

Photo: Wondimu Bekele.

total of nine soil samples (3 slope categories * 3 fields per slope category) were collected.

After sieving air dried soil samples with 2 mm steel mesh, texture, soil organic carbon (SOC), total nitrogen (N_{tot}), and exchangeable potassium (K_{exch}) were analyzed. Soil texture was determined following the hydrometric method [34]. The concentration of SOC was assessed following the Walkley and Black method [35], while total nitrogen (N_{tot}) was determined by wet-digestion, distillation, and titration procedures of the Kjeldahl method as described by Black et al. [36]. The exchangeable potassium (K_{exch}) was determined by a flame emission spectrophotometer [36].

2.3 Data Analysis

Data were analyzed using SPSS 20 computer software (IBM Co., Armonk, NY, USA). The differences in soil properties due to soil bunds compared with nearby non-conserved plots using a t-test. Variations in soil properties between slope categories as well as differences between the three sections (below a bund, middle point, and above a bund) within the soil bunds were assessed using analysis of variance (one-way ANOVA) at $p \leq 0.05$. The Least Significant Difference (LSD) was applied to evaluate differences between means.

3. Results

3.1 Variation of Soil Properties in between Fields with Soil Bunds and No Bunds

The texture analysis showed that fields without soil bunds showed significantly (p<0.05) greater sand and silt fractions and fewer fractions of clay than fields treated with soil bunds (Table 1). In the steep, moderate and lower slope areas, SOC was significantly greater ($p < 0.05$) in fields treated with soil bunds than no bund fields. The variations in SOC between bunds and no bunds were slight increased from steep slope to lower slope, where the fields with soil bunds in steep, middle and lower slope were greater by 25%, 39% and 42%, respectively, than those without bunds. The significant difference in N_{tot} was observed at steep slopes where fields with soil bunds had significantly ($p < 0.05$) greater values than no bunds. The K_{exch} was significantly ($p < 0.05$) greater in fields treated with soil bunds than without soil bunds at steep, middle and lower slopes. The K_{exch} was 63%-129% greater in fields with soil bunds than without, the highest difference at steeper slopes.

3.2 Spatial Variation of Soil Properties within Soil Bunds

In between two consecutive soil bunds, at steep slopes, concentrations of clay, SOC, and K_{exch} were significantly ($p < 0.05$) greater above a bund than middle and below a bund, and the opposite trend was observed for sand (Table 2). This was true for mid and lower slope categories. The significant differences in N_{tot} between above a bund, midpoint and below a bund were observed only at the lower slope category.

3.3 Effect of Slope and Bunds on Soil Properties

In fields with soil bunds and with no bunds, the fractions of sand and clay were significantly ($p < 0.05$) varied between steep and lower slopes. Sand fractions were greater at steep slope whereas clay was greater at lower slopes (Table 1). The differences were 50% and 14% of sand in fields with soil bunds and with no bunds, respec-

Table 1. Soil texture, soil organic carbon (SOC), total nitrogen (N_{tot}), and exchangeable potassium (K_{exch}) at 0 cm-20 cm depth soils of fields with and without soil bunds in steep, middle and lower slope positions of the Fanta Watershed (mean ± standard deviation), southwest Ethiopia.

Slope position	Soil bunds, n=9	Without soil bunds, n=3	*p*-value
Sand, %			
Steep	36.4 ± 0.84a[a]	45.7 ± 3.05a[b]	0.0
Middle	30.9 ± 1.69b[a]	42.3 ± 0.57ab[b]	0.0
Lower	24.3 ± 5.0c[a]	40.0 ± 1.0b[b]	0.0
p-value	0.0	0.028	
Clay, %			
Steep	36.9 ± 1.69a[a]	29.0 ± 0.00a[b]	0.0
Middle	41.1 ± 1.17a[a]	30.7 ± 1.53a[b]	0.0
Lower	55.8 ± 9.64b[a]	33.00 ± 1.00b[b]	0.003
p-value	0.0	0.01	
Silt, %			
Steep	26.66 ± 5.27a[a]	25.33 ± 3.06a[a]	0.233
Middle	28.1 ± 0.78a[a]	26.67 ± 0.58a[b]	0.016
Lower	19.9 ± 5.12b[a]	27.0 ± 0.00a[b]	0.043
p-value	0.0	0.55	
Soil organic carbon, %			
Steep	1.58 ± 0.04a[a]	1.269 ± 0.018a[b]	0.0
Middle	1.77 ± 0.03b[a]	1.27 ± 0.02bc[b]	0.0
Lower	1.97 ± 0.12c[a]	1.39 ± 0.041c[b]	0.0
p-value	0.0	0.0	0.0
Total nitrogen , %			
Steep	0.22 ± 0.05a[a]	0.14 ± 0.03a[b]	0.01
Middle	0.29 ± 0.04bc[a]	0.20 ± 0.07ab[a]	0.18
Lower	0.31 ± 0.05c[a]	0.26 ± 0.05b[a]	0.21
p-value	0.01	0.11	
$K_{exch,}$ Cmol (+)/kg			
Steep	0.278 ± 0.018a[a]	0.118 ± 0.0549a[b]	0.0
Middle	0.327 ± 0.018a[a]	0.201 ± 0.0166bc[b]	0.002
Lower	0.429 ± 0.059b[a]	0.231 ± 0.008c[b]	0.0
p-value	0.0	0.04	

Note: Mean and standard deviation followed by different small letters in the superscript indicate significant ($p < 0.05$) differences between soil bunds and no bund (row comparison). Significant ($p < 0.05$) variations between slope positions (column comparison) were shown by different small letters.

Table 2. Soil texture, concentration of soil organic carbon (SOC), total nitrogen (N_{tot}), exchangeable potassium (K_{exch}) in upper, middle and lower sections in intra-soil bunds in the steep, middle and lower slope position in the Fanta watershed of Omo-Gibe basin, Ethiopia (mean ± standard deviation, n = 3).

Slope position	Parameters	Location in between soil bunds				
		Upper section	Middle section	Lower section	Total	*p*-value
Steep slope position	Sand, %	38.0 ± 1.0a	37.0 ± 0.0a	34.3 ± 1.53b	36.4 ± 1.88	0.01
	Silt, %	27.0 ± 0.0a	26.0 ± 0.0b	26.7 ± 5.77a	26.6 ± 5.27	0.03
	Clay, %	35.0 ± 1.0a	37.0 ± 0.0b	38.7 ± 0.58c	36.9 ± 1.69	0.002
	SOC, %	1.51 ± 0.03a	1.56 ± 0.02ab	1.67 ± 0.03b	1.58 ± 0.03	0.001
	N_{tot}, %	0.19 ± 0.03a	0.22 ± 0.05a	0.25 ± 0.03a	0.22 ± 0.04	0.239
	K_{exch}, Cmol (+)/kg	0.26 ± 0.01a	0.28 ± 0.00b	0.29 ± 0.01b	0.28 ± 0.02	0.007
Middle slope position	Sand, %	33 ± 0.0a	30.3 ± 0.56b	29.3 ± 0.58c	30.9 ± 1.69	0.0
	Silt, %	27.3 ± 5.77a	28.7 ± 5.77b	28.3 ± 5.77ab	28.1 ± 7.83	0.07
	Clay, %	40.0 ± 0.0a	41.0 ± 0.0a	42.3 ± 1.15b	41.1 ± 1.16	0.015
	SOC, %	1.74 ± 0.01a	1.76 ± 0.01ab	1.81 ± 0.04b	1.77 ± 0.03	0.04
	N_{tot}, %	0.26 ± 0.04a	0.28 ± 0.04a	0.32 ± 0.03a	0.29 ± 0.04	0.29
	K_{exch}, Cmol (+)/kg	0.31 ± 0.01a	0.33 ± 0.01b	0.35 ± 0.00c	0.33 ± 0.02	0.0
Lower slope position	Sand, %	28.3 ± 1.12a	25.7 ± 1.12a	19.0 ± 5.29b	24.3 ± 5.00	0.03
	Silt, %	25.7 ± 2.08a	19.3 ± 1.12b	14.7 ± 3.06c	19.9 ± 1.72	0.0
	Clay, %	46.0 ± 2.65a	55.0 ± 2.00b	66.3 ± 7.02c	55.78 ± 9.64	0.004
	SOC, %	1.86 ± 0.04a	1.95 ± 0.01a	2.10 ± 0.12b	1.97 ± 0.12	0.018
	N_{tot}, %	0.27 ± 0.03a	0.31 ± 0.03ab	0.35 ± 0.04b	0.31 ± 0.05	0.069
	K_{exch}, Cmol (+)/kg	0.37 ± 0.01a	0.43 ± 0.02b	0.49 ± 0.04c	0.43 ± 0.06	0.006

Note: Mean and standard deviation followed by different small letters had significant difference (p<0.05) between sections in intra-bund area.

tively. Also, clay differed by 34% and 12% in fields with soil bunds and with no bunds, respectively. Unlike fields without soil bunds, significant difference in silt fraction between steep and lower slope was observed in fields with soil bunds. The SOC and K_{exch} were significantly ($p < 0.05$) greater at a lower slope than steep slopes, both at fields with soil bunds and with no bunds. In soil bunds, the lower slopes showed 20% greater SOC and 37% greater K_{exch} than steep slope, which was 9% of SOC and 49% of K_{exch} in fields without soil bunds. In fields with soil bunds, N_{tot} was significantly ($p < 0.05$) greater at lower slope areas than steep slopes, which was insignificant in fields with no bunds.

4. Discussion

4.1 Effects of Soil Bunds on Soil Fertility

Soil bunds, constructed along contour by digging a ditch and accumulating excavated soil at a down slope, are cross-slope barriers against surface runoff and thus, reduce soil loss. Studies reported soil bunds' effect in reducing erosion from 50%-90% [12,13,25]. The greater clay concentration and less sand in fields with soil bunds than no bunds in cultivated for more than seven years indicated that soil erosion has removed small-sized particles. The erosion-mitigating ability of the soil bunds has resulted in a greater concentration of clay fractions in fields with

soil bunds. Due to its greater size, sand fractions remain behind while the finer materials are easily removed by erosion [37]. Studies by Bezabih et al. [27] in Dedo district of Southwest Ethiopia and Mengistu et al. [28] in northern Ethiopia reported that soils treated with soil bunds have higher clay fractions compared to no bund plots. Greater SOC in fields with physical SWC measures was reported in Silluh valley of northern Ethiopia [38]. However, Wolka et al. [22,26] and Hailu et al. [39] reported insignificant variation of soil sand and clay fractions in between fields with and without soil bunds in Goromti and Bokole areas. Differences in land management, length of intervention period and severity of erosion would have affected.

On slopping cultivated land, soil erosion removes SOC and thus, is a process of degrading soil quality [40,41]. The conservation measures are important to conserve SOC, which is a major soil property in determining soil quality, in cultivated sloping lands. In the Fanta watershed, the greater SOC in fields with soil bunds than with no bunds could be mainly due to the erosion controlling ability of the soil bunds. The retention of clay in fields with soil bunds could also imply the alongside retention of SOC, as associations between clay and SOC have been documented [42]. Our study showed that soil bunds could retain soil particles together with SOC in all slope categories (steep, middle and lower), indicating the need for such SWC practices in the different slope categories. The capacity of soil bunds to retain surface runoff could positively influence soil moisture and thus, crop yield as reported in Zimbabwe [43] and Ethiopia [28], which can partly enhance SOC concentration. Also, in fields with soil bunds, conservation of the dissolved SOC through surface runoff retention is an additional advantage [13]. The greater SOC in fields with soil bunds than with no bunds in the present study agreed with findings in Kenya [44] and Ethiopia [39]. The role of soil bunds in reducing soil erosion was also observed from its greater N_{tot} and K_{exch} than in fields with no soil bunds. However, Mengistu et al. [28] reported insignificant differences in N_{tot} and K_{exch} between fields with and without no conservation measures on different slope positions in Anjeni watershed, northern Ethiopia, which could be associated to severity of erosion and soil management activities. On sloping and conventionally cultivated land, the nutrient rich topsoil removal could affect cropland productivity. Thus, soil bunds are highly important to maintain cropland fertility and thus, food security of smallholders.

4.2 Soil Properties in Plots between Two Bunds

In Fanta watershed, more than seven years old soil bunds showed differences in soil properties between three locations (above bund, middle, below bund) in between bunds due to topsoil transfer to downslope. Soil bunds, a barrier against surface runoff, could accumulate soil above the bund. That means, the downslope side of soil bunds is a loser, while the upper slope side of next soil bund gains sediment. Van Oost et al. [45] reported that tillage erosion could also transfer 70 kg $m^{-1}yr^{-1}$-260 kg $m^{-1}yr^{-1}$ of soil when non-mechanized agriculture is practiced. That means, both water erosion and tillage could transport topsoil to downslope and deposit above the bund [46]. Thus, the sand fractions, due to their greater size, remain below the bund, while more clay accumulates at lower section, above soil bund. Our result agrees with the findings of Lin et al. [47], which reported greater clay fractions in lower section in purple-soil area of China. A related study by Siriri et al. [31] also reported greater clay at lower section of terrace in Uganda. In our study area, the downslope transfer of topsoil resulted in greater SOC, N_{tot} and K_{exch} at above soil bunds than below soil bunds. Studies on spatial variation of soil properties in intra-soil bund areas are rare. Wolka et al. [22] reported insignificant intra-bund soil properties in two years old soil bunds in Bokole watershed of Ethiopia. Studies on the other cross-slope barrier soil and water conservation measures such as *Fanya juu* and stone bunds in Ethiopia [29,30,48], plant hedgerow in Honduras and China [47,49], and bench terrace in Uganda [31] reported greater concentrations of SOC and nutrients at above the conservation measure than below the barrier. In the Fanta watershed, in the present study area, erosion below the bund and deposition above the bund, which resulted in spatial variation of soil quality, could have resulted in spatial variation of crop yield but not addressed in this study. Adaptive soil fertility management techniques in between bunds can improve soil quality below the bunds.

4.3 Effect of Slope Gradient on Soil Properties in Treated and Non-Treated Fields

In fields with soil bunds and no bunds, the steep slope showed greater sand and less clay than lower slope (Table 1), perhaps due to long time erosion and deposition. That means, the fine particles including clay are removed from upper slope position and deposited in lower slope area, while the large sized sand could remain behind. After physical soil and water conservation measures, less erosion is expected than in fields with soil bunds [12,15] than fields with no soil bunds. This implies a greater transfer of soil from steep slope to the lower slope in fields with no soil bunds, particularly on cereal dominating agricultural landscapes. Since soil erosion and sediment yields are a function of slope [50,51], steep slopes could have more erosion and thus, greater deposition at a lower slope.

Due to deposition of SOC and nutrient rich topsoil at

lower slopes, greater SOC, N_{tot} and K_{exch} were observed at lower slopes than steep slopes. Our result supports Amare et al. [30] and Bezabih et al. [27], which reported greater SOC and nutrients at the slope position than steeper slope position in Anjeni watershed of northern Ethiopia and Dedo district of southwest Ethiopia. Hailu et al. [39] also reported the association of SOC with land slope positions where fertile soil deposits at lower slope positions. Due to surface runoff, the greater soil moisture at lower slopes could enhance plant growth and biomass production, which in turn can increase SOC. Insignificant variation in N_{tot} was observed along slope gradient, particularly in fields without soil bunds due to overall low soil N_{tot}. Implementing sufficient conservation measures is important to sustain soil quality of cultivated sloping land.

5. Conclusions

Soil and water conservation measures are practiced for controlling adverse effects of severe soil erosion on sloping cultivated lands. Soil bunds have been widely implemented to protect against erosion and soil degradation of sloping cultivated lands. Our study on more than seven years old soil bunds revealed that fields with soil bunds showed significantly greater clay fractions than fields with no soil bunds. The greater SOC and nutrients in fields with soil bunds revealed comparatively better soil fertility than in bunds than non-treated fields. The increase in clay, SOC, N_{tot}, and K_{exch} concentrations with decreasing slope gradients in fields with soil bunds and with no soil bunds showed long-term erosion from steeper slopes and deposition at foot slope fields. In intra-soil bund area, above soil bunds were more fertile than below soil bunds. Our study revealed that soil bunds are important cross-slope barriers which could support sustaining soil quality against erosion as differences in soil properties between fields with soil bunds and no bunds were revealed. In between bunds, soil fertility is better just above the bund. We suggest implementation of soil bunds in the study area and other areas with similar agro-ecology and soil type. The spatial variation of soil quality in between bunds could be compensated by applying selective soil fertility management techniques below the bunds to enhance nutrient concentrations and crop yield.

Conflict of Interest

There is no conflict of interest.

Acknowledgement

The first author acknowledges Agriculture and Natural Resources Management office of Gena Bosa Woreda for partial financial and technical assistance for field work. Farmers who allowed their plots for soil sampling are acknowledged.

References

[1] Pimentel, D., Burgess, M., 2013. Soil erosion threatens food production. Agriculture. 3(3), 443-463.

[2] Tully, K., Sullivan, C., Weil, R., et al., 2015. The state of soil degradation in Sub-Saharan Africa: Baselines, trajectories, and solutions. Sustainability. 7(6), 6523-6552.

[3] Zingore, S., Mutegi, J., Agesa, B., et al., 2015. Soil degradation in sub-Saharan Africa and crop production options for soil rehabilitation. Better Crops. 99(1), 24-26.

[4] Muchena, F.N., Onduru, D.D., Gachini, G.N., et al., 2005. Turning the tides of soil degradation in Africa: Capturing the reality and exploring opportunities. Land Use Policy. 22(1), 23-31.

[5] Karamage, F., Zhang, C., Ndayisaba, F., et al., 2016. Extent of cropland and related soil erosion risk in Rwanda. Sustainability. 8(7), 609.

[6] FAO, 2019. Proceedings of the global symposium on soil erosion 2019. Food and Agriculture Organization of United Nations: Rome.

[7] Hurni, H., Abate, S., Bantider, A., et al., 2010. Land degradation and sustainable land management in the highlands of Ethiopia. Global Change and Sustainable Development. 5, 187-207.

[8] Borrelli, P., Robinson, D.A., Fleischer, L.R., et al., 2017. An assessment of the global impact of 21st century land use change on soil erosion. Nature Communications. 8(1), 2013.

[9] Hurni, H., 1983. Soil formation rates in Ethiopia. FAO/MOA Joint Project, EHRS, Working Paper No.2, Addis Ababa.

[10] Bewket, W., Sterk, G., 2003. Assessment of soil erosion in cultivated fields using a survey methodology for rills in the Chemoga watershed, Ethiopia. Agriculture, Ecosystems & Environment. 97(1-3), 81-93.

[11] Tefera, B., Sterk, G., 2010. Land management, erosion problems and soil and water conservation in Fincha'a watershed, western Ethiopia. Land Use Policy. 27(4), 1027-1037.

[12] Adimassu, Z., Mekonnen, K., Yirga, C., et al., 2014. Effect of soil bunds on runoff, soil and nutrient losses, and crop yield in the central highlands of Ethiopia. Land Degradation & Development. 25(6), 554-564.

[13] Wolka, K., Biazin, B., Martinsen, V., et al., 2020. Soil and water conservation management on hill slopes in

southwest Ethiopia. I. Effects of soil bunds on surface runoff, erosion and loss of nutrients. Science of the Total Environment. 757, 142877.

[14] Tenywa, M.M., Bekunda, M., 2009. Managing soils in Sub-Saharan Africa: Challenges and opportunities for soil and water conservation. Journal of Soil and Water Conservation. 64(1), 44A-48A.

[15] Wolka, K., Mulder, J., Biazin, B., 2018. Effects of soil and water conservation techniques on crop yield, runoff and soil loss in Sub-Saharan Africa: A review. Agricultural Water Management. 207, 67-79.

[16] Holden, S., Shiferaw, B., 2004. Land degradation, drought and food security in a less-favoured area in the Ethiopian highlands: A bio-economic model with market imperfections. Agricultural Economics. 30(1), 31-49.

[17] Bewket, W., 2007. Soil and water conservation intervention with conventional technologies in northwestern highlands of Ethiopia: Acceptance and adoption by farmers. Land Use Policy. 24(2), 404-416.

[18] Abera, W., Tamene, L., Tibebe, D., et al., 2019. Characterizing and evaluating the impacts of national land restoration initiatives on ecosystem services in Ethiopia. Land Degradation & Development. 31, 37-52.

[19] Haregeweyn, N., Tsunekawa, A., Nyssen, J., et al., 2015. Soil erosion and conservation in Ethiopia. Progress in Physical Geography. 39(6), 750-774.

[20] Porter, C., Goyal, R., 2016. Social protection for all ages? Impacts of Ethiopia's Productive Safety Net Program on child nutrition. Social Science & Medicine. 159, 92-99.

[21] Adimassu, Z., Kessler, A., 2015. Impact of the productive safety net program on farmers' investments in sustainable land management in the Central Rift Valley of Ethiopia. Environmental Development. 16, 54-62.

[22] Wolka, K., Biazin, B., Martinsen, V., et al., 2021. Soil and water conservation management on hill slopes in southwest Ethiopia. II. Modeling effects of soil bunds on surface runoff and maize yield using AquaCrop. Journal of Environmental Management. 296, 113187.

[23] Desta, L., Carucci, V., Wendemagenehu, A., et al., 2005. Community based participatory watershed development: A guideline. Ministry of Agriculture and Rural Development: Addis Ababa, Ethiopia.

[24] Amdemariam, T., Selassie, Y.G., Haile, M., et al., 2011. Effect of soil and water conservation measures on selected soil physical and chemical properties and barley (Hordeum spp.) yield. Journal of Environmental Science and Engineering. 5(11), 1483-1495.

[25] Herweg, K., Ludi, E., 1999. The performance of selected soil and water conservation measures—case studies from Ethiopia and Eritrea. Catena. 36, 99-114.

[26] Wolka, K., Moges, A., Yimer, F., 2011. Effects of level soil bunds and stone bunds on soil properties and its implications for crop production: The case of Bokole watershed, Dawuro zone, Southern Ethiopia. Agricultural Science. 2, 357-363.

[27] Bezabih, B., Abebayehu, A., Tadesse, M., et al., 2016. The effect of land management practices on soil physical and chemical properties in Gojeb Sub-river Basin of Dedo District, Southwest Ethiopia. Journal of Soil Science and Environmental Management. 7(10), 154-165.

[28] Mengistu, D., Bewket, W., Lal, R., 2015. Conservation effects on soil quality and climate change adaptability of Ethiopian watersheds. Land Degradation & Development. 27(6), 1603-1621.

[29] Alemayehu, A.A., Getu, L.A., Addis, H.K., 2020. Impacts of stone bunds on selected soil properties and crop yield in Gumara-Maksegnit watershed Northern Ethiopia. Cogent Food & Agriculture. 6(1), 1785777.

[30] Amare, T., Terefe, A., Selassie, Y.G., et al., 2013. Soil properties and crop yields along the terraces and toposequece of Anjeni Watershed, Central Highlands of Ethiopia. Journal of Agricultural Science. 5(2), 134.

[31] Siriri, D., Tenywa, M.M., Raussen, T., et al., 2005. Crop and soil variability on terraces in the highlands of SW Uganda. Land Degradation & Development. 16(6), 569-579.

[32] Wolancho, K.W., 2015. Evaluating watershed management activities of campaign work in Southern nations, nationalities and peoples' regional state of Ethiopia. Environmental Systems Research. 4, 1-13.

[33] SNNPRS-BoFED, 2004. "Regional Atlas", Southern Nations, Nationalities and Peoples' Regional State, Bureau of Finance and Economic Development, Awassa, Ethiopia.

[34] Bouyoucos, G.J., 1962. Hydrometer method improved for making particle size analysis of soil. Agronomy. 54, 464-465.

[35] Walkley, A., Black, I.A., 1934. An examination of the degtjareff method for determining soil organic matter and a proposed modification of the chromic acid titration method. Soil Science. 37, 29-38.

[36] Black, C.A., Evans, D.D., White, J.L., et al., 1965. Methods of soil analysis. Part 1. Physical and mineralogical properties, including statistics of measurement and sampling. American Society of Agronomy,

Inc: Madison, Wisconsin.

[37] Wang, L., Shi, Z.H., 2015. Size selectivity of eroded sediment associated with soil texture on steep slopes. Soil Science Society of America Journal. 79(3), 917.

[38] Hishe, S., Lyimo, J., Bewket, W., 2017. Soil and water conservation effects on soil properties in the Middle Silluh Valley, northern Ethiopia. International Soil and Water Conservation Research. 5(3), 231-240.

[39] Hailu, W., Moges, A., Yimer, F., 2012. The effects of "Fanya juu" soil conservation structure on selected soil physical & chemical properties: The case of Goromti watershed, Western Ethiopia. Resources Environment. 2, 132-140.

[40] Chappell, A., Baldock, J., Sanderman, J., 2015. The global significance of omitting soil erosion from soil organic carbon cycling schemes. Nature Climate Change. 6(2), 187-191.

[41] Olson, K.R., Al-Kaisi, M., Lal, R., et al., 2016. Impact of soil erosion on soil organic carbon stocks. Journal of Soil and Water Conservation. 71(3), 61-67.

[42] Hassink, J., 1997. The capacity of soils to preserve organic C and N by their association with clay and silt particles. Plant and Soil. 191, 77-87.

[43] Mupangwa, W., Twomlow, S., Walker, S., 2012. Dead level contours and infiltration pits for risk mitigation in smallholder cropping systems of southern Zimbabwe. Physics and Chemistry of the Earth, Parts A/B/C. 47-48, 166-172.

[44] Saiz, G., Wandera, F.M., Pelster, D.E., et al., 2016. Long-term assessment of soil and water conservation measures (Fanya-juu terraces) on soil organic matter in South Eastern Kenya. Geoderma. 274, 1-9.

[45] Van Oost, K., Govers, G., De Alba, S., et al., 2006. Tillage erosion: A review of controlling factors and implications for soil quality. Progress in Physical Geography. 30(4), 443-466.

[46] Nyssen, J., Poesen, J., Gebremichael, D., et al., 2007. Interdisciplinary on-site evaluation of stone bunds to control soil erosion on cropland in Northern Ethiopia. Soil and Tillage Research. 94, 151-163.

[47] Lin, C., Tu, S., Huang, J., et al., 2009. The effect of plant hedgerows on the spatial distribution of soil erosion and soil fertility on sloping farmland in the purple-soil area of China. Soil and Tillage Research. 105(2), 307-312.

[48] Vancampenhout, K., Nyssen, J., Gebremichael, D., et al., 2006. Stone bunds for soil conservation in the northern Ethiopian highlands: Impacts on soil fertility and crop yield. Soil and Tillage Research. 90(1-2), 1-15.

[49] Walle, R.J., Sims, B.G., 1999. Fertility gradients in naturally formed terraces on Honduran hillside farms. Agronomy Journal. 91, 350-353.

[50] Koulouri, M., Giourga, C., 2007. Land abandonment and slope gradient as key factors of soil erosion in Mediterranean terraced lands. Catena. 69(3), 274-281.

[51] Ziadat, F.M., Taimeh, A.Y., 2013. Effect of rainfall intensity, slope, land use and antecedent soil moisture on soil erosion in an arid environment. Land Degradation & Development. 24(6), 582-590.

BILINGUAL PUBLISHING CO.
Pioneer of Global Academics Since 1984

Journal of Environmental & Earth Sciences
https://ojs.bilpublishing.com/index.php/jees

ARTICLE

Rings Structures on Ice Lake Baikal

V. K. Balkhanov*

Institute of Physical Materials Science of the Siberian Branch of Russian Academy of Sciences, Ulan-Ude, Russia

ARTICLE INFO

Article history
Received: 30 March 2022
Accepted: 10 May 2022
Published Online: 12 May 2022

Keywords:
Convection
Baikal
Thermal conductivity
Hydrodynamics

ABSTRACT

On the cosmic picture of the ice surface lake Baikal discovered a dark ring a diameter of 7-8 km. The author shall give a physical interpretation of the given phenomenon, having expected that shaping rings are connected with a surge of the warm natural gas from sedimentary a thick mass of the bottom of the Baikal. Convection is formed in thick mass of water in the manner of torah around surge of the natural gas, which carries become warm water before surface (the lower edge ice) side from pole of the natural gas. The mechanism heatconductivity heat gets to the upper edge of the ice, where snow and ice begin intensive to melt. As a result thawed patch is formed on snow-clad ice in the manner of a ring.

1. Background

About 23 years ago, by order of the Ministry of Natural Resources of Russia, daily space monitoring of the Baikal natural territory began with the help of the UniScan receiving station and the EOStation software complex, which operate in Moscow (ScanEx RDC) and Irkutsk (Baikal Center LLC). With the help of these satellite data, unique ring formations with a diameter of 7-8 km were discovered, which are formed on the snow-covered ice field of Lake Baikal (Figure 1). Rings appear one or two at a time, but not every year. Undoubtedly, the formation of rings is not a new phenomenon, and it has occurred in previous years. But without satellite monitoring, it was impossible to detect them. Although the rings are of considerable size, it is almost impossible to see them from the ice and even from the mountain ranges surrounding the basin of the lake.

Rings on Lake Baikal became famous in April 2009, when they became widely discussed on the internet. The author first observed them on a computer monitor on April 4, 2009, when pictures of the rings were posted on the internet [1]. I immediately proposed a physical mechanism for the formation of rings, and established a system of equations describing convection. Even earlier, the presence of rings was established by employees of the Limnological Institute, in particular Nikolai Granin. He suggested that the rings may arise due to the rise of deep waters,

*Corresponding Author:
V. K. Balkhanov,
Institute of Physical Materials Science of the Siberian Branch of Russian Academy of Sciences, Ulan-Ude, Russia;
Email: ballar@yandex.ru

DOI: https://doi.org/10.30564/jees.v4i1.4576

which are caused by eruptions of mud volcanoes. At the same time, in the central part of the future ring structure, the temperature rises (on average by half a degree compared to other parts of the lake), and the so-called anticyclonic current (circular flow directed counterclockwise) is formed. The current enhances vertical water exchange, as a result of which the ice cover is destroyed more strongly over the zones of maximum flow velocities [2,3]. The dark circles visible in the images are areas with minimal ice thickness. With an average thickness of the ice cover at the southern end of Lake Baikal of 70 centimeters within a radius of two kilometers from the center of the rings, it does not exceed 43 centimeters. Thin ice is more saturated with water than the average for the lake, and this contrast is clearly observed from space. Our consideration clarifies the picture proposed by Nikolai Granin - we abandon the anticyclonic flow as the cause of the formation of rings, and instead of mud volcanoes we consider emissions of natural gas. The latter is due to the fact that after the sinking of the underwater vehicle "Paisis" (http://nabaimar.ru/baikal/) in 1977 and 1991, the locations of mud volcanoes became known, the coordinates of which do not coincide with the coordinates of the rings in question.

Figure 1. Circular rings 1 (near the Svyatoy Nos Peninsula) and 2 (near the southern tip of Lake Baikal) on Lake Baikal. Picture from 4.04.2009.

In 2008-2010, MIR underwater vehicles sank to the bottom of Lake Baikal [4,5]. Studies conducted by scientists were widely covered by the media and the internet. In particular, one of the moments of the descent of one of the devices was shown on television. At the same time, footage of natural gas emissions from the bottom of the lake literally flashed in the form of a clearly visible jet of bubbles against the background of the water column. These shots were shown at night local time, so the author, unfortunately, did not have time to photograph them. But natural gas emissions and their demonstration in a television report undoubtedly took place.

2. Physical Interpretation of Ring Formation

Lake Baikal is geologically a graben lake, a section of the earth's crust bounded by steeply inclined gaps, confined to the rift zone (the Rift is a large linear tectonic structure of the earth's crust, hundreds to thousands of km long). Rifts are characterized by increased heat flow and seismic activity, and direct rift depressions are characterized by a powerful thickness of sedimentary rocks, several kilometers away, where a lot of organic matter accumulates. Increased thermal field and temperature gradient cause intense gas formation [6]. The release of natural gas, in particular methane, from the bottom of the lake in summer is observed due to bubbles rising to the water's surface and in winter the formation of "proparin" (ice-free surface of the water) with a size of 0.5 m - 100 m across. In addition to such relatively small proparins, space images of Lake Baikal revealed dark rings of an abnormally large size - with a diameter of 7-8 km (Figure 1) [1]. In April 2009, the rings were discovered west of Cape Lower Headboard of the Svyatoy Nos peninsula (Figure 1, circumference 1) and at the southern tip of Lake Baikal (Figure 1, circumference 2). In Figure 2 and Figure 3 rings are "tied" to the bathymetric map Baikal, where the geographical coordinates of the centers of the rings are also indicated (Bathymetric maps are geographical maps that display the underwater relief using isobaths, supplemented by depth marks). The fact that in the process of formation of rings the determining role is played by heat fluxes can be seen in Figure 4, where it is shown how as a result of heating is disturbed the strength of the ice, and it is crushed into ice blocks of different sizes. I associated the formation of rings on the surface of the ice with the giant convection of the entire water column around the release of natural gas. In the middle part of the rings, the temperature of the subglacial water is higher, according to the observations of Nikolai Granin on the rest of the water. This leads to the melting of snow and the ice itself.

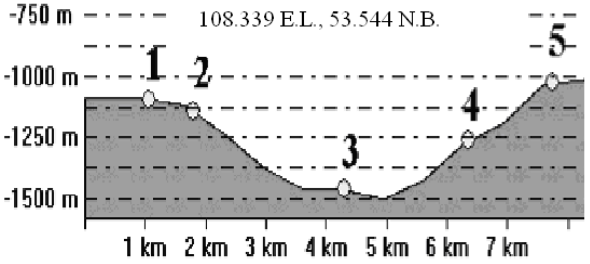

Figure 2. A section of the ring 1 in latitude on the bathymetric map near the Peninsula of the Holy Nose. 1 and 5 are the outer edge of the ring, 2 and 4 are the inner edge of the ring, and 3 are the center of the ring. At the top are the geographical coordinates of the center of the ring.

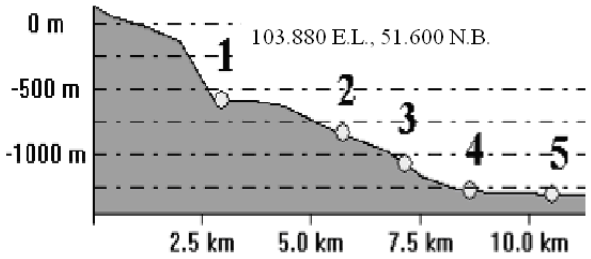

Figure 3. A section of ring 2 in longitude on a bathymetric map near the southern tip of Lake Baikal. The numbers indicate: 1 and 5 - the outer edge of the ring, 2 and 4 - the inner edge of the ring, 3 - the center of the ring. At the top are the geographical coordinates of the center of the ring.

Figure 4. The destruction of the ice field was a result of the warming of the ice near the southern end of Lake Baikal. Photo from the International Space Station "MCS" from 25.04.2009.

The water of Lake Baikal is characterized by the fact that in the spring the temperature throughout the depth practically does not change and is usually $T_0 = 3.2 - 3.4\ ^\circ C$. Only near the surface, from a depth of 150-200 m, the temperature gradually decreases to almost 0 °C afloat. The resulting temperature gradient is so insignificant that water convection does not occur (we are distracted from the internal currents of the water column that are not associated with temperature convection). Already here it can be seen that the problem under consideration is significantly different from the well-known Convection of Benard - Rayleigh. However, the outflow of natural gas from the sedimentary layer of the bottom disrupts the mechanical balance of water. The water column comes into a convective current, which, due to symmetry, takes a shape close to the torus, as shown in Figure 5. Contacting the lower point with warmer natural gas, as a result of the rotation of the water column, heat is carried to the upper point. The following system of equations makes it possible to prove that the temperature distribution on the surface of water in the middle part of the rings has a maximum. This picture is indicated by a completely similar phenomenon accompanying the explosion of a hydrogen bomb, as in Figure 6. The difference only that the convection we are considering arises from the laminar rise of natural gas, and the convection associated with the explosion of a hydrogen bomb arises from the rise of the turbulent flow of combustible products. (As far as the author knows, foreign researchers call the model in question - the model of the explosion of an atomic bomb). However, in both cases, convection takes the form of a torus. A well-known example of the rotation of smoke rings can be given.

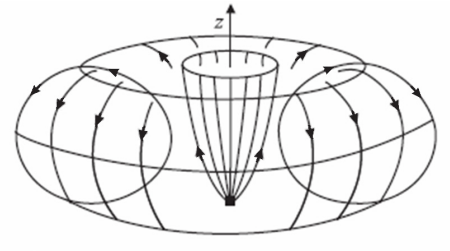

Figure 5. A high-quality picture of the surfacing of a warm jet of natural gas and the convective flow of water around the jet in the form of an oblate torus. A shaded square at the bottom of the upward jet indicates the size of the source.

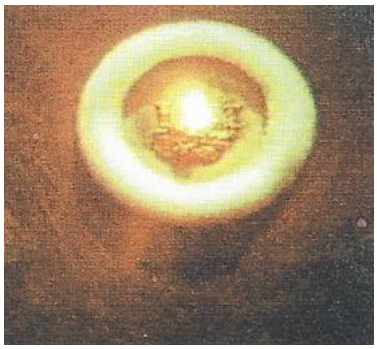

Figure 6. Hydrogen bomb explosion (top view).

3. Convective Flow Equation System

Let us proceed to a theoretical description of the convective flow. Such a description is possible only if we consider the equations of hydrodynamics (navier-Stokes equation and continuity equation) and the thermal conductivity equation together. We'll start with the thermal conductivity equation, which looks like this:

$$\frac{\partial T}{\partial t} + \left(\vec{V} \cdot \nabla\right) T = \chi \nabla^2 T. \qquad (1)$$

Coefficient χ is called the thermal diffusivity coefficient. Its presence in Equation (1) means that the thermal properties of water are described by only one parameter.

The convection we are considering is a stationary process in which all quantities do not clearly depend on time. For such quantities, the partial derivative in time turns to zero. In the absence of an external heat source, the water mass has a stationary temperature distribution T_0, depending on the location only. Convection occurs due to the fact that an extraneous source of heat is introduced into the liquid. As a result of a stationary temperature distribution T_0 a small addition of temperature is applied T. It follows that in order to describe convection by Equation (1), the value of T must be replaced by the sum T_0+T. Then Equation (1) will take the following form:

$$\left(\vec{V}\cdot\nabla\right)T_0+\left(\vec{V}\cdot\nabla\right)T=\chi\nabla^2T_0+\chi\nabla^2T. \quad (2)$$

Convective flow as a mechanical movement occurs at a slow speed. Therefore, speed V in Equation (2) is a first-order quantity of smallness, as is the small addition of temperature T. Separating quantities of different orders of smallness and neglecting the second-order term, we obtain the following equations:

$$\nabla^2T_0=0. \quad (3)$$

$$\left(\vec{V}\cdot\nabla\right)T_0=\chi\nabla^2T. \quad (4)$$

Equation (3) for our problem of theoretical description of convection can be immediately solved. For the equilibrium state of water in the Earth's gravitational field, the temperature T_0 may depend only on the depth of z, where the z-axis is directed from the bottom to the water surface (Figure 7). Then Equation (3) has two solutions. One of them corresponds to the constant value of the equilibrium temperature: T_0= *const*. The second solution will be a linear dependence on depth:

$$T_0=c-Az, \quad (5)$$

where c and A are constant integrations defined by the condition of the problem. For of the Baikal water column, both cases are realized. Of the Baikal water column, both cases are realized. First, from the bottom of the lake to some depth with an elevation of 150-200 m from the surface of the water, the equilibrium water temperature is constant and is 3.2-3.4 °C.

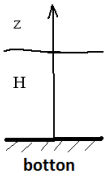

Figure 7. The depth of Lake H, the z-axis is directed from the bottom of the lake to the water's surface.

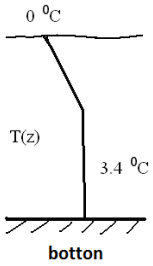

Figure 8. Equilibrium temperature profile of the water mass in the spring on Lake Baikal.

Then the temperature is linearly compared with the temperature of the surface layer of water corresponding to the season. In the month of April, when it is possible to observe rings on Lake Baikal, the temperature of Celsius on the surface is zero (Figure 8). We can see that in the spring the equilibrium temperature decreases evenly, which is why in solution (5) there is a minus sign before the constant A. If we assume that the depth is 1 km, and up to the mark of 800 m from the bottom, the temperature is constant and equal to 3.4 °C, then the solution of Equation (3) can be written as follows:

$$T_0\left({}^0C\right)=\begin{cases}3.4, & z=0-800\ м\\ 17-\dfrac{3.4}{200}\,z, & z=800-1000\ м\end{cases}.$$

Let us now turn to the Navier-Stokes equation:

$$\frac{\partial\vec{V}}{\partial t}+\left(\vec{V}\cdot\nabla\right)\vec{V}=-\frac{\nabla P}{\rho}+\nu\nabla^2\vec{V}+\vec{g}, \quad (6)$$

supplemented by the continuity equation:

$$\nabla\cdot\vec{V}=0. \quad (7)$$

where ν is viscosity coefficient, g is the acceleration of free fall, P is the pressure, ρ is density of water.

Velocity V is a small velocity of convective water flow, so $\left(\vec{V}\cdot\nabla\right)\vec{V}$ as a second-order term of the small can be omitted. In addition, we consider the stationary course. In this case, Equation (6) takes the following form:

$$0=-\frac{\nabla P}{\rho}+\nu\nabla^2\vec{V}+\vec{g}. \quad (8)$$

In the absence of an external heat source, the density of water has a constant and equilibrium value ρ_0. With slight heating, the volume of water increases, respectively, the density decreases. In the first order of approximation of the small addition of temperature T, which is a consequence of the appearance of an external heat source, the addition to the density will be proportional to this temperature T. Thus, the density becomes equal to:

$$\rho=\rho_0-\beta\rho_0T. \quad (9)$$

Here is the multiplier β is called the coefficient of thermal expansion. In the range from 0 °C to 3.4 °C it can be considered permanent.

In the pressure, let's highlight the atmospheric pressure P_A on the surface of the water, hydrostatic pressure $-\rho_0 g z$ a column of water, and a small additive *P* associated with the convective flow. Thus, in Equation (8), the value *P* is replaced by the following expression:

$$P_A + \rho_0 g (H - z) + P, \tag{10}$$

where H is the depth of the lake. Substituting Equations (9) and (10) into Equation (8), in the first order of approximation by *P*, *V* and *T* we get:

$$0 = -\frac{\nabla P}{\rho_0} + \beta \vec{g} T + \nu \nabla^2 \vec{V}. \tag{11}$$

To eliminate the pressure *P*, let's use Equation (11) on the left with two rotor operators $\nabla \times (\nabla \times ...)$. Using the rules of vector analysis, and taking into account the continuity Equation (7), the result is:

$$\nu \left(\nabla^2\right)^2 \vec{V} = \beta \nabla \left(\vec{g} \cdot \nabla T\right) - \beta \vec{g} \nabla^2 T. \tag{12}$$

We obtained Equations (3), (4), (7) and (12), which, supplemented by boundary conditions, completely determine the spatial distribution of temperature *T* and velocity $\vec{V}$ convective flow (describe the known "mushroom" formed during an atomic explosion).

4. Surfacing Natural Gas Jets

Convection in the form of a violation of mechanical equilibrium occurs when an external heat source appears. For Rayleigh-Bénard convection, the source of heat is a heated bottom. For the convection we are considering, the source of heat is a jet of heated natural gas introduced into the water column. Its mass element Δm carries the element of heat $\Delta Q = \Delta m C_p T_s$. In here C_p is specific heat of the jet at constant pressure, T_s is temperature measured from the equilibrium temperature of the surrounding water column. Let ρ_s be density of natural gas, and $\rho_s < \rho_0$, so that the jet floats in the form of a pillar with a round cross-section. If r_s is the cross-sectional radius of the jet, Δz_s is the jet height element, then the mass element will be

$$\Delta m = \rho_s \pi \Delta r_s^2 \Delta z_s.$$

During the time Δt natural gas floats to a height $\Delta z_s = V_s \Delta t$, where V_s is the speed of the jet surfacing. Combining all the expressions, we get that in a unit of time a column of natural gas carries heat:

$$\frac{\Delta Q}{\Delta t} = \pi \rho_s C_p T_s V_s r_s^2. \tag{13}$$

Jet surfacing is a regular and stationary process. Ignoring also the dissipation of heat, we come to the position that the expression (13) is a constant value. Thus,

$$T_s V_s r_s^2 = const. \tag{14}$$

Consider the rise of a jet of natural gas in a viscous continuous column of water. Its surfacing is a stationary laminar current. The equation of motion of the jet is derived from the equations of hydrodynamics in a similar way to convective motion and leads to Equation (12), but only with the non-zero left side, and the values provided with the index *s*:

$$\left(\vec{V}_s \cdot \nabla\right) \vec{V}_s = -\nabla \frac{P}{\rho_s} - \beta_s \vec{g} T_s + \nu_s \nabla^2 \vec{V}_s. \tag{15}$$

All the terms of Equation (15) are of the same order, so

$$\frac{V_s^2}{z_s} \sim \beta_s g T_s \sim \nu_s \frac{V_s}{r_s^2}.$$

Solving these equations together with Equation (14), we find that the jet emerges in the form of a figure of rotation with the *z*-axis, moreover (Zeldovich relations [6]):

$$r_s \sim \sqrt{z_s},\ V_s = const,\ T_s \sim \frac{1}{z_s}. \tag{16}$$

Expression (16) will be boundary conditions for the problem of determining the spatial distribution of the temperature of the water column, especially interesting for us the distribution of temperature at the surface. Let's rewrite the last ratio in Equation (16) as follows:

$$T\left(\sqrt{x^2 + y^2} = r, z = H\right) \sim \frac{1}{z}. \tag{17}.$$

This ratio describes the distribution of temperature in the convective flow at the point of contact with the jet. A laminar jet emerges from the sedimentary stratum of the bottom from a hole of some finite size, the minimum size of which can be found from the expression (14) and conditions $\rho_s V = \max$ [7]. Regularity $r_s \sim \sqrt{z_s}$, it is convenient to specify and write in the following form:

$$r_s = \sqrt{D z_s}. \tag{18}$$

Below we define its numerical value for the value of *D*.

5. Spatial Temperature Distribution

The above system of Equations (3), (4), (7) and Equation (12), describing convection, has not yet received proper mathematical research. But they can be solved in one approximate case. Namely, near the water's surface, we can assume that the convective flow of water is almost parallel to the water's surface. This means that when $z = H$ speed component V_R in the plane *x y* will have a lot more vertical components V_z. Let's project Equation (12)

onto a plane *x y*:

$$\nu \left(\nabla^{2}\right)^{2} V_R = \beta\, g\, \nabla_R \frac{\partial T}{\partial z}, \tag{19}$$

where ∇_R is determined by the ratio $\nabla_R^{2} = \frac{\partial^{2}}{\partial x^{2}} + \frac{\partial^{2}}{\partial y^{2}}$.

Near $z = H$ speed V_R can depend only on the radial in the plane *x y* of the coordinate *r*. Then the expression on the left in Equation (19) is a function only of *r*. In order for Equation (19) and the expression on the right to depend only on *r*, the temperature *T* must be a linear function of *z*. Thus,

$$T(r,z) = u(r) + v(r)\ z. \tag{20}$$

Since the temperature $T(r,z)$ counted from the value T_0, which with $z = H$ is zero, then and $T(r, z = H) = 0$. From here it can be seen that the functions $u(r)$ and $v(r)$ have different signs. In addition, at the point of contact of the convective flow with the natural gas jet, when $r = \sqrt{D\ z}$, the boundary condition Equation (17) must be met. This can be achieved if $T(r,z)$ select the following form [8]:

$$T(r,z) = a\ h^{2}\ T_m \left(\frac{1}{r^{2}} - b\frac{h\ z}{r^{4}}\right). \tag{21}$$

Indeed, substituting $r = \sqrt{D\ z}$, get

$$T(r_s) = T(r,z) = \frac{a\ H^{2}\ T_m}{D}\left(1 - b\frac{H}{D}\right)\frac{1}{z},$$

in agreement with Equation (17). Permanent *a*, *b* and T_m to be determined below.

When writing the solution in the form of Equation (21), we actually followed the general method, when solutions of a system of equations like Equation (7) and Equation (12) are searched in such a way as to satisfy the boundary conditions of the problem. The solution Equation (19) has a remarkable feature – dependence $T(r, z = H)$ has max. It follows that at a point max,

$$R_m = \sqrt{2b}\ H, \tag{22}$$

and, in addition,

$$a = 4\ b. \tag{23}$$

So, for the ring in Figure 2 R_m=2.78 km and *H*=1.46 km, from where *b*=1.81 and *a*=7.25. To establish the meaning of a quantity *D* in the formula (18), suppose that at the point of contact of water with the jet, the temperature T_s=0 °C (ice and snow do not melt on it). At a point maximum temperature T_m=4 °C (the ice is not melting yet, and the snow has already melted). Then, substituting $r = \sqrt{D\ z}$ in Equation (21), for *D* we obtain a quadratic equation whose smallest solution will be:

$$D_m = 4 \text{ km}. \tag{24}$$

We see that the dimensionless quantities *a* and *b* have values of the order of one. This circumstance once again justifies the choice of a solution in the form Equation (21). Here are the following values related to the ring in Figure 3:

R_m=2.76 km and *H*=1.05 km, *b*=3.45, *a*=13.8 and *D*=5.17 km.

They differ significantly from similar values for the values of ring No 1 (Figure 2). This difference seems to be related both to the approximation used in solving Equation (12) and to the difference in bottom relief for both rings.

To obtain other approximate solutions near the middle of the ring, it is necessary to involve the entire set of boundary conditions. However, information on the physical characteristics of the natural gas jet is not yet available. Therefore, scant experimental data (in fact, only space images and a bathymetric map were used) do not yet allow for a more detailed analysis of the phenomenon of the formation of giant rings on ice.

6. Convective Instability

Consider the question of the criterion for the occurrence of instability of the water column in the form of a torus around the release of natural gas from the bottom of Lake Baikal. For the Rayleigh-Bénard convection, a similar question is set out in the book *Theory of Elasticity* [6]. Let's look for the perturbation of velocity and temperature described by Equations (3), (4), (7) and Equation (12) in exponential form:

$$\exp(i\ \vec{k}\cdot\vec{r}) = \exp\left(i\ k_R\ r + i\ k_z\ z\right). \tag{25}$$

On the right in the exponent we write $i\ k_R\ r$, because we are considering a cylindrically symmetrical case. The appearance of instability will mean the emergence of the root of the equations,

$$\text{Im}\ k_R\ (\text{Re}) = 0,\ \text{Im}\ k_z\ (\text{Re}) = 0. \tag{26}$$

Im means taking an imaginary part. The number of Rayleigh Re will be determined below.

Taking into account Equation (25), this system of equations takes the following form:

$$\frac{d^{2} T_0}{d z^{2}} = 0, \tag{27.a}$$

$$-V_z\ \frac{d\ T_0}{d\ z} = \chi\ k_R^{2}\ T + \chi\ k_z^{2}\ T, \tag{27.b}$$

$$i\ k_R\ V_R + i\ k_z\ V_z = 0, \tag{27.c}$$

$$\nu\left(k_R^{2} + k_z^{2}\right)^{2} V_R = -\beta\ g\ k_R\ k_z\ T. \tag{27.d}$$

Here it is advisable to move on to one equation. For

example, excluding speed components V_R and V_z, we get the equation for temperature T:

$$\left[\left(k_R^2+k_z^2\right)^3-\mathrm{Re}\ k_R^2\right]T=0. \tag{28}$$

And here the number of Rayleigh Re is a dimensional quantity. If the wave number k is measured in units of some length ΔH, then the Number of Relays will be dimensionless:

$$\mathrm{Re}=\frac{\beta\, g\, \Delta H^4\ \left(-d\, T_0/d\, z\right)}{\nu\, \chi}. \tag{29}$$

It was noted above that at a significant part of the depth the temperature $T_0=const$. This means turning the Rayleigh number to zero and no convection. Since convection undoubtedly takes place, a component must be added to the right side, arising from the fact that the water column is not in contact with a solid surface, but with a heated liquid stream of natural gas. In an area where the temperature is linearly dependent on the depth, we have $-d\, T_0/d\, z=A$. Substituting in Equation (28) $k_z^2=-d^2/d\, z^2$, get:

$$\left[\left(\frac{d^2}{d\, z^2}-k_R^2\right)^3+\mathrm{Re}\ k_R^2\right]T=0. \tag{30}$$

This equation formally coincides with the corresponding equation in the book *Theory of Elasticity* [6]. Therefore, you can immediately write the critical values for the Rayleigh number and the radial component of the wave number:

$$\mathrm{Re}_c=1708,\ k_{Rc}=3.12/\Delta H. \tag{31}$$

Replacing in Equation (28) $k_R^2=-\frac{1}{r}\frac{\partial}{\partial\, r}\left(r\frac{\partial}{\partial\, r}\right)$, get:

$$\left[\left(\frac{1}{r}\frac{\partial}{\partial\, r}r\frac{\partial}{\partial\, r}-k_z^2\right)^3-\mathrm{Re}\ \frac{1}{r}\frac{\partial}{\partial\, r}r\frac{\partial}{\partial\, r}\right]T=0. \tag{32}$$

As far as is known, no such equation has been analyses. Such an analysis should give the same value for Re_c, that both the given in Equation (31) and the numerical value for k_{zc}. However, the value for k_{zc} can be found without actually solving Equation (32). Indeed, by substituting Equation (32) with Equation (28), you can immediately find:

$$k_{zc}=3.97/\Delta H. \tag{33}$$

Further, since it is obvious that,

$$k_{Rc}\sim 1/R_m,\ k_{zc}\sim 1/H,$$

then from the ratios (31) and (33), after exclusion ΔH, followed by Equation (22), which, by this, gets another justification. Due to different boundary conditions for our problem, and for the Rayleigh-Bénard convection, the numerical values in formulas (31) and (33) will generally be different. However, the conclusion about the linear relationship (22) between the radius of the rings and the depth of the lake will remain.

7. Conclusions

It was established that the formation of rings on the ice surface of Lake Baikal is associated with giant convection of the water column due to the release of warm natural gas from the sedimentary bottom of Lake Baikal. Natural gas, rising to the surface, cools, but manages to warm up the surrounding cold water. As a result, convection forms in the water column in the form of a torus around the release of natural gas, which carries warm water to the surface (lower edge of the ice) away from the column of natural gas. By the mechanism of thermal conductivity, the heat reaches the upper edge of the ice, where ice and snow begin to melt intensively. As a result, a protalin in the form of a ring is formed on snow-covered ice. Convection in the form of a torus is described by joint solutions of the equations of hydrodynamics and the equation of thermal conductivity. From these equations, a system of equations describing convection in the form of a torus is obtained. By the mechanism of thermal conductivity, the heat reaches the upper edge of the ice, where ice and snow begin to melt intensively. As a result, a protalin in the form of a ring is formed on snow-covered ice. Convection in the form of a torus is described by joint solutions of the equations of hydrodynamics and the equation of thermal conductivity. From these equations, a system of equations describing convection in the form of a torus is obtained. An approximate solution for the spatial distribution of temperature near the water surface is given. The latter is due to the fact that our system of equations has not yet received proper mathematical research. Indeed, let us recall that about 15 years have passed since the discovery of the Bénard cells and their mathematical description by Rayleigh. The question of convective instability is considered. In solving this question, it was established that the radius of the rings is linearly related to the depth of the lake.

Conflict of Interest

There is no conflict of interest.

Funding

Work done in Laboratory Electromagnetic Diagnostics Institute of Physical Materials Science of the Siberian Branch RAS.

References

[1] Balkhanov, V.K., Bashkuev, Y.B., Khaptanov, V.B., 2010. Formation of circular rings on the snow-covered ice field of Lake Baikal. Technical Physics. 55(9), 1266-1269.
DOI: https://doi.org/10.1134/s1063784210090057

[2] Granin, N.G., 2009. The ringed Baikal. Nauka iz Pervykh Ruk [Science First Hand]. 3, 22-23. (in Russian)

[3] Granin, N.G., Vyusht, A., Gnatovsky, R.Yu., et al., 2005. IV Vereshchagin Baikal Conference. p. 52-53.

[4] Baikal, L., 1993. Atlas. Federal Survey for Geodesy and Mapping Publishing House: Moscow. p. 160.

[5] Map of the Lake Baikal, 1992. Main Directorate of Navigation and Oceanography of the Ministry of Defense of the USSR.

[6] Landau, L.D., Lifshitz, E.M., 1986. Theory of elasticity. (3rd ed.), Butterworth-Heinemann: Oxford.

[7] Kompaneets, A.S., 1974. A course of theoretical physics Vol. 2 statistical laws. Mir Publishers: Moscow. pp. 480.

[8] Convective currents: Collection of scientific works, Perm, PSPI, 1989. pp. 120.

BILINGUAL
PUBLISHING CO.
Pioneer of Global Academics Since 1984

Tel.:+65 65881289
E-mail: contact@bilpublishing.com
Website:ojs.bilpublishing.com

2661-3190
01
9 772661 319227